Universidad Politécnica de Cartagena

ESCUELA INTERNACIONAL DE DOCTORADO

PROGRAMA DE DOCTORADO EN TECNOLOGÍAS INDUSTRIALES

TESIS DOCTORAL

TÉCNICAS NUMÉRICAS NO LINEALES PARA EL TRATAMIENTO DE DATOS CON DISCONTINUIDADES

Presentada por Concepción Solano Lorente para optar al grado de Doctora
por la Universidad Politécnica de Cartagena

Dirigida por:
Dr. Juan Ruiz Álvarez

Cartagena, 2023

Universidad Politécnica de Cartagena

ESCUELA INTERNACIONAL DE DOCTORADO

DOCTORAL PROGRAMME IN INDUSTRIAL TECHNOLOGIES

PhD THESIS

NONLINEAR NUMERICAL TECHNIQUES FOR THE PROCESSING OF DATA WITH DISCONTINUITIES

Presented by Concepción Solano Lorente
to the Technical University of Cartagena in fulfilment of
the thesis requirement for the award of PhD

Supervisor:
Dr. Juan Ruiz Álvarez

Cartagena, 2023

Contents

Agradecimientos **8**

Resumen **9**

Abstract **11**

1 Introduction **13**
1.1 Numerical Integration 13
1.2 Hermite splines 14
1.3 Super resolution 15
1.4 Conclusions and future work 16

2 Numerical integration rules with improved accuracy close to discontinuities **17**
2.1 Introduction 17
2.2 Obtainment of adapted numerical integration formulas 17
2.2.1 Error formula for the corrected trapezoid rule 18
2.2.2 Correction terms and error formula for the corrected Simpson's $\frac{1}{3}$ rule . . . 21
2.3 Modified Newton-Cotes integration formulas 27
2.3.1 Correction terms for commonly used Newton-Cotes formulas 35
2.4 Numerical experiments 35
2.4.1 A study of the numerical accuracy attained through the proposed numerical integration formulas 36
2.4.2 Example: Solving Sturm-Liouville boundary problems using the Green functions and numerical integration 38
2.5 Conclusions 40

3 Adapting cubic Hermite splines to the presence of singularities through correction terms **43**
3.1 Introduction 43
3.2 Some preliminaries about classical cubic Hermite splines 44

3.3 Accurate approximation of first order derivatives using splines and data in the point-values . . . 48
3.4 Analysis of the absence of the Gibbs phenomenon close to jump discontinuities in the cubic Hermite spline using corrected first order derivatives . . . 56
3.5 Full accuracy of the adapted Hermite interpolation . . . 58
3.6 The adaption as a post-processing procedure . . . 65
3.6.1 The cubic Hermite spline with corrected first order derivatives as a post-processing procedure . . . 65
3.6.2 The fully accurate cubic Hermite spline as a post-processing procedure . . . 66
3.7 Numerical experiments . . . 67
3.7.1 Accuracy analysis of the interpolation, first and second order derivatives obtained through the classical and corrected splines . . . 67
3.7.2 Elimination of the Gibbs phenomenon using adapted first order derivatives 72
3.7.3 Regularity . . . 73
3.8 Conclusions . . . 73

4 Image super resolution **78**
4.1 Introduction . . . 78
4.2 Harten's framework for multiresolution . . . 79
4.3 The Cell-average Multiresolution Setting . . . 81
4.4 Relationship between multiresolution schemes and subdivision schemes (zoom) . . . 83
4.5 Towards a super resolution algorithm . . . 84

5 Conclusions and future works **86**
5.1 Conclusions . . . 86
5.2 Future lines of research . . . 87

References **88**

List of Figures

2.1 An example of a function with discontinuities (solid line) placed at a position x^*. We have labeled the domain to the left of the discontinuity as $-$ and the one to the right as $+$. We have also represented with a dashed line the prolongation of the functions through Taylor expansions at both sides of the discontinuity. 18

2.2 Two examples of functions with discontinuities (solid line) placed in different intervals at a position x^*. We have labeled the domain to the left of the discontinuity as $-$ and the one to the right as $+$. We have also represented with a dashed line the prolongation of the functions through Taylor expansions at both sides of the discontinuity. 22

2.3 Three examples of functions with discontinuities (solid line) placed in different intervals at a position x^*. We have labeled the domain to the left of the discontinuity as $-$ and the one to the right as $+$. We have also represented with a dashed line the prolongation of the functions through Taylor expansions at both sides of the discontinuity. 36

2.4 Grid refinement analysis for the numerical integration of the function in (2.54). To the left, using the simple trapezoid rule and the corrected simple trapezoid rule. At the center, using the simple Simpson's 1/3 rule and the corrected one. To the right, using the simple Simpson's 3/8 rule and the corrected one. In all the cases, the error of the corrected formulas decreases following the theoretical rate. 37

2.5 Grid refinement analysis for the numerical integration of the function in (2.54). To the left, using the composite trapezoid rule and the corrected composite trapezoid rule. At the center, using the composite Simpson's 1/3 rule and the corrected one. To the right, using the composite Simpson's 3/8 rule and the corrected one. In all the cases, the error of the corrected formulas decrease following the theoretical rate. 38

3.1 Representation of the Hermite basis for $s \in [0, 1]$. 46

3.2 In this figure we can see an example of discontinuity in the function and its derivatives placed in the interval $[x_j, x_{j+1}]$ at a position $x^* = x_j + \alpha$. 48

3.3 Functions in (3.68) and (3.69) used in the numerical experiments. 68

3.4 In this figure we represent the results of the grid refinement analysis for the accuracy of the corrected and classical splines and their first and second order derivatives using the infinity norm shown in Tables 3.1, 3.2 and 3.3. The original data has been sampled from the function in (3.68). In the first row we show the error E^l for the corrected and classical spline, in the second one we show the error for the first order derivative, and finally, the error for the second order derivative. The x axis represents de resolution level l: the increase of l implies the reduction of the grid-spacing of the low resolution data. Thus, the slope of the dashed lines represents the accuracy of each method. 71

3.5 In this figure we represent the results of the grid refinement analysis for the accuracy of the corrected and classical splines and their first and second order derivatives using the infinity norm shown in Tables 3.4, 3.5 and 3.6. The original data has been sampled from the function in (3.69). As in Figure 3.4, in the first row we show the error E^l for the corrected and classical spline, in the second one we show the error for the first order derivative, and finally, the error for the second order derivative. The x axis represents de resolution level l: the increase of l implies the reduction of the grid-spacing of the low resolution data. Thus, the slope of the dashed lines represents the accuracy of each method. 71

3.6 In the first row, we present the reconstruction or approximation $g(x)$ of the function in (3.68) with red circles. Initially we sample the function at a high resolution of 256 points and we represent it with blue crosses. Then we subsample the data to obtain a low resolution version of 16 points, and we represent it with solid black circles. The second and third row are dedicated to present the error in the first and second order derivatives, respectively. The first column presents the results of the classical cubic Hermite spline, the second one presents those obtained by the classical cubic Hermite spline with corrected first order derivatives. Finally, the third one presents the results attained by the corrected cubic Hermite spline with corrected first order derivatives. 74

3.7 Approximation of the first order derivative (first column), and second order derivative (second column) of the function in (3.68) sampled with 16 points to obtain the low resolution data. The blue dots represent the first or the second order derivative of the function. The coloured stars represent the first or the second order derivatives of the polynomial pieces of the spline $g(x)$. Each colour of the stars represents a different polynomial piece of the spline. The first row presents the result for the classical spline. The second row shows the result for the classical spline with corrected first order derivatives. The third row shows the results for the corrected spline with corrected first order derivatives. 75

3.8 Approximation of the first order derivative (first column) and second order derivative (second column) of the function in (3.69) sampled with 16 points to obtain the low resolution data. The blue dots represent the first or the second order derivative of the function. The coloured stars represent the first or the second order derivatives of the polynomial pieces of the spline $g(x)$. Each colour of the stars represents a different polynomial piece of the spline. The first row presents the result for the classical spline. The second row shows the result for the classical spline with corrected first order derivatives. The third row shows the results for the corrected spline with corrected first order derivatives. 76

4.1 High resolution mesh where two low resolution images have been placed (represented by large black dot and large white dot) separated by 0.5 pixels in diagonal direction. The points where we do not have information from the two low-resolution images are represented by a small black dot. 85

List of Tables

2.1 Grid refinement analysis in the infinity norm for the integral shown in (2.61) using two composite quadrature rules. The first part of the table shows the trapezoidal rule (T.R.) and the corrected trapezoidal rule (C.T.R.). The bottom part shows the Simpson's 1/3 Rule (S. 1/3 R.) and the corrected Simpson's rule (C.S. 1/3 R.). 41

2.2 Correction terms to be subtracted from the most common integration formulas. . . 41

2.3 Grid refinement analysis for the simple quadrature rules. The first part of the table shows the trapezoidal rule (T.R.) and the corrected trapezoidal rule (C.T.R.). The central part shows the Simpson's 1/3 Rule (S. 1/3 R.) and the corrected Simpson's rule (C.S. 1/3 R.). Finally the bottom part shows the Simpson's 3/8 Rule (S. 3/8 R.) and the corrected Simpson's 3/8 rule (C.S. 3/8 R.). We have used the function in (2.54). 42

2.4 Grid refinement analysis for the composite quadrature rules. The first part of the table shows the trapezoidal rule (T.R.) and the corrected trapezoidal rule (C.T.R.). The central part shows the Simpson's 3/8 Rule (S. 3/8 R.) and the corrected Simpson's rule (C.S. 3/8 R.). Finally the bottom part shows the Simpson's 1/3 Rule (S. 1/3 R.) and the corrected Simpson's 1/3 rule (C.S. 1/3 R.). We have used the function in (2.54). 42

3.1 Grid refinement analysis for the accuracy of the corrected and classical splines using the infinity norm at the high resolution nodes. The original data has been sampled from the function in (3.68). The low resolution nodes have been sampled with $m = 2^l$ nodes and the high resolution data with $32m$ points. 69

3.2 Grid refinement analysis for the accuracy of the first order derivative at the low resolution nodes of the corrected and classical splines using the infinity norm. The original data has been sampled from the function in (3.68). The low resolution nodes have been sampled with $m = 2^l$ nodes and the high resolution data with $32m$ points. 69

3.3 Grid refinement analysis for the accuracy of the second order derivatives at the high resolution nodes of the corrected and classical splines using the infinity norm. The original data has been sampled from the function in (3.68). The low resolution nodes have been sampled with $m = 2^l$ nodes and the high resolution data with $32m$ points. 70
3.4 Grid refinement analysis for the accuracy of the corrected and classical splines using the infinity norm at the high resolution nodes. The original data has been sampled from the function in (3.69). The low resolution nodes have been sampled with $m = 2^l$ nodes and the high resolution data with $32m$ points. 70
3.5 Grid refinement analysis for the accuracy of the first order derivative at the nodes of the corrected and classical splines using the infinity norm. The original data has been sampled from the function in (3.69). The low resolution nodes have been sampled with $m = 2^l$ nodes and the high resolution data with $32m$ points. 72
3.6 Grid refinement analysis for the accuracy of the second order derivatives at the high resolution nodes of the corrected and classical splines using the infinity norm. The original data has been sampled from the function in (3.69). The low resolution nodes have been sampled with $m = 2^l$ nodes and the high resolution data with $32m$ points. 72

Agradecimientos

Me gustaría expresar mi más sincero agradecimiento: A mi director, Dr. Juan Ruiz Álvarez, por el apoyo, el ánimo y la motivación a lo largo de todo el periodo de esta tesis. Me siento afortunada por haber contado con su trabajo, sus consejos y su profesionalidad. Hago extensivo mi agradecimiento a todos los coautores de las publicaciones, Dr. Sergio Amat Plata, Dr. Zhilin Li y Dr. Juan Carlos Trillo Moya. Sin sus inestimables colaboraciones no hubiese sido posible realizar este trabajo. A toda mi familia, en especial a mis padres, mis hermanos y mi marido por haberme ayudado, y animado a llegar hasta aquí. Y finalmente, a mis hijos, por darme la energía suficiente para finalizar esta etapa tan importante junto a vosotros.

Resumen

En esta tesis de doctorado, hemos intentado diseñar algoritmos capaces de manejar datos discontinuos. Hemos centrado nuestra atención en tres aplicaciones principales:

- Integración numérica más términos de corrección. En esta parte de la tesis, construimos y analizamos una nueva técnica no lineal que permite obtener integraciones numéricas precisas de cualquier orden utilizando datos que contienen discontinuidades, y cuando el integrando solo se conoce en puntos de la malla. La novedad de la técnica consiste en la inclusión de términos de corrección con una expresión cerrada que depende del tamaño de los saltos de la función y sus derivadas en las discontinuidades, cuya posición se supone conocida. La adición de estos términos permite recuperar la precisión de las fórmulas clásicas de integración numérica cerca de las discontinuidades, ya que estos términos de corrección tienen en cuenta el error que cometen las fórmulas clásicas de integración hasta su precisión en las zonas de suavidad de los datos. Por lo tanto, los términos de corrección se pueden agregar durante la integración o como un post-proceso, lo cual es útil si el cálculo principal de la integral ya se ha realizado utilizando fórmulas clásicas. Durante nuestra investigación, logramos concluir varios experimentos numéricos que confirmaron las conclusiones teóricas alcanzadas. Los resultados de esta parte de la tesis se incluyeron en el artículo [1], publicado en la revista *Mathematics and Computers in Simulation*, una revista internacional que pertenece al primer cuartil del *Journal of Citation Reports*.

- Interpolación de Hermite más términos de corrección. Esta técnica (sin términos de corrección) se utiliza clásicamente para reconstruir datos suaves cuando la función y sus derivadas de primer orden están disponibles en ciertos nodos. Si las derivadas de primer orden no están disponibles, es fácil establecer un sistema de ecuaciones imponiendo algunas condiciones de regularidad sobre los nodos. Este proceso conduce a la construcción de un spline de Hermite. El problema del spline de Hermite descrito es que se pierde la precisión si los datos contienen singularidades (nos centraremos fundamentalmente en discontinuidades en la función o en la primera derivada, aunque también analizaremos qué ocurre cuando hay discontinuidades en la segunda derivada). La consecuencia es la aparición de oscilaciones, si hay una discontinuidad abrupta en la función, que afecta globalmente la precisión del spline, o el suavizado de las singularidades, si las discontinuidades están en las derivadas de la función.

Nuestro objetivo en esta parte de la tesis es la construcción y análisis de una nueva técnica que permite el cálculo preciso de derivadas de primer orden de una función cerca de las singularidades utilizando un spline cúbico de Hermite. La idea es corregir el sistema de ecuaciones del spline para alcanzar la precisión deseada incluso cerca de las singularidades. Una vez que hemos calculado las derivadas de primer orden con suficiente precisión, se agrega un término de corrección al spline de Hermite en los intervalos que contienen una singularidad. El objetivo es reconstruir funciones suaves a trozos con precisión $O(h^4)$ incluso cerca de las singularidades. El proceso de adaptación requerirá algún conocimiento sobre la posición del salto, así como del tamaño de los saltos en la función y algunas derivadas en dicha posición. Esta técnica puede usarse como post-proceso, donde agregamos un término de corrección al spline cúbico de Hermite clásico. Durante nuestra investigación, obtuvimos pruebas para la precisión y regularidad del spline corregido y sus derivadas. También analizamos el mecanismo que elimina el fenómeno Gibbs cerca del salto en la función. Además, también realizamos varios experimentos numéricos que confirmaron los resultados teóricos obtenidos. Los resultados de esta parte de la tesis se incluyeron en el artículo [2], publicado en la revista *Journal of Scientific Computing*, una revista internacional que pertenece al primer cuartil del *Journal of Citation Reports*.

- Super resolución. Aunque se presenta en última posición, este tema marcó el comienzo de esta tesis, donde centramos nuestra atención en algoritmos de multiresolución. La super resolución busca mejorar la calidad de imágenes y videos con baja resolución agregando detalles más finos, lo que resulta en una salida más nítida y clara. Esta parte de la tesis es muy breve y solo trata de reflejar el trabajo que se realizó para obtener el D.E.A., ya que poco después centramos nuestra atención en otras líneas de investigación que aparentaban ser algo más prometedoras para la elaboración de esta tesis.

Abstract

In this PhD thesis we have tried to design algorithms capable of dealing with discontinuous data. We have centred our attention in three main applications:

- Numerical integration plus correction terms. In this part of the thesis we constructed and analyzed a new nonlinear technique that allows obtaining accurate numerical integrations of any order using data that contains discontinuities, and when the integrand is only known at grid points. The novelty of the technique consists in the inclusion of correction terms with a closed expression that depends on the size of the jumps of the function and its derivatives at the discontinuities, that are supposed to be known. The addition of these terms allows recovering the accuracy of classical numerical integration formulas close to the discontinuities, as these correction terms account for the error that the classical integration formulas commit up to their accuracy at smooth zones. Thus, the correction terms can be added during the integration or as post-processing, which is useful if the main calculation of the integral has been already done using classical formulas. During our research, we managed to conclude several numerical experiments that confirmed the theoretical conclusions reached. The results of this part of the thesis were included in the article [1] published in the journal *Mathematics and Computers in Simulation*, an international journal that belongs to the first quartile of the *Journal of Citation Reports*.

- Hermite interpolation plus correction terms. This technique (without correction terms) is classically used to reconstruct smooth data when the function and its first order derivatives are available at certain nodes. If first order derivatives are not available, it is easy to set a system of equations imposing some regularity conditions at the data nodes in order to obtain them. This process leads to the construction of a Hermite spline. The problem of the described Hermite splines is that the accuracy is lost if the data contains singularities (we will center our attention on discontinuities in the function or in the first derivative, although we will also analyze what happens when there are discontinuities in the second derivative). The consequence is the appearance of oscillations, if there is a jump discontinuity in the function, that globally affects the accuracy of the spline, or the smearing of singularities, if the discontinuities are in the derivatives of the function.

  Our objective in this part of the thesis is devoted to the construction and analysis of a new technique that allows for the computation of accurate first order derivatives of a function

close to singularities using a cubic Hermite spline. The idea is to correct the system of equations of the spline in order to attain the desired accuracy even close to the singularities. Once we have computed the first order derivatives with enough accuracy, a correction term is added to the Hermite spline in the intervals that contain a singularity. The aim is to reconstruct piecewise smooth functions with $O(h^4)$ accuracy even close to the singularities. The process of adaption will require some knowledge about the position of the singularity and the jumps of the function and some of its derivatives at the singularity. The whole process can be used as a post-processing, where a correction term is added to the classical cubic Hermite spline. During our research, we obtained proofs for the accuracy and regularity of the corrected spline and its derivatives. We also analysed the mechanism that eliminates the Gibbs phenomenon close to jump discontinuities in the function. In addition, we also performed several numerical experiments that confirmed the theoretical results obtained. The results of this part of the thesis were included in the article [2] published in the *Journal of Scientific Computing*, an international journal that belongs to the first quartile of the *Journal of Citation Reports*.

- Super resolution. While it is presented in the last position, this marked the beginning of this thesis, where we focused our attention on multiresolution algorithms. Super resolution seeks to enhance the quality of low-resolution images and videos by adding finer details, resulting in a sharper and clearer output. These algorithms operate by analyzing different levels of image data and combining them to create a higher-resolution version. Applications for these algorithms can be found across industries, including surveillance, medical imaging, and media, to improve visual fidelity. Although the study of super resolution was the starting point of the thesis, we soon shifted our focus to the study of other algorithms in the context of numerical approximation. These alternative approaches proved to be more promising in terms of results that could be published. Nevertheless, this first part of the research served to obtain the D.E.A.

Chapter 1

Introduction

In the context of numerical analysis, the approximation of data exhibiting discontinuities is a challenge, and has lead to an extensive exploration and innovation in the field. This thesis is about the design of some numerical methods that try to handle with such discontinuities. Through the path of our investigation, we have explored two fundamental approaches: classical approximations plus correction terms and multiresolution algorithms. Exploring these techniques, we had the purpose of designing new tools that would allow us to achieve a more accurate approximation of data with abrupt transitions or sharp discontinuities, which are prevalent in various real-world scenarios.

In what follows, we present a brief summary of each part of the research, including the structure of this document.

1.1 Numerical Integration

Classical integration formulas, such as the trapezoidal rule, the Simpson's rule, or the Newton-Cotes formulas, are based on the integration of interpolatory polynomials over an interval. The classical problem that arises from using such interpolatory polynomials is the loss of accuracy whenever the original data does not present enough regularity. In this chapter, we introduce a new method inspired by the *Immersed interface method* (IIM) [3], created as a high-resolution technique for the discretization of elliptic partial differential equations with interfaces. Several references can be found in the literature about the numerical integration of functions with pole discontinuities [4, 5, 6, 7]. The problem of obtaining quadrature rules adapted to the presence of finite discontinuities in this context can also be found in the literature [8, 9], but we have not found many references about the subject. In this chapter, we pretend to obtain adapted integration formulas that manage to take into account the presence of finite discontinuities in the function or the derivatives through the addition of correction terms with closed explicit expressions. To find these correction terms, we need to know the position of the singularities plus the jumps in the function and its derivatives at the discontinuities. We are interested in the cases when the

function that is to be integrated is given as discretised data points that do not coincide with the position of the discontinuity, and we want to use these data in order to recover an approximation of the definite integral of the function in an interval. In this case, the new technique can be used as a post-processing that makes explicit use of the position of the discontinuity and the jumps in the function and its derivatives at the discontinuity. Only with this information, we can compute the correction terms that allow increasing the accuracy close to the discontinuity. Our aim is to show that, through this new technique, it is possible to reach the maximum theoretical accuracy in terms of the length of the stencil. We will present some numerical experiments and one application of the formulas proposed.

This part of the thesis is included in Chapter 2, where the work is organized as follows: Section 2.2 describes how to obtain correction terms for the trapezoid rule and Simpson's rule. Section 2.3 presents a generalization for Newton-Cotes formulas. Section 2.3.1 presents expressions of the correction terms for commonly used Newton-Cotes Formulas. Section 2.4 presents some numerical experiments that endorse the theoretical results. Finally, Section 2.5 presents the conclusions.

1.2 Hermite splines

In the classic literature, we can find that a spline can be constructed defining polynomial pieces that join together under certain regularity or differentiability requirements at these joints. Such regularity properties are the reason why splines are used very often in computer aided geometric design (CAGD) for industrial and professional design applications. Some examples are the representation of geometrical objects in one or several dimensions [10, 11, 12, 13, 14], the solution of PDEs or ODEs [15, 16, 17], image processing [18, 19, 20] and many others.

Sometimes the data used to construct the spline presents singularities. In the cases where the discontinuity is in the function, some kinds of splines are known to introduce oscillations close to the discontinuities [21, 22]. These oscillations classically appear when truncating the Fourier series of a discontinuous function and have been widely studied [23, 24, 25, 26]. Global expansions, such as Fourier series, are affected by the presence of local discontinuities. The usual result is non-uniform convergence and oscillations of the partial sums. D. Gottlieb and C.-W. Shu showed that it is possible to recover high order information from these slowly and non-uniformly convergent global approximations [27, 28, 29, 30, 31]. Some other interesting and related works are [25, 32, 33]. By splitting a function with singularities in two parts, a smooth one and another one containing the information of the singularity, K. S. Eckhoff [34, 35] presented a way of modifying the Fourier's method to obtain numerical techniques that allow us to compute derivatives and integrals with a high order of accuracy.

In this work, our approach is different from all previous techniques, although the philosophy might be similar: to reconstruct piecewise smooth functions from discretized data, taking into account the presence of singularities. In our case, we approach the problem using cubic Hermite splines plus correction terms in order to attain adaption close to the singularities.

Recently, some papers have been published about the modification of cubic splines that aim

to solve the problems caused by the oscillations that appear close to the discontinuities [36, 37]. In those previous papers the authors try to exploit the properties of a nonlinear mean in the construction of the spline, through which we automatically adapt the interpolation to the presence of discontinuities in the function, thus eliminating the Gibbs oscillations. One drawback is that this technique cannot provide full accuracy close to the singularity, and it smears the discontinuities.

This part of the thesis is included in Chapter 3, and is organized as follows. First of all, in Section 3.2 we introduce the classical way of constructing cubic Hermite splines. Section 3.3 explains how to obtain adapted first order derivatives using a Hermite spline. There, we present the first main result of this chapter: a theorem about the accuracy of the adapted first order derivatives. Section 3.4 presents a study about the elimination of the Gibbs phenomenon in the classical spline when using the corrected first order derivatives. Section 3.5 introduces an adapted Hermite spline and analyses theoretically the accuracy of the interpolation near singularities, which is the second main result of this work. Section 3.6 exposes how the correction terms can be used as a post-processing of the classical cubic Hermite spline. Section 3.7 presents some numerical experiments which show how the new algorithm performs using univariate functions. In particular, experiments about the accuracy and regularity of the function and the two first order derivatives are presented, jointly with some tests that show the elimination of the Gibbs phenomenon close to jump discontinuities in the function. Finally, Section 3.8 presents the conclusions.

1.3 Super resolution

Super resolution, in the context of Harten's multiresolution algorithms, represents a powerful concept for enhancing the detail and quality of images or data. Harten's framework provides a very suitable context for processing data at multiple scales, and super resolution uses this framework to improve the resolution of images or data. The key idea is to enhance the level of detail and precision in low-resolution data by incorporating information from other low resolution images or from the interpolation of data at several scales of the multiresolution process. This is achieved through the reconstruction operator, which plays a fundamental role in Harten's framework. By employing data-dependent reconstruction operators, super resolution methods can generate more accurate and detailed representations of the underlying data, especially near singularities or areas with abrupt changes. This enables better adaptability and more precise treatment of fine details in images or data, leading to improved results in applications like image processing, signal analysis, etc.

One of the main advantages of Harten's multiresolution approach in the context of super resolution is its adaptability. Super resolution techniques can be created to fit the specific needs of a given problem or dataset by adjusting the reconstruction operators. This adaptability is particularly valuable when dealing with noisy or low-resolution data, common challenges in various fields. By incorporating information from different resolution levels and using nonlinear prediction schemes, super resolution techniques can effectively mitigate the effects of noise and improve the overall quality of the reconstructed data. The ability to handle data-dependent reconstruction ope-

rators, such as Essentially Non Oscillatory (ENO) techniques, enables more accurate and flexible processing. In our case, we will use different data-dependent algorithm to create super resolution algorithms. This part of the thesis was used to obtain the D.E.A., but was not eventually continued as we found other lines of research that appeared more promising.

1.4 Conclusions and future work

This part of the thesis is included in Chapter 5. In this section we outline the conclusions based on the findings obtained throughout the thesis. Additionally, we show some paths to explore in the future, opening a door for further research and refinement of the ideas and methods introduced in this work.

Chapter 2

Numerical integration rules with improved accuracy close to discontinuities

2.1 Introduction

In this chapter we explore the limitations of classical integration formulas like the trapezoidal and Simpson's rules when dealing with data that lacks regularity. We introduce a novel method inspired by the Immersed Interface Method (IIM), initially designed for solving partial differential equations with interfaces [3]. This new approach aims to adapt integration formulas for functions with finite discontinuities by incorporating correction terms with explicit expressions, knowing the positions of singularities and jumps in the function and its derivatives. The technique becomes particularly interesting when the function is represented as discrete data points that do not align with the location of the discontinuity. We show that the algorithm can also be used as a post-processing, where the knowledge about the discontinuity's position and jumps allows to enhance the accuracy near the points of discontinuity. Along the chapter we show how this technique can allow achieving the highest possible accuracy in terms of the stencil's length. Through numerical experiments, we manage to support the theoretical results obtained.

2.2 Obtainment of adapted numerical integration formulas

We consider the space of finite sequences V and a uniform partition X of the interval $[a, b]$ in J subintervals,

$$X = \{x_i\}_{i=0}^{J}, \quad x_0 = a, \quad h = x_i - x_{i-1}, \quad x_J = b.$$

We will consider a piecewise smooth function f discretized through the point values,

$$f_i = f(x_i), \quad f = \{f_i\}_{i=0}^{J}, \tag{2.1}$$

that, therefore, conserves the information of f only at the x_i nodes. We also assume that discontinuities are placed far enough from each other, that their position is known exactly, and that $x_i \neq x^*$, where x^* denotes the location of the discontinuity. Figures 2.1, 2.2, and 2.3 present the kind of discontinuities that we will be dealing with in this work. We will refer to these figures along the chapter. From these considerations, we can directly proceed to obtain the correction terms and error formulas for these cases. Let us start with the trapezoidal rule.

2.2.1 Error formula for the corrected trapezoid rule

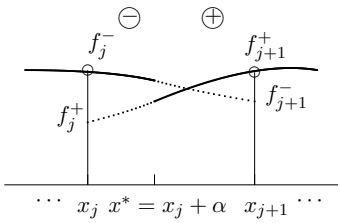

Figure 2.1: An example of a function with discontinuities (solid line) placed at a position x^*. We have labeled the domain to the left of the discontinuity as $-$ and the one to the right as $+$. We have also represented with a dashed line the prolongation of the functions through Taylor expansions at both sides of the discontinuity.

We can consider the situation presented in Figure 2.1. Let us denote by $E(f)$ the error committed by the classical trapezoidal rule and by $E^*(f)$ the error by the corrected rule. The classical trapezoid rule for a uniform grid of mesh-size h and its error [38] at smooth zones reads,

$$\begin{aligned} I(f) &= \frac{h}{2}\left(f_j + f_{j+1}\right), \\ E(f) &= -\frac{h^3}{12} f''(\eta), \quad \eta \in [x_j, x_{j+1}]. \end{aligned} \tag{2.2}$$

The position η appears here due to the use of the integral mean value theorem (see Theorem 1.3, page 4 of [38]). We can see that the expression of the error of the integral is qualitative in the sense that we know that it is $O(h^3)$ if the integrand is smooth, but we do not know the exact value of η. This is a classical result (it can be found, for example, before expression (5.1.4) in page 253 of [8]). The approximation error is of order $O(h^2)$ if there is a jump in the first derivative in the interval $[x_j, x_{j+1}]$ or $O\left(h\right)$ if there is a jump discontinuity in the function. One way of rising the order of accuracy in the previous cases is to use the location of the discontinuity x^*. Let us suppose that x^* is known exactly. In order to obtain the area below the curve in the interval $[x_j, x^*]$ (the area in the interval $[x^*, x_{j+1}]$ can be obtained in a similar way), we can just use the Taylor expansion of the value f_{j+1}^+ around x^* and then change the values from the $+$ side in terms of the $-$ side

using the jump relations. Let us use the notation,

$$\begin{aligned}
[f] &= f^+(x^*) - f^-(x^*), \\
\left[f'\right] &= f_x^+(x^*) - f_x^-(x^*), \\
\left[f''\right] &= f_{xx}^+(x^*) - f_{xx}^-(x^*), \\
\left[f'''\right] &= f_{xxx}^+(x^*) - f_{xxx}^-(x^*), \cdots
\end{aligned} \tag{2.3}$$

for the jumps in the function and its derivatives at x^*. Then, using Taylor expansions at both sides of the discontinuity, the expressions for f_j^-, f_j^+, f_{j+1}^- and f_{j+1}^+ can be written as,

$$\begin{aligned}
f^-(x_j) = f_j^- &= f^-(x^*) - f_x^-(x^*)\alpha + O(h^2), \\
f^+(x_j) = f_j^+ &= f^+(x^*) - f_x^+(x^*)\alpha + O(h^2), \\
f^-(x_{j+1}) = f_{j+1}^- &= f^-(x^*) + f_x^-(x^*)(h-\alpha) + O(h^2), \\
f^+(x_{j+1}) = f_{j+1}^+ &= f^+(x^*) + f_x^+(x^*)(h-\alpha) + O(h^2),
\end{aligned} \tag{2.4}$$

and subtracting we obtain,

$$\begin{aligned}
f_j^+ &= f_j^- + [f] - [f']\alpha + O(h^2), \\
f_{j+1}^+ &= f_{j+1}^- + [f] + [f'](h-\alpha) + O(h^2).
\end{aligned} \tag{2.5}$$

Now, let us try to analyze the error formula for the corrected trapezoid rule. We will use the following lemma, which proof is a classical result and can be found, for example, on page 143 of [38],

Lemma 1 *Let t be a real number, different from the nodes $x_0, x_1, \cdots, x_n$. Being n the degree, the polynomial interpolation error to $f(x)$ at t is $f(t) - p_n(t) = (t-x_0)\cdots(t-x_n)f[x_0, \cdots, x_n, t]$, where $f[x_0, \cdots, x_n, t]$ denotes the $(n+1)$-th order divided difference.*

If we denote by $E_{[a,b]}(f)$ the error of integration in the interval $[a, b]$, now we can state the following theorem:

Theorem 1 *Let $f(x) \in C^2([x_0, x^*] \cup [x^*, x_n])$ except at a point $x^* \in (x_j, x_{j+1})$. We denote the function to the left of x^* by $f^-(x)$ and to the right of x^* as $f^+(x)$. If we know the following jumps in the function and its derivatives at x^* and they are finite, $[f] = f^+(x^*) - f^-(x^*), [f'] = f'^+(x^*) - f'^-(x^*)$, then the subtraction of the correction term,*

$$C = \frac{(-h+2\alpha)}{2}[f] + \frac{\left(h\alpha - \alpha^2\right)}{2}[f'], \tag{2.6}$$

to the trapezoid numerical integration formula in the interval $[x_j, x_{j+1}]$ that contains the discontinuity assures that the error is equal to,

$$E^*(f) + C = E_{[x_j, x^*]}(f) + E_{[x^*, x_{j+1}]}(f) + O(h^4), \tag{2.7}$$

with

$$E_{[x_j,x^*]}(f) = -\frac{1}{12}\left(\alpha^3 f^-_{xx}(\eta^-)\right) + O(h^4),$$

and

$$E_{[x^*,x_{j+1}]}(f) = -\frac{1}{12}\left((h-\alpha)^3 f^+_{xx}(\eta^+)\right) + O(h^4),$$

and $\eta^- \in [x_j, x^*], \eta^+ \in [x^*, x_{j+1}]$.

At the $-$ part of the interval we will denote

$$E(f)_{[x_j,x^*]} = \int_{x_j}^{x_j+\alpha} (f^-(x) - p(x))\, dx,$$

where $p(x)$ is the polynomial of degree 1 taking the values f_j^- and f_{j+1}^+ at the interval endpoints x_j and x_{j+1}, respectively. We write this error using the Lagrange's form of the polynomial and take into account that there is a discontinuity at $x^* = x_j + \alpha$, so we can use the expressions in (3.17),

$$\begin{aligned} p(x) &= \frac{x-x_{j+1}}{x_j - x_{j+1}} f_j^- + \frac{x-x_j}{x_{j+1}-x_j} f_{j+1}^+ \\ &= \frac{x-x_{j+1}}{x_j - x_{j+1}} f_j^- + \frac{x-x_j}{x_{j+1}-x_j} f_{j+1}^- + \frac{x-x_j}{x_{j+1}-x_j}\left([f] + \left[f'\right](h-\alpha) + O(h^2)\right) \\ &= p^-(x) + \frac{x-x_j}{x_{j+1}-x_j}\left([f] + \left[f'\right](h-\alpha) + \frac{[f'']}{2}(h-\alpha)^2 + O(h^3)\right). \end{aligned} \tag{2.8}$$

Then, using (2.8) and denoting by $p^-(x)$ to the piecewise polynomial to the left of the discontinuity, the error can be expressed as,

$$\begin{aligned} E^{*-}(f) &= \int_{x_j}^{x_j+\alpha} (f^-(x) - p^-(x))\, dx = -\frac{1}{12}\alpha^3 f^-_{xx}(\eta^-) \\ &= \int_{x_j}^{x_j+\alpha} (f^-(x) - p(x))\, dx \\ &+ \int_{x_j}^{x_j+\alpha} \frac{x-x_j}{x_{j+1}-x_j}\left([f] + \left[f'\right](h-\alpha) + \frac{[f'']}{2}(h-\alpha)^2\right)\, dx + O(h^4) \\ &= \int_{x_j}^{x_j+\alpha} (f^-(x) - p(x))\, dx + \frac{1}{2h}\left(\alpha^2[f] + \alpha^2(h-\alpha)[f'] + \frac{\alpha^2}{2}(h-\alpha)^2[f'']\right) \\ &+ O(h^4) \\ &= E(f)_{[x_j,x^*]} + C^- + \frac{\alpha^2}{4h}(h-\alpha)^2[f''] + O(h^4), \end{aligned} \tag{2.9}$$

with $\eta^- \in [x_j, x^*]$, where we have used the error for the classical trapezoid rule. So we have that in the interval $[x_j, x^*]$ the error is,

$$E^{*-}(f) = E(f)_{[x_j,x^*]} + C^- + \frac{\alpha^2}{4h}(h-\alpha)^2[f''] + O(h^4) = -\frac{1}{12}\alpha^3 f^-_{xx}(\eta^-), \tag{2.10}$$

with $\eta^- \in [x_j, x^*]$,

$$C^- = \frac{\alpha^2}{2h}[f] + \frac{\alpha^2(h-\alpha)}{2h}[f'].$$

Replicating the process for the interval $[x^*, x_{j+1}]$, but this time expressing the quantities from the $-$ side in terms of the $+$ side (or just by symmetry), we obtain that,

$$E^{*+}(f) = E(f)_{[x^*,x_{j+1}]} + C^+ - \frac{\alpha^2}{4h}(h-\alpha)^2[f''] + O(h^4) = -\frac{1}{12}(h-\alpha)^3 f^+_{xx}(\eta^+), \tag{2.11}$$

with $\eta^+ \in [x^*, x_{j+1}]$,

$$C^+ = -\left(\frac{(h-\alpha)^2}{2h}[f] - \frac{(h-\alpha)^2\alpha}{2h}[f']\right).$$

Adding the errors obtained in both intervals, as expressed in (2.10) and (2.11), it is easy to check that the terms of the error that are $O(h^3)$ disappear and we get,

$$\begin{aligned} E^*(f) &= E^{*-}(f) + E^{*+}(f) = E(f)_{[x^*,x_{j+1}]} + C^- + E(f)_{[x_j,x^*]} + C^+ \\ &= E(f)_{[x^*,x_{j+1}]} + E(f)_{[x_j,x^*]} + C + O(h^4), \end{aligned}$$

where,

$$C = C^+ + C^- = \frac{(-h+2\alpha)}{2}[f] + \frac{\left(h\alpha - \alpha^2\right)}{2}[f'],$$

that allows us finishing the proof.

2.2.2 Correction terms and error formula for the corrected Simpson's $\frac{1}{3}$ rule

In this section we will proceed to analyze how to adapt Simpon's rule following the same process that we used to adapt the trapezoidal rule in the previous Subsection. Simpson's rule is obtained by integrating a parabola in the corresponding interval. In this case we need to enlarge the stencil and we will need to use the three data values (f_{j-1}, f_j, f_{j+1}), placed at the positions (x_{j-1}, x_j, x_{j+1}) in order to build the parabola. In this occasion we must consider two cases: when the discontinuity is in the interval $[x_{j-1}, x_j]$ or in the interval $[x_j, x_{j+1}]$, as shown in the plots of Figure 2.2. The classical Simpson's $\frac{1}{3}$ rule for a uniform grid of mesh-size h and its error [38] at smooth zones reads,

$$\begin{aligned} I(f) &= \frac{h}{3}\left(f_j + 4f_{j+1} + f_{j+2}\right), \\ E(f) &= -\frac{h^5}{90}f^{(4)}(\eta), \quad \eta \in [x_j, x_{j+2}]. \end{aligned} \tag{2.12}$$

Now we can state the following theorem.

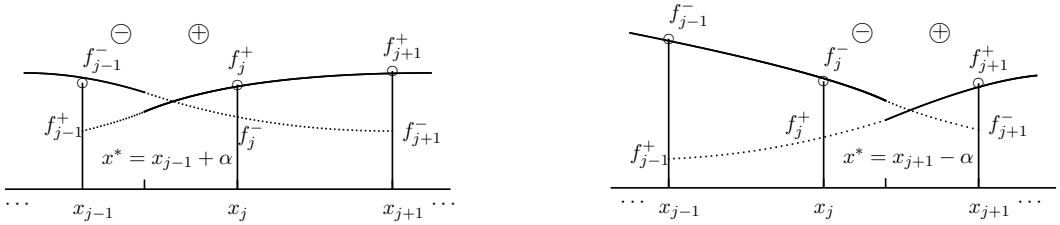

Figure 2.2: Two examples of functions with discontinuities (solid line) placed in different intervals at a position x^*. We have labeled the domain to the left of the discontinuity as $-$ and the one to the right as $+$. We have also represented with a dashed line the prolongation of the functions through Taylor expansions at both sides of the discontinuity.

Theorem 2 *Let $f(x) \in C^3([x_0, x^*] \cup [x^*, x_n])$ except at a point $x^* \in (x_j, x_{j+1})$. We denote the function to the left of x^* by $f^-(x)$ and to the right of x^* as $f^+(x)$. If we know the following jumps in the function and its derivatives at x^* and they are finite, $[f] = f^+(x^*) - f^-(x^*), [f'] = f'^+(x^*) - f'^-(x^*), [f''] = f''^+(x^*) - f''^-(x^*)$, then the subtraction of the correction term,*

$$C = \gamma \left(\alpha - \frac{h}{3}\right) [f] + \frac{\alpha}{6} (3\alpha - 2h) [f'] + \gamma \frac{\alpha^2}{6} (\alpha - h) [f''], \tag{2.13}$$

to the Simpson's numerical integration formula, with $\gamma = 1$, if the discontinuity is placed at an odd interval, and $\gamma = -1$, if the discontinuity is placed at an even interval, assures that the error is equal to,

$$\begin{aligned} E(f) + C = {} & \frac{\alpha^2}{36} \left(3\alpha^2 + 6h^2 - 8h\alpha\right) [f'''] + \frac{f^+_{xxx}(\eta_2)}{6} \left(-\frac{\alpha^4}{4} + \frac{h^2\alpha^2}{2}\right) \\ & + \frac{f^-_{xxx}(\eta_3)}{24} \left(\frac{\alpha^4}{4} - h\alpha^3 + h^2\alpha^2\right) + O(h^5). \end{aligned} \tag{2.14}$$

If the discontinuity falls at an odd interval, then $\eta_2 \in [x_{j+1} - \alpha, x_{j+1}], \eta_3 \in [x_{j-1}, x_{j-1} + \alpha]$. If the discontinuity falls at an even interval, the case is symmetric and $\eta_2 \in [x_{j-1}, x_{j-1} + \alpha], \eta_3 \in [x_{j+1} - \alpha, x_{j+1}]$.

- We start by the case when the discontinuity is placed in the interval $[x_{j-1}, x_j]$.

  1. As in the trapezoidal rule, we know that for the $+$ part of the integral,

  $$E^{*+}(f) = \int_{x_{j-1}+\alpha}^{x_{j+1}} (f^+(x) - p^+(x))\, dx.$$

  The interpolating polynomial $p(x)$ in the Lagrange form is,

  $$\begin{aligned} p(x) = {} & \frac{(x - x_j)(x - x_{j+1})}{(x_{j-1} - x_j)(x_{j-1} - x_{j+1})} f^-_{j-1} + \frac{(x - x_{j-1})(x - x_{j+1})}{(x_j - x_{j-1})(x_j - x_{j+1})} f^+_j \\ & + \frac{(x - x_{j-1})(x - x_j)}{(x_{j+1} - x_{j-1})(x_{j+1} - x_j)} f^+_{j+1}. \end{aligned} \tag{2.15}$$

Proceeding in the same way as we did in (3.17) for the trapezoid rule, we can use the expression of f_{j-1}^{-} in terms of the quantities from the + side to write,

$$f_{j-1}^{-} = f_{j-1}^{+} - [f] + [f']\alpha - [f'']\frac{\alpha^2}{2} + [f''']\frac{\alpha^3}{6} + O(h^4). \tag{2.16}$$

Now we can write,

$$\begin{aligned} p(x) &= \frac{(x-x_j)(x-x_{j+1})}{(x_{j-1}-x_j)(x_{j-1}-x_{j+1})}\left(f_{j-1}^{+} - [f] + [f']\alpha - [f'']\frac{\alpha^2}{2} + [f''']\frac{\alpha^3}{6}\right) \\ &+ \frac{(x-x_{j-1})(x-x_{j+1})}{(x_j-x_{j-1})(x_j-x_{j+1})}f_j^{+} + \frac{(x-x_{j-1})(x-x_j)}{(x_{j+1}-x_{j-1})(x_{j+1}-x_j)}f_{j+1}^{+} \\ &= p^{+}(x) + \frac{(x-x_j)(x-x_{j+1})}{(x_{j-1}-x_j)(x_{j-1}-x_{j+1})}\left(-[f] + [f']\alpha - [f'']\frac{\alpha^2}{2} + [f''']\frac{\alpha^3}{6}\right) \\ &+ O(h^4). \end{aligned} \tag{2.17}$$

Then, the error for the integral at the + side in the interval $[x^*, x_{j+1}]$, as shown in Figure 2.1 to the left, can be expressed as,

$$\begin{aligned} E^{*+}(f) &= \int_{x_{j-1}+\alpha}^{x_{j+1}} (f^{+}(x) - p^{+}(x))\, dx = \int_{x_{j-1}+\alpha}^{x_{j+1}} (f^{+}(x) - p(x))\, dx \\ &+ \int_{x_{j-1}+\alpha}^{x_{j+1}} \frac{(x-x_j)(x-x_{j+1})}{(x_{j-1}-x_j)(x_{j-1}-x_{j+1})}\left(-[f] + [f']\alpha - [f'']\frac{\alpha^2}{2} + [f''']\frac{\alpha^3}{6}\right)\, dx + O(h^5) \\ &= E(f)_{[x^*,x_{j+1}]} \\ &- \frac{1}{72}\frac{-\left(6\,[f] - 6\,\alpha\,[f'] + 3\,\alpha^2[f''] - \alpha^3[f''']\right)\left(-4\,h^3 + 2\,\alpha^3 - 9\,h\alpha^2 + 12\,h^2\alpha\right)}{h^2} + O(h^5) \\ &= E(f)_{[x^*,x_{j+1}]} + C^{+} + O(h^5), \end{aligned} \tag{2.18}$$

and we also have that,

$$E^{*+}(f) = \int_{x_{j-1}+\alpha}^{x_{j+1}} (x-x_{j-1})(x-x_j)(x-x_{j+1})f^{+}[x_{j-1}, x_j, x_{j+1}, x]\, dx. \tag{2.19}$$

The polynomial in the integrand of (2.19) changes the sign in the interval $(x_{j-1} + \alpha, x_{j+1})$. Thus, we can not use the integral mean value theorem. Instead, we can define the function

$$w(x) = \int_{x_{j-1}+\alpha}^{x} (x-x_{j-1})(x-x_j)(x-x_{j+1})\, dx,$$

that satisfies, $w(x_{j-1}+\alpha) = 0$, and $w(x) > 0$ for $x \in (x_{j-1}+\alpha, x_{j+1}-\alpha)$ and $w(x) < 0$ for $x \in (x_{j+1}-\alpha, x_{j+1})$. Then, we can divide the integral in two parts,

$$\begin{aligned} E^{*+}(f) &= \int_{x_{j-1}+\alpha}^{x_{j+1}} w'(x)f^{+}[x_{j-1}, x_j, x_{j+1}, x]\, dx \\ &= \int_{x_{j-1}+\alpha}^{x_{j+1}-\alpha} w'(x)f^{+}[x_{j-1}, x_j, x_{j+1}, x]\, dx \\ &+ \int_{x_{j+1}-\alpha}^{x_{j+1}} w'(x)f^{+}[x_{j-1}, x_j, x_{j+1}, x]\, dx. \end{aligned} \tag{2.20}$$

Integrating by parts the first integral,

$$\int_{x_{j-1}+\alpha}^{x_{j+1}-\alpha} w'(x) f^+[x_{j-1}, x_j, x_{j+1}, x]\ dx = \left[w(x) f^+[x_{j-1}, x_j, x_{j+1}, x]\right]_{x_{j-1}+\alpha}^{x_{j+1}-\alpha}$$
$$- \int_{x_{j-1}+\alpha}^{x_{j+1}-\alpha} w(x) \frac{d}{dx} f^+[x_{j-1}, x_j, x_{j+1}, x]\ dx.$$

Using now that $w(x_{j+1}-\alpha) = 0$, due to the symmetry of the polynomial that appears in the integrand of $w(x)$ in a uniform grid, that (see 3.2.17 page 147 of Atkinson [38])

$$\frac{d}{dx} f^+[x_{j-1}, x_j, x_{j+1}, x] = f^+[x_{j-1}, x_j, x_{j+1}, x, x], \tag{2.21}$$

and the integral mean value theorem, we get,

$$\begin{aligned}
&- \int_{x_{j-1}+\alpha}^{x_{j+1}-\alpha} w(x) f^+[x_{j-1}, x_j, x_{j+1}, x, x]\ dx = \\
&- f^+[x_{j-1}, x_j, x_{j+1}, \xi_1, \xi_1] \int_{x_{j-1}+\alpha}^{x_{j+1}-\alpha} w(x)\ dx = \\
&f^+[x_{j-1}, x_j, x_{j+1}, \xi_1, \xi_1] \left(-\frac{1}{5}(2\alpha^5) + 2\alpha^4 h - \frac{1}{3}(10\alpha^3 h^2) + 2\alpha^2 h^3 - \frac{1}{15}(4h^5) \right) \\
&= \frac{f^+_{xxxx}(\eta_1)}{24} O\left(h^5\right),
\end{aligned} \tag{2.22}$$

for some $\xi_1, \eta_1 \in [x_{j-1}+\alpha, x_{j+1}-\alpha]$. For the second integral in (2.20), $w'(x)$ does not change the sign in $[x_{j+1}-\alpha, x_{j+1}]$ so we can apply the integral mean value theorem,

$$\begin{aligned}
\int_{x_{j+1}-\alpha}^{x_{j+1}} w'(x) f^+[x_{j-1}, x_j, x_{j+1}, x]\ dx &= f^+[x_{j-1}, x_j, x_{j+1}, \xi_2] \int_{x_{j+1}-\alpha}^{x_{j+1}} w'(x)\ dx \\
&= \frac{f^+_{xxx}(\eta_2)}{6} \left(-\frac{\alpha^4}{4} + \frac{h^2\alpha^2}{2} \right),
\end{aligned}$$

for some $\xi_2, \eta_2 \in [x_{j+1}-\alpha, x_{j+1}]$. Thus,

$$\int_{x_{j-1}+\alpha}^{x_{j+1}} w'(x) f^+[x_{j-1}, x_j, x_{j+1}, x]\ dx = \frac{f^+_{xxxx}(\eta_1)}{24} O(h^5) + \frac{f^+_{xxx}(\eta_2)}{6} \left(-\frac{\alpha^4}{4} + \frac{h^2\alpha^2}{2} \right).$$

So, from (2.18) we get that the corrected error for the integral in the + side of the left plot of Figure 2.2 is,

$$E(f)_{[x^*, x_{j+1}]} + C^+ + O(h^5) = E^{*+}(f) = \frac{f^+_{xxxx}(\eta_1)}{24} O(h^5) + \frac{f^+_{xxx}(\eta_2)}{6} \left(-\frac{\alpha^4}{4} + \frac{h^2\alpha^2}{2} \right), \tag{2.23}$$

with $\xi_2, \eta_2 \in [x_{j+1}-\alpha, x_{j+1}]$ and $\xi_1, \eta_1 \in [x_{j-1}+\alpha, x_{j+1}-\alpha]$.

2. For the integral in the $-$ side of the left plot of Figure 2.2, we want to obtain the error

$$E^{*-}(f) = \int_{x_{j-1}}^{x_{j-1}+\alpha} (f^-(x) - p^-(x))\, dx.$$

From (2.15) we can express the quantities from the $+$ side in terms of the $-$ side using the jump conditions in (3.16), as we did before,

$$\begin{aligned}
p(x) &= \frac{(x-x_j)(x-x_{j+1})}{(x_{j-1}-x_j)(x_{j-1}-x_{j+1})} f^-_{j-1} \\
&+ \frac{(x-x_{j-1})(x-x_{j+1})}{(x_j-x_{j-1})(x_j-x_{j+1})} \left(f^-_j + [f] + [f'](h-\alpha) + [f'']\frac{(h-\alpha)^2}{2} + [f''']\frac{(h-\alpha)^3}{6} \right) \\
&+ \frac{(x-x_{j-1})(x-x_j)}{(x_{j+1}-x_{j-1})(x_{j+1}-x_j)} \left(f^-_{j+1} + [f] + [f'](h+\alpha) + [f'']\frac{(h+\alpha)^2}{2} + [f''']\frac{(h+\alpha)^3}{6} \right) + O(h^4) \\
&= p^-(x) + \frac{(x-x_{j-1})(x-x_{j+1})}{(x_j-x_{j-1})(x_j-x_{j+1})} \left([f] + [f'](h-\alpha) + [f'']\frac{(h-\alpha)^2}{2} + [f''']\frac{(h-\alpha)^3}{6} \right) \\
&+ \frac{(x-x_{j-1})(x-x_j)}{(x_{j+1}-x_{j-1})(x_{j+1}-x_j)} \left([f] + [f'](h+\alpha) + [f'']\frac{(h+\alpha)^2}{2} + [f''']\frac{(h+\alpha)^3}{6} \right) + O(h^4).
\end{aligned} \tag{2.24}$$

Now, the error for the integral on the $-$ side, as shown in Figure 2.2 to the left, can be expressed as,

$$\begin{aligned}
E^-(f) &= \int_{x_{j-1}}^{x_{j-1}+\alpha} (f^-(x) - p^-(x))\, dx = \int_{x_{j-1}}^{x_{j-1}+\alpha} (f^-(x) - p(x))\, dx \\
&+ \int_{x_{j-1}}^{x_{j-1}+\alpha} \frac{(x-x_{j-1})(x-x_{j+1})}{(x_j-x_{j-1})(x_j-x_{j+1})} \left([f] + [f'](h-\alpha) + [f'']\frac{(h-\alpha)^2}{2} + [f''']\frac{(h-\alpha)^3}{6} \right) dx \\
&+ \int_{x_{j-1}}^{x_{j-1}+\alpha} \frac{(x-x_{j-1})(x-x_j)}{(x_{j+1}-x_{j-1})(x_{j+1}-x_j)} \left([f] + [f'](2h-\alpha) + [f'']\frac{(2h-\alpha)^2}{2} + [f''']\frac{(2h-\alpha)^3}{6} \right) dx + O(h^5) \\
&= E(f) - \frac{1}{72} \left(\frac{\alpha^2 \left(-54\,h + 12\,\alpha\right)[f]}{h^2} + \frac{\alpha^2 \left(54\,h\alpha - 12\,\alpha^2 - 36\,h^2\right)[f']}{h^2} + \frac{\alpha^2 \left(6\,\alpha^3 + 24\,h^2\alpha - 27\,h\alpha^2\right)[f'']}{h^2} \right. \\
&+ \left. \frac{\alpha^2 \left(-2\,\alpha^4 + 9\,h\alpha^3 - 12\,h^3\alpha - 6\,h^2\alpha^2 + 12\,h^4\right)[f''']}{h^2} \right) + O(h^5) \\
&= E(f)_{(x_{j-1},x^*)} + C^- + O(h^5) = \int_{x_{j-1}}^{x_{j-1}+\alpha} (x-x_{j-1})(x-x_j)(x-x_{j+1}) f^-[x_{j-1}, x_j, x_{j+1}, x]\, dx.
\end{aligned} \tag{2.25}$$

It is not difficult to see that the polynomial in the integrand does not change the sign in the interval $(x_{j-1}, x_{j-1}+\alpha)$. Thus, using the integral mean value theorem

$$\begin{aligned}
E^{*-}(f) &= \int_{x_{j-1}}^{x_{j-1}+\alpha} (x-x_{j-1})(x-x_j)(x-x_{j+1}) f^-[x_{j-1}, x_j, x_{j+1}, x]\, dx \\
&= f^-[x_{j-1}, x_j, x_{j+1}, \xi_3] \int_{x_{j-1}}^{x_{j-1}+\alpha} (x-x_{j-1})(x-x_j)(x-x_{j+1})\, dx \\
&= \frac{f^-_{xxx}(\eta_3)}{24} \left(\frac{\alpha^4}{4} - h\alpha^3 + h^2\alpha^2 \right),
\end{aligned} \tag{2.26}$$

for some $\xi_3, \eta_3 \in [x_{j-1}, x_{j-1}+\alpha]$. So, from (2.25) we get that the corrected error for the left part of the integral is,

$$E(f)_{(x_{j-1},x^*)} + C^- + O(h^5) = E^{*-}(f) = \frac{f^-_{xxx}(\eta_3)}{24}\left(\frac{\alpha^4}{4} - h\alpha^3 + h^2\alpha^2\right), \tag{2.27}$$

for some $\xi_3, \eta_3 \in [x_{j+1}-\alpha, x_{j+1}]$.

Adding the error terms C^+ and C^- obtained in (2.18) and (2.25), we obtain

$$C^+ + C^- = -\left(-\left(\alpha - \frac{h}{3}\right)[f] + \frac{\alpha}{6}(3\alpha - 2h)[f'] - \frac{\alpha^2}{6}(\alpha - h)[f''] + \frac{\alpha^2}{36}\left(3\alpha^2 + 6h^2 - 8h\alpha\right)[f'']\right). \tag{2.28}$$

Let us denote the terms up to $O(h^3)$ by,

$$C = -\left(-\left(\alpha - \frac{h}{3}\right)[f] + \frac{\alpha}{6}(3\alpha - 2h)[f'] - \frac{\alpha^2}{6}(\alpha - h)[f'']\right). \tag{2.29}$$

Adding now the errors in the intervals $[x^*, x_{j+1}]$ and $[x_{j-1}, x^*]$ as expressed respectively in (2.23) and (2.27), and denoting again

$$E(f) = E(f)_{[x_{j-1},x^*]} + E(f)_{[x^*,x_{j+1}]},$$

we obtain from (2.29) and (2.28),

$$\begin{aligned} E^*(f) = E^{*+}(f) + E^{*-}(f) = E(f) + C + O(h^5) = \frac{\alpha^2}{36}\left(3\alpha^2 + 6h^2 - 8h\alpha\right)[f''] + \frac{f^+_{xxx}(\eta_2)}{6}\left(-\frac{\alpha^4}{4} + \frac{h^2\alpha^2}{2}\right) \\ + \frac{f^-_{xxx}(\eta_3)}{24}\left(\frac{\alpha^4}{4} - h\alpha^3 + h^2\alpha^2\right), \end{aligned} \tag{2.30}$$

with $\eta_2 \in [x_{j+1}-\alpha, x_{j+1}], \eta_3 \in [x_{j-1}, x_{j-1}+\alpha]$.

- If the discontinuity is placed in the interval (x_j, x_{j+1}) at a distance α from x_{j+1}, that is the case presented in Figure 2.2 to the right, the case is symmetrical and the correction term is:

$$C = -\left(\left(\alpha - \frac{h}{3}\right)[f] + \frac{\alpha}{6}(3\alpha - 2h)[f'] + \frac{\alpha^2}{6}(\alpha - h)[f'']\right).$$

In this case the error reads,

$$\begin{aligned} E^*(f) = E(f) + C + O(h^5) = \frac{\alpha^2}{36}\left(3\alpha^2 + 6h^2 - 8h\alpha\right)[f''] + \frac{f^+_{xxx}(\eta_2)}{6}\left(-\frac{\alpha^4}{4} + \frac{h^2\alpha^2}{2}\right) \\ + \frac{f^-_{xxx}(\eta_3)}{24}\left(\frac{\alpha^4}{4} - h\alpha^3 + h^2\alpha^2\right), \end{aligned} \tag{2.31}$$

with $\eta_2 \in [x_{j-1}, x_{j-1}+\alpha], \eta_3 \in [x_{j+1}-\alpha, x_{j+1}]$.

Remark 1 *Theorems 1 and 2 imply that we can use the classical composite trapezoidal rule or the composite Simpson's rule to obtain the integral over a large interval and, then, add the corresponding correction terms (2.6) or (2.13) to obtain $O(h^2)$ or $O(h^4)$ global accuracy respectively, if discontinuities are present in the data. Mind that the correction terms are typically added to take into account the effect of the set of discontinuities, which cardinal is usually small (one dimension lower) compared with the number of points in the data. Thus, it is enough if the correction terms provide the order of the global error of the classical composite integration rule. The integral can be obtained through classical quadrature rules and then add the corrections as post-processing.*

2.3 Modified Newton-Cotes integration formulas

The Trapezoidal rule and the Simpson's $\frac{1}{3}$ formula, which we have analyzed in previous sections, are the first two cases of Newton-Cotes integration formulas. In what follows, we will try to obtain expressions for the errors of corrected integration formulas of any order. To do so, we present some previous lemmas that we will use afterward in the proofs.

Lemma 2 *Let $f(x) \in C^{n+1}([a,\, x^*] \cup [x^*,\, b])$ except at a point $x^* \in (a, b)$. We denote the function to the left of x^* by $f^-(x)$ and to the right of x^* as $f^+(x)$. If we know the following jumps in the function and its derivatives at x^* and they are finite, $[f] = f^+(x^*) - f^-(x^*), [f'] = f'^+(x^*) - f'^-(x^*), \cdots, [f^{(n)}] = f^{(n)+}(x^*) - f^{(n)-}(x^*)$, then at any node x_i we can express any value of $f^+(x_i)$ in terms of the jumps and the continuous extension of the function from the other side of the discontinuity (see for example, Figures 2.1, 2.2, 2.3), that is:*

$$f_i^+ = f_i^- + [f] + [f'](x_i - x^*) + \frac{1}{2}[f''](x_i - x^*)^2 + \cdots + \frac{1}{n!}[f^{(n)}](x_i - x^*)^n + O(h^{n+1}). \quad (2.32)$$

Isolating, we can obtain f_i^- in terms of f_i^+.

The proof is direct using Taylor expansions.

We denote by $\lfloor x \rfloor$ greatest integer less than or equal to x and $\lceil x \rceil$ the least integer greater than or equal to x.

Lemma 3 *We consider an interpolating polynomial of degree n in the Lagrange form in the interval $[a, b]$, constructed using $n+1$ points belonging to a piecewise continuous function that contains a discontinuity at $x^* \in (a, b)$ and that is n times piecewise continuously differentiable. We follow the same notation as before and denote the information to the left of the discontinuity with the $-$ symbol and to the right with the $+$ symbol. Then in the interval of interest $[a, b]$:*

- *We can express this polynomial as a continuous extension in the $-$ region of the polynomial at the $+$ region, plus additional terms as,*

$$p_n(x) = \sum_{i=0}^{n+1} f^+(x_i) \prod_{j=0, j\neq i}^{j=n+1} \frac{x - x_j}{x_i - x_j} + Q^-(x) = p_n^+(x) + Q^-(x). \quad (2.33)$$

If we denote by,

$$\tilde{f}_i = [f] + [f'](x_i - x^*) + \frac{1}{2}[f''](x_i - x^*)^2 + \cdots + \frac{1}{n!}[f^{(n)}](x_i - x^*)^n + O(h^{n+1}), \tag{2.34}$$

then $Q^-(x)$ contains all the information of the discontinuity and takes the expression,

$$Q^-(x) = \sum_{i=0}^{\lfloor \frac{x^*-a}{h} \rfloor} \tilde{f}_i \prod_{j=0, j\neq i}^{j=n+1} \frac{x - x_j}{x_i - x_j}, \tag{2.35}$$

- *We can express this polynomial as a continuous extension in the + region of the polynomial at the − region, plus additional terms as,*

$$p_n(x) = \sum_{i=0}^{n+1} f^-(x_i) \prod_{j=0, j\neq i}^{j=n+1} \frac{x - x_j}{x_i - x_j} + Q^+(x) = p_n^+(x) + Q^+(x).$$

In this case $Q^+(x)$ takes the expression,

$$Q^+(x) = \sum_{i=\lceil \frac{x^*-a}{h} \rceil}^{n+1} \tilde{f}_i \prod_{j=0, j\neq i}^{j=n+1} \frac{x - x_j}{x_i - x_j},$$

The proof is direct using Lemma 6 and replacing f_i in the Lagrange form of the polynomial

$$p_n(x) = \sum_{i=0}^{n+1} f_i \prod_{j=0, j\neq i}^{j=n+1} \frac{x - x_j}{x_i - x_j},$$

by the values f_i^+ or f_i^- provided in (2.32), depending of f_i belonging to the + or − side.

Lemma 4 *We consider the integral of the polynomial interpolation error from Lemma 5 in the smooth interval $[x_0, x^*]$,*

$$E_n = \int_{x_0}^{x^*} (f(x) - p_n(x))\ dx = \int_{x_0}^{x^*} (x - x_0) \cdots (x - x_n) f[x_0, \cdots, x_n, x]\ dx.$$

- *If there is not a change of sign in the polynomial of the integrand in the interval $[x_0, x^*]$, the error can be written as,*

$$E_n = \frac{f^{(n+1)}(\xi)}{(n+1)!} h^{n+2} \int_0^{\frac{x^*-x_0}{h}} \mu(\mu - 1) \cdots (\mu - n + 1)(\mu - n)\ d\mu \tag{2.36}$$

for some $\xi \in [x_0, x_n]$.

- *If there is a change of sign in the polynomial of the integrand in the interval $[x_0, x^*]$, the error can be written as,*

$$E_n = \int_{x_0}^{x^*} (f(x) - p_n(x))\ dx = \frac{f^{(n+1)}(\xi_1)}{(n+1)!} h^{n+2} \int_0^{\frac{x^*-x_0}{h}} \mu(\mu-1)\cdots(\mu-n+1)(\mu-n)\ d\mu$$
$$+ \frac{f^{(n+2)}(\xi_2)}{(n+2)!} h^{n+3} \int_0^{\frac{x^*-x_0}{h}} \mu(\mu-1)\cdots(\mu-n+1)(\mu-n)(\mu-\frac{x^*-x_0}{h})\ d\mu. \tag{2.37}$$

for some $\xi_1, \xi_2 \in [x_0, x_n]$.

First, if there is not a change of sign in the polynomial of the integrand in the smooth interval $[x_0, x^*]$, we can directly use the integral mean value theorem and the fact that,

$$f[x_0, \cdots, x_n] = \frac{f^{(n)}(\xi)}{n!} \quad \text{for some } \xi \in [x_0, \cdots, x_n], \tag{2.38}$$

to write,

$$E_n = \int_{x_0}^{x^*} (f(x) - p_n(x))\ dx = \int_{x_0}^{x^*} (x-x_0)\cdots(x-x_n) f[x_0, \cdots, x_n, x]\ dx$$
$$= \frac{f^{(n+1)}(\xi)}{(n+1)!} \int_{x_0}^{x^*} (x-x_0)\cdots(x-x_n)\ dx.$$

for some $\xi \in [x_0, x_n]$. Applying the change of variables $x = x_0 + \mu h, 0 \le \mu \le n$, we can write,

$$E_n = \frac{f^{(n+1)}(\xi)}{(n+1)!} \int_{x_0}^{x^*} (x-x_0)\cdots(x-x_n)\ dt$$
$$= \frac{f^{(n+1)}(\xi)}{(n+1)!} h^{n+2} \int_0^{\frac{x^*-x_0}{h}} \mu(\mu-1)\cdots(\mu-n+1)(\mu-n)\ d\mu.$$

Secondly, If there is a change of sign in the polynomial of the integrand in the smooth interval $[x_0, x^*]$, we can define

$$w(y, x) = \int_y^x (t-x_0)\cdots(t-x_n)\ dt, \tag{2.39}$$

that satisfies that, at smooth zones,

$$w(x_0, x_0) = w(x_0, x_n) = 0, \quad w(x_0, x) > 0 \quad \text{for } x_0 < x < x_n,$$

when n is even, and

$$w(x_0, x_0) = 0, \quad w(x_0, x) < 0 \quad \text{for } x_0 < x < x_n,$$

when n is odd. In [39] (page 309) there is a complete proof of these facts.

Now, we can write,

$$E_n = \int_{x_0}^{x^*} w'(x_0, x) f[x_0, \cdots, x_n, x] \; dx. \tag{2.40}$$

Integrating by parts and using that $w(x_0, x_0) = 0$,

$$\begin{aligned} \int_{x_0}^{x^*} w'(x_0, x) f[x_0, \cdots, x_n, x] \; dx &= [w(x_0, x) f[x_0, \cdots, x_n, x]]_{x_0}^{x^*} - \int_{x_0}^{x^*} w(x_0, x) \frac{d}{dx} f[x_0, \cdots, x_n, x] \; dx \\ &= w(x_0, x^*) f[x_0, \cdots, x_n, x^*] - \int_{x_0}^{x^*} w(x_0, x) \frac{d}{dx} f[x_0, \cdots, x_n, x] \; dx. \end{aligned} \tag{2.41}$$

Using now (2.38), we can write,

$$w(x_0, x^*) f[x_0, \cdots, x_n, x^*] = \frac{f^{(n+1)}(\xi_1)}{(n+1)!} w(x_0, x^*) = \frac{f^{(n+1)}(\xi_1)}{(n+1)!} \int_{x_0}^{x^*} (t - x_0) \cdots (t - x_n) \; dt.$$

for some $\xi_1 \in [x_0, x^*]$. Applying again the change of variables $t = x_0 + \mu h, 0 \leq \mu \leq n$, we can write,

$$\int_{x_0}^{x^*} (t - x_0) \cdots (t - x_n) \; dt = h^{n+2} \int_0^{\frac{x^* - x_0}{h}} \mu(\mu - 1) \cdots (\mu - n + 1)(\mu - n) \; d\mu.$$

Thus, we have that,

$$w(x_0, x^*) f[x_0, \cdots, x_n, x^*] = \frac{f^{(n+1)}(\xi_1)}{(n+1)!} h^{n+2} \int_0^{\frac{x^* - x_0}{h}} \mu(\mu - 1) \cdots (\mu - n + 1)(\mu - n) \; d\mu, \tag{2.42}$$

for some $\xi_1 \in [x_0, x_n]$.

For the last integral in (2.41) we can use the fact that (see 3.2.17 page 147 of Atkinson [38])

$$\frac{d}{dx} f[x_0, \cdots, x_n, x] = f[x_0, \cdots, x_n, x, x], \tag{2.43}$$

the integral mean value theorem, and (2.38) to write

$$\begin{aligned} -\int_{x_0}^{x^*} w(x_0, x) \frac{d}{dx} f[x_0, \cdots, x_n, x] \; dx &= -\int_{x_0}^{x^*} w(x_0, x) f[x_0, \cdots, x_n, x, x] \; dx \\ &= -f[x_0, \cdots, x_n, \eta_2, \eta_2] \int_{x_0}^{x^*} w(x_0, x) \; dx \\ &= -\frac{f^{(n+2)}(\xi_2)}{(n+2)!} \int_{x_0}^{x^*} \int_{x_0}^{x} (t - x_0) \cdots (t - x_n) \; dt dx, \end{aligned}$$

for some $\eta_2, \xi_2 \in [x_0, x_n]$. Now we can change the order of integration and apply the change of variables $t = x_0 + \mu h, 0 \leq \mu \leq n$:

$$\begin{aligned}\int_{x_0}^{x^*} \int_{x^*}^{x} (t-x_0)\cdots(t-x_n)\ dtdx &= \int_{x_0}^{x^*} \int_{t}^{x^*} (t-x_0)\cdots(t-x_n)\ dxdt \\ &= \int_{x_0}^{x^*} (t-x_0)\cdots(t-x_n)(d-t)\ dt \\ &= -h^{n+3} \int_0^{\frac{x^*-x_0}{h}} \mu(\mu-1)\cdots(\mu-n+1)(\mu-n)(\mu-\frac{x^*-x_0}{h})\ d\mu.\end{aligned} \tag{2.44}$$

Thus, we can write that

$$\begin{aligned}&-\int_{x_0}^{x^*} w(x_0,x)\frac{d}{dx} f[x_0,\cdots,x_n,x]\ dx \\ &= \frac{f^{(n+2)}(\xi_2)}{(n+2)!} h^{n+3} \int_0^{\frac{x^*-x_0}{h}} \mu(\mu-1)\cdots(\mu-n+1)(\mu-n)(\mu-\frac{x^*-x_0}{h})\ d\mu.\end{aligned} \tag{2.45}$$

Joining the partial results in (2.45) and (2.42), we finish the proof,

$$\begin{aligned}E_n &= \int_{x_0}^{x^*} (f(x)-p_n(x))\ dx = \int_{x_0}^{x^*} (x-x_0)\cdots(x-x_n) f[x_0,\cdots,x_n,x]\ dx \\ &= \frac{f^{(n+1)}(\xi_1)}{(n+1)!} h^{n+2} \int_0^{\frac{x^*-x_0}{h}} \mu(\mu-1)\cdots(\mu-n+1)(\mu-n)\ d\mu \\ &+ \frac{f^{(n+2)}(\xi_2)}{(n+2)!} h^{n+3} \int_0^{\frac{x^*-x_0}{h}} \mu(\mu-1)\cdots(\mu-n+1)(\mu-n)(\mu-\frac{x^*-x_0}{h})\ d\mu,\end{aligned}$$

for some $\xi_1, \xi_2 \in [x_0, x_n]$. From Lemma 4 we can get the following corollary.

Corollary 1 *If the smooth interval is $[x^*, x_n]$:*

- *If there is not a change of sign in the polynomial of the integrand in the interval $[x^*, x_n]$, the error can be written as,*

$$E_n = \int_{x^*}^{x_n} (f(x)-p_n(x))\ dx = (-1)^{n+2} \frac{f^{(n+1)}(\xi)}{(n+1)!} h^{n+2} \int_0^{\frac{x_n-x^*}{h}} \mu(\mu-1)\cdots(\mu-n+1)(\mu-n)\ d\mu \tag{2.46}$$

  for some $\xi \in [x_0, x_n]$.

- *If there is a change of sign in the polynomial of the integrand in the interval $[x^*, x_n]$, the*

error can be written as,

$$E_n = \int_{x^*}^{x_n} (f(x) - p_n(x))\ dx = -\frac{f^{(n+1)}(\xi_1)}{(n+1)!} h^{n+2} \int_{\frac{x^*-x_0}{h}}^{\frac{x_n-x_0}{h}} \mu(\mu-1)\cdots(\mu-n+1)(\mu-n)\ d\mu$$
$$+ \frac{f^{(n+2)}(\xi_2)}{(n+2)!} h^{n+3} \int_{\frac{x^*-x_0}{h}}^{\frac{x_n-x_0}{h}} \mu(\mu-1)\cdots(\mu-n+1)(\mu-n)(\mu-\frac{x_n-x_0}{h})\ d\mu. \tag{2.47}$$

for some $\xi_1, \xi_2 \in [x_0, x_n]$.

First, if there is not a change of sign in the polynomial of the integrand in the interval $[x^*, x_n]$, we just need to do the change of variables $y = x_n - x$ and proceed as in Lemma 4,

$$\begin{aligned} E_n &= \int_{x^*}^{x_n} (f(x) - p_n(x))\ dx = \int_{x^*}^{x_n} (x-x_0)\cdots(x-x_n) f[x_0, \cdots, x_n, x]\ dx \\ &= (-1)^{n+2} \int_0^{x_n-x^*} (y-(x_n-x_0))\cdots(y-(x_n-x_{n-1}))y f[x_0, \cdots, x_n, x_n-y]\ dy \\ &= (-1)^{n+2} \frac{f^{(n+1)}(\xi)}{(n+1)!} \int_0^{x_n-x^*} (y-nh)\cdots(y-h)y\ dy. \end{aligned}$$

for some $\xi \in [x_0, x_n]$. Applying the change of variables $y = \mu h, 0 \le \mu \le n$, we can write,

$$E_n = (-1)^{n+2} \frac{f^{(n+1)}(\xi)}{(n+1)!} h^{n+2} \int_0^{\frac{x_n-x^*}{h}} \mu(\mu-1)\cdots(\mu-n+1)(\mu-n)\ d\mu.$$

Secondly, if there is a change of sign in the polynomial of the integrand in the smooth interval $[x^*, x_n]$, we can define

$$w(x_n, x) = \int_{x_n}^{x} (t-x_0)\cdots(t-x_n)\ dt. \tag{2.48}$$

that satisfies, by the symmetry of the polynomials used, that at smooth zones,

$$w(x_n, x_n) = w(x_n, x_0) = 0, \quad w(x_n, x) < 0 \quad \text{for } x_0 < x < x_n,$$

when n is even, and

$$w(x_n, x_n) = 0, \quad w(x_n, x) < 0 \quad \text{for } x_0 < x < x_n,$$

when n is odd.

Following similar arguments to those in [39] (page 309), or just using symmetry arguments, the proof of these facts can be easily obtained.

Now, we can write the error as in Lemma 4,

$$E_n = \int_{x^*}^{x_n} w'(x_n, x) f[x_0, \cdots, x_n, x] \; dx.$$

and integrate by parts,

$$\begin{aligned}\int_{x^*}^{x_n} w'(x_n, x) f[x_0, \cdots, x_n, x] \; dx &= [w(x_n, x) f[x_0, \cdots, x_n, x]]_{x^*}^{x_n} - \int_{x^*}^{x_n} w(x_n, x) \frac{d}{dx} f[x_0, \cdots, x_n, x] \; dx \\ &= -w(x_n, x^*) f[x_0, \cdots, x_n, x^*] - \int_{x^*}^{x_n} w(x_n, x) \frac{d}{dx} f[x_0, \cdots, x_n, x] \; dx.\end{aligned} \tag{2.49}$$

Proceeding exactly as in Lemma 4 and observing that,

$$w(x_n, x^*) = -w(x^*, x_n),$$

we obtain

$$w(x_n, x^*) f[x_0, \cdots, x_n, x^*] = -\frac{f^{(n+1)}(\xi_1)}{(n+1)!} h^{n+2} \int_{\frac{x^* - x_0}{h}}^{\frac{x_n - x_0}{h}} \mu(\mu - 1) \cdots (\mu - n + 1)(\mu - n) \; d\mu, \tag{2.50}$$

for some $\xi_1 \in [x_0, x_n]$.

For the last integral in (2.49) we can proceed again as in Lemma 4 to write

$$\begin{aligned}-\int_{x^*}^{x_n} w(x_n, x) \frac{d}{dx} f[x_0, \cdots, x_n, x] \; dx &= -\int_{x^*}^{x_n} w(x_n, x) f[x_0, \cdots, x_n, x, x] \; dx \\ &= -f[x_0, \cdots, x_n, \eta_2, \eta_2] \int_{x^*}^{x_n} w(x_n, x) \; dx \\ &= -\frac{f^{(n+2)}(\xi_2)}{(n+2)!} \int_{x^*}^{x_n} \int_{x_n}^{x} (t - x_0) \cdots (t - x_n) \; dt dx,\end{aligned}$$

for some $\eta_2, \xi_2 \in [x_0, x_n]$. Now we can change the order of integration and apply the change of variables $t = x_0 + \mu h, 0 \le \mu \le n$:

$$\begin{aligned}-\int_{x^*}^{x_n} \int_{x_n}^{x} (t - x_0) \cdots (t - x_n) \; dt dx &= -\int_{x^*}^{x_n} \int_{t}^{x_n} (t - x_0) \cdots (t - x_n) \; dx dt \\ &= -\int_{x^*}^{x_n} (t - x_0) \cdots (t - x_n)(x_n - t) \; dt \\ &= h^{n+3} \int_{\frac{x^* - x_0}{h}}^{\frac{x_n - x_0}{h}} \mu(\mu - 1) \cdots (\mu - n + 1)(\mu - n)(\mu - \frac{x_n - x_0}{h}) \; d\mu.\end{aligned} \tag{2.51}$$

Thus, we can write that

$$\begin{aligned} &-\int_{x^*}^{x_n} w(x_n,x)\frac{d}{dx}f[x_0,\cdots,x_n,x]\ dx \\ &= \frac{f^{(n+2)}(\xi_2)}{(n+2)!}h^{n+3}\int_{\frac{x^*-x_0}{h}}^{\frac{x_n-x_0}{h}} \mu(\mu-1)\cdots(\mu-n+1)(\mu-n)(\mu-\frac{x_n-x_0}{h})\ d\mu. \end{aligned} \tag{2.52}$$

Joining the partial results in (2.50) and (2.52), we finish the proof,

$$\begin{aligned} E_n &= \int_{x^*}^{x_n}(f(x)-p_n(x))\ dx = \int_{x^*}^{x_n}(x-x_0)\cdots(x-x_n)f[x_0,\cdots,x_n,x]\ dx \\ &= -\frac{f^{(n+1)}(\xi_1)}{(n+1)!}h^{n+2}\int_{\frac{x^*-x_0}{h}}^{\frac{x_n-x_0}{h}} \mu(\mu-1)\cdots(\mu-n+1)(\mu-n)\ d\mu \\ &+ \frac{f^{(n+2)}(\xi_2)}{(n+2)!}h^{n+3}\int_{\frac{x^*-x_0}{h}}^{\frac{x_n-x_0}{h}} \mu(\mu-1)\cdots(\mu-n+1)(\mu-n)(\mu-\frac{x_n-x_0}{h})\ d\mu, \end{aligned}$$

for some $\xi_1, \xi_2 \in [x^*, x_n]$.

Theorem 3 *We suppose that the piecewise continuous function f has discontinuities at x^* up to the n-th derivative. The subtraction of the correction term,*

$$C = \int_a^{x^*} Q^+(x)\ dx + \int_{x^*}^b Q^-(x)\ dx \tag{2.53}$$

to the numerical integration formula, assures that the error is:

- *If the discontinuity is placed in the interval $[x_0, x_1]$*

$$E^*(f) = E(f) + C = C_n^1\frac{(f^-)^{(n+1)}(\xi_1)}{(n+1)!}h^{n+2} + C_n^2\frac{(f^+)^{(n+1)}(\xi_2)}{(n+1)!}h^{n+2} + C_n^3\frac{(f^+)^{(n+2)}(\xi_3)}{(n+2)!}h^{n+3},$$

  with $\xi_1, \xi_2, \xi_3 \in [x_0, x_n]$, and

$$\begin{aligned} C_n^1 &= \int_0^{\frac{x^*-x_0}{h}} \mu(\mu-1)\cdots(\mu-n+1)(\mu-n)\ d\mu, \\ C_n^2 &= \int_{\frac{x^*-x_0}{h}}^{\frac{x_n-x_0}{h}} \mu(\mu-1)\cdots(\mu-n+1)(\mu-n)\ d\mu. \\ C_n^3 &= \int_{\frac{x^*-x_0}{h}}^{\frac{x_n-x_0}{h}} \mu(\mu-1)\cdots(\mu-n+1)(\mu-n)(\mu-n)\ d\mu. \end{aligned}$$

- *If the discontinuity is placed in the interval $[x_{n-1}, x_n]$,*

$$E(f) + C = C_n^1\frac{(f^-)^{(n+1)}(\xi_1)}{(n+1)!}h^{n+2} + C_n^2\frac{(f^-)^{(n+2)}(\xi_2)}{(n+2)!}h^{n+3} + (-1)^{n+2}C_n^3\frac{(f^+)^{(n+1)}(\xi_3)}{(n+1)!}h^{n+2},$$

with $\xi_1, \xi_2, \xi_3 \in [x_0, x_n]$, *and*

$$C_n^1 = \int_0^{\frac{x^*-x_0}{h}} \mu(\mu-1)\cdots(\mu-n+1)(\mu-n)\ d\mu,$$
$$C_n^2 = \int_0^{\frac{x^*-x_0}{h}} \mu(\mu-1)\cdots(\mu-n+1)(\mu-n)(\mu-\frac{x^*-x_0}{h})\ d\mu.$$
$$C_n^3 = \int_0^{\frac{x_n-x^*}{h}} \mu(\mu-1)\cdots(\mu-n+1)(\mu-n)\ d\mu.$$

- *In any other case,*

$$E^*(f) = E(f) + C = C_n^1 \frac{(f^-)^{(n+1)}(\xi_1)}{(n+1)!}h^{n+2} + C_n^2 \frac{(f^-)^{(n+2)}(\xi_2)}{(n+2)!}h^{n+3} + C_n^3 \frac{(f^+)^{(n+1)}(\xi_3)}{(n+1)!}h^{n+2} + C_n^4 \frac{(f^+)^{(n+2)}(\xi_4)}{(n+2)!}h^{n+3}.$$

with $\xi_1, \xi_2, \xi_3, \xi_4 \in [x_0, x_n]$, *and*

$$C_n^1 = \int_0^{\frac{x^*-x_0}{h}} \mu(\mu-1)\cdots(\mu-n+1)(\mu-n)\ d\mu,$$
$$C_n^2 = \int_0^{\frac{x^*-x_0}{h}} \mu(\mu-1)\cdots(\mu-n+1)(\mu-n)(\mu-\frac{x^*-x_0}{h})\ d\mu,$$
$$C_n^3 = \int_{\frac{x^*-x_0}{h}}^{\frac{x_n-x_0}{h}} \mu(\mu-1)\cdots(\mu-n+1)(\mu-n)\ d\mu.$$
$$C_n^4 = \int_{\frac{x^*-x_0}{h}}^{\frac{x_n-x_0}{h}} \mu(\mu-1)\cdots(\mu-n+1)(\mu-n)(\mu-n)\ d\mu.$$

The proof is straightforward using Lemmas 3, 4 and Corollary 1.

2.3.1 Correction terms for commonly used Newton-Cotes formulas

In Table 2.2 we present some expressions for the correction terms C in (2.53). In Table 2.2 we have used the notation $C_{n,j}, j = 1\cdots n$, being n the degree of the interpolating polynomial used to obtain the integration rule. Thus, for the trapezoidal rule there is only the term $C_{1,1}$. For the Simpson's 1/3 rule there are two terms: $C_{2,1}$ if the discontinuity falls at an odd interval and $C_{2,2}$ if the discontinuity falls at an odd interval. For the Simpson's 3/8 rule, there are three terms: $C_{3,1}$ if $\left(\lceil\frac{x^*}{h}\rceil mod\ 3\right) = 1$, $C_{3,2}$ if $\left(\lceil\frac{x^*}{h}\rceil mod\ 3\right) = 2$ and $C_{3,3}$ if $\left(\lceil\frac{x^*}{h}\rceil mod\ 3\right) = 0$. For higher orders, the notation is similar. Just to show an example, in Figure 2.3 we should use $C_{3,1}$ in the case presented to the left, $C_{3,2}$ in the case presented at the middle and $C_{3,3}$ in the case to the right.

2.4 Numerical experiments

In this section we analyze the numerical accuracy obtained by the integration formulas proposed in previous sections. In the first subsection, we present some grid refinement analysis for functions

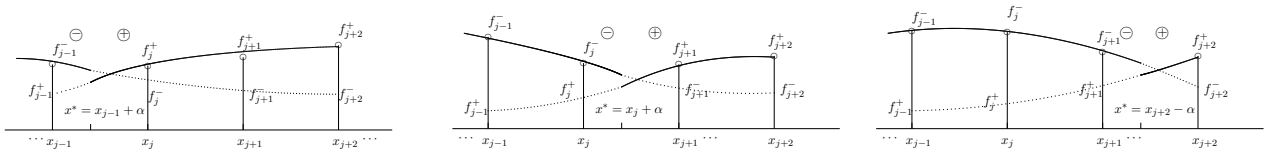

Figure 2.3: Three examples of functions with discontinuities (solid line) placed in different intervals at a position x^*. We have labeled the domain to the left of the discontinuity as $-$ and the one to the right as $+$. We have also represented with a dashed line the prolongation of the functions through Taylor expansions at both sides of the discontinuity.

with discontinuities. In the second subsection we include an example of a practical application of the formulas, jointly with a numerical analysis of the accuracy obtained.

2.4.1 A study of the numerical accuracy attained through the proposed numerical integration formulas

In this section we will apply the classical and corrected simple and composite trapezoid rule, Simpson's 1/3 rule and Simpson's 3/8 rule to data obtained from the discretisation of the function in (2.54), that presents jumps in the function and all the derivatives. We will consider that we start from discretized data and that the location of the discontinuity, as well as the jump conditions, are known exactly. As it was motivated in the abstract and the introduction, we suppose that the function is only known at data points.

$$f(x) = \begin{cases} \cos(\pi x) + 10, & \text{if } a \leq x < b, \\ \sin(\pi x), & \text{if } b \leq x \leq c. \end{cases} \tag{2.54}$$

The results observed in the experiments are similar for any other piecewise continuous function that we have explored.

In the grid refinement experiments, the error E_i is calculated as the absolute value of the difference between the exact integral and the approximated one, obtained via the simple or composite quadrature rules. The order of accuracy is obtained in general as,

$$O_i = \frac{\ln(E_i/E_{i+1})}{\ln(n_i/n_{i+1})}, \tag{2.55}$$

being E_i the error obtained for a grid of n_i points and E_{i+1}, the error obtained for a grid of n_{i+1} points (in the experiments, $n_{i+1} = 2n_i$ for the trapezoid rule and the Simpson's $\frac{3}{8}$ rule or $n_{i+1} = 2n_i + 1$ for the Simpson's $\frac{1}{3}$ rule).

Let us first check the numerical order attained by the simple quadrature rules. For this first experiment we initially set $a = 0$, $c = 0.5$. Then, we divide the interval $[a, c]$ in the number of panels used by the simple quadrature rule that we want to check. The grid-spacing is represented by h and we set $b = (n + d)h$, where d is a number in the interval $[0, 1]$, and $n = 0, 1, 2, \ldots$, depending

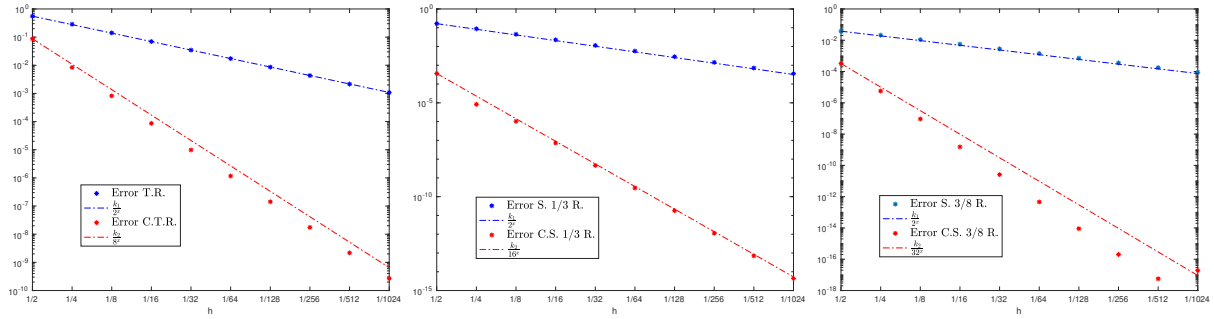

Figure 2.4: Grid refinement analysis for the numerical integration of the function in (2.54). To the left, using the simple trapezoid rule and the corrected simple trapezoid rule. At the center, using the simple Simpson's 1/3 rule and the corrected one. To the right, using the simple Simpson's 3/8 rule and the corrected one. In all the cases, the error of the corrected formulas decreases following the theoretical rate.

on the number of panels that the particular rule uses. The value of n and d is maintained during the whole experiment. In the experiments that we present $n = 0, d = 0.4$, but similar results can be obtained with other values. Once we have calculated the error for the simple rule in absolute value, we divide the interval $[a, c]$ by two and we repeat the process keeping the value of n and d. The results are presented in Figure 2.4. We can see that in all the cases, the error of the corrected formulas decreases following the theoretical rate and the noncorrected formulas present an error that corresponds to the first term of the corrections presented in Table 2.2, that is $O(h)$. To the left of Figure 2.4, we present the results for the simple trapezoid rule in blue and for the corrected simple trapezoid rule in red. The error for the noncorrected rule decreases as the dashed line in blue, which shows the division of the error by two each time that the mesh size is divided by two ($O(h)$ order of accuracy). The corrected trapezoid rule behaves very similarly to the dashed line in red, which divides the error by eight when the mesh side is divided by two ($O(h^3)$ order of accuracy). At the center, the error for the non corrected Simpson's $\frac{1}{3}$ decreases as the dashed line in blue, which represents $O(h)$ order of accuracy. The error for the corrected Simpson's $\frac{1}{3}$ is represented by the dashed line in red, which represents $O(h^4)$ order of accuracy. To the right, the error for the noncorrected Simpson' $\frac{3}{8}$ rule decreases with $O(h)$ order of accuracy, while the corrected one decreases with $O(h^4)$ order of accuracy. We can also observe the numerical results in table 2.3.

In Table 2.4 we present a second grid refinement experiment for the composite rules. In this case, we start from a point value discretization of the data with $n = 2^i, i = 3, 5, \ldots, 12$ points for the trapezoid and the Simpson's $\frac{3}{8}$ rule. For the Simpson's $\frac{1}{3}$ we set $n = 2^i + 1, i = 3, 5, \ldots, 12$. The order presents some variability in the case of the Simpson's $\frac{1}{3}$, (as well as the order of the noncorrected rules). Even so, in Figure 2.5 we can observe that the decreasing of the errors presented in Table 2.4 coincides with the expected theoretical one, also represented in the graphs.

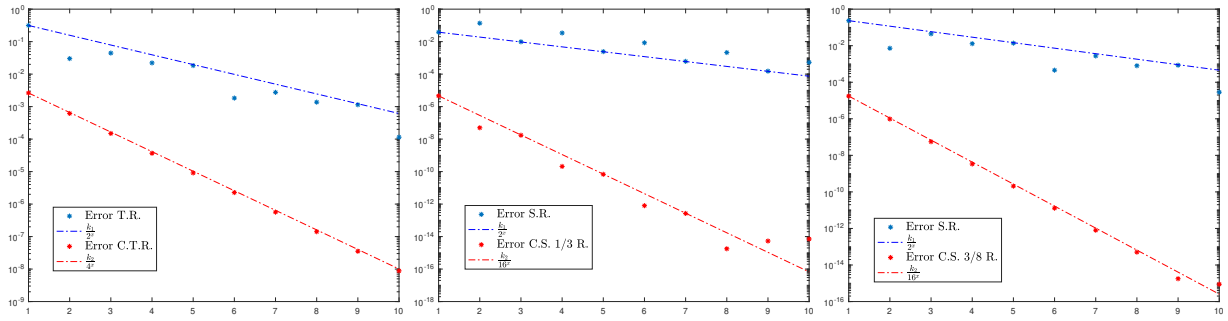

Figure 2.5: Grid refinement analysis for the numerical integration of the function in (2.54). To the left, using the composite trapezoid rule and the corrected composite trapezoid rule. At the center, using the composite Simpson's 1/3 rule and the corrected one. To the right, using the composite Simpson's 3/8 rule and the corrected one. In all the cases, the error of the corrected formulas decrease following the theoretical rate.

In Figure 2.5 to the left, we present the results for the composite trapezoid rule in blue and for the corrected composite trapezoid rule in red. We can see that the noncorrected rule shows a decrease in the error very similar to the dashed line in blue, which shows the division of the error by two each time that the mesh size is divided by two ($O(h)$ order of accuracy). The corrected trapezoid rule behaves very similarly to the dashed line in red, which divides the error by four when the mesh side is divided by two ($O(h^2)$ order of accuracy). At the center of Figure 2.5, the non corrected Simpson's $\frac{1}{3}$ rule behaves very similarly to the dashed line in blue, which represents $O(h)$ order of accuracy. The corrected Simpson's $\frac{1}{3}$ rule behaves very similarly to the dashed line in red, which represents $O(h^4)$ order of accuracy. Similar behavior can be observed for the Simpson' $\frac{3}{8}$ rule (at the right in Figure 2.5): the noncorrected rule presents $O(h)$ order of accuracy, while the corrected one presents $O(h^4)$. We can see that the orders of accuracy of the corrected composite rules correspond to those of the classical composite rules at smooth zones.

2.4.2 Example: Solving Sturm-Liouville boundary problems using the Green functions and numerical integration

In this section we present an example that shows a practical application of the corrected numerical integration formulas introduced before.

Let us consider a Sturm-Liouville one dimensional two-point boundary value problem [40],

$$u_{xx}(x) = f(x), \quad a < x < b, \tag{2.56}$$

with specified boundary conditions $u(a) = u_a$, $u(b) = u_b$. The solution can be expressed as,

$$u(x) = \frac{x-b}{a-b}u_a + \frac{x-a}{b-a}u_b + \int_a^b G(x,\xi)f(\xi)\ d\xi, \tag{2.57}$$

where $G(x,\xi)$ is the *Green's function*, defined as the solution of,

$$G_{\xi\xi}(x,\xi) = \delta(x-\xi), \quad a < \xi < b, \tag{2.58}$$

with homogeneous boundary conditions $G(x,a) = 0, G(x,b) = 0$. We also know that in the one-dimensional case, the function G presents known jump conditions (see for example [41])

$$\begin{aligned} [G(\xi,\xi)] &= \lim_{x\to\xi^+} G(x,\xi) - \lim_{x\to\xi^-} G(x,\xi) = 0, \\ [G_x(\xi,\xi)] &= \lim_{x\to\xi^+} G_x(x,\xi) - \lim_{x\to\xi^-} G_x(x,\xi) = 1, \end{aligned} \tag{2.59}$$

which are known as *connection conditions*. We consider the case when the values of $f(x)$ and $G(x)$ are given at grid points. We include the exact jump conditions at the discontinuities of the integrand in (2.57) in order to get an accurate computation of the numerical quadratures. Thus, we apply the modified integration formulas presented in previous sections to compute the integral in (2.57) numerically. This approach is preferred if we want to obtain the approximated solution at some points instead of the entire domain and it is often called an integral equation approach. The interested reader can see [41, 42, 43, 44, 45, 46, 47] and the references therein for more discussions about the discrete *Green function*.

Let us consider a Sturm-Liouville two-point boundary value problem of the type shown in (2.56), with specified boundary conditions $u(0) = 0$, $u(1) = 0$

$$u_{xx}(x) = f(x), \quad 0 < x < 1 \tag{2.60}$$

The solution of this problem can be expressed as,

$$u(x) = \int_0^1 G(x,\xi) f(\xi)\, d\xi. \tag{2.61}$$

Following (2.58), we have that, for our problem, $G(x)$ is the *Green function* that can be defined as the solution of

$$G_{xx}(x) = \delta(x-\xi), \quad 0 < \xi < 1, \tag{2.62}$$

with specified boundary conditions $G(x,0) = 0, G(x,1) = 0$, where $\delta(x)$ represents the Dirac delta function. Integrating twice G_{xx} and applying the boundary conditions, and the connection conditions in (2.59), we obtain that the expression for the Green's function is

$$G(x,\xi) = \begin{cases} x(\xi-1), & \text{if } 0 \le x < \xi, \\ (x-1)\xi, & \text{if } \xi \le x \le 1. \end{cases} \tag{2.63}$$

Given $f(x) \in C[0,\alpha) \cup (\alpha,1]$, as mentioned before, we assume that the functions f and G are given in discrete form, and that we know the jumps in the integrand of (2.61) and its derivatives. In our experiment, we selected $f(x)$ as follows,

$$f(x) = \begin{cases} 1, & \text{if } 0 \le x < \alpha, \\ 0, & \text{if } \alpha \le x \le 1. \end{cases} \tag{2.64}$$

For this $f(x)$ and the boundary conditions $u(0) = 0$, $u(1) = 0$, we can obtain very easily (just integrating) the analytical solution of the problem in (2.56) with $a = 0$ and $b = 1$,

$$u(x) = \begin{cases} \frac{x^2}{2} + (\frac{\alpha^2}{2} - \alpha)x, & \text{if } 0 \leq x < \alpha, \\ \frac{\alpha^2}{2}(x-1), & \text{if } \alpha \leq x \leq 1. \end{cases} \tag{2.65}$$

We use this expression to check against the numerical solution.

Note that the expression in (2.61) implies that we need to do a numerical integration for every point of the solution that we want to obtain. The function G is bivariate and we particularize the x variable in order to obtain a univariate function. Thus, in the numerical integration we typically have to deal with the discontinuity of $G(x, \xi)$ plus the discontinuities that $f(x)$ might contain. The discretization of G in the ξ direction must have the same number of points as the function f, but can have an arbitrary number of points in the x direction. In our experiments, if n is the number of points in the ξ direction, we select a number of points in the x direction equal to $m = 4n$, in order to assure that the discontinuity of G falls sometimes between grid points of f.

The error in the approximated solution is computed in the infinity norm in the interval $[0, 1]$ and the order of accuracy is obtained in general as,

$$\bar{O}_i = \frac{\ln(E_i^\infty / E_{i+1}^\infty)}{\ln(n_i / n_{i+1})}. \tag{2.66}$$

For the trapezoid rule, E_i^∞ is the error in the infinity norm obtained for a grid of n_i points, and E_{i+1}^∞ is the error obtained for a grid of $n_{i+1} = 2n_i$ points. For the Simpson 1/3 rule, we select n_i points to compute E_i^∞, and $n_{i+1} = 2n_i + 1$ to compute E_{i+1}^∞, just to assure an odd number of points in the computation.

We check the solution of the problem (2.60) obtained through the expression in (2.61), using the classical trapezoid rule and the Simpson 1/3 rule and we compare them with the result obtained using their modified versions. The results are listed in Table 2.1 when $\alpha = \frac{\pi}{4}$. We can see that, in this case, the modified quadrature formulas provide the exact solution up to the machine precision. The average of the orders for the original quadrature formulas are only approximately $O(h)$.

Note that a finite element method (FEM) can be used to solve the interface problem presented in this subsection. The key point is whether the location of the discontinuity is a nodal point or not. If not, the solution to the FEM will not be very accurate near the discontinuity since the computed mass matrix and the load vector are likely to lose accuracy using traditional numerical quadrature techniques. Note also that the optimal error estimates for the FEM are based on average norms (L^2, H^1, energy) that cannot tell the point-wise accuracy, while the approach presented in this manuscript can provide point-wise error estimates.

2.5 Conclusions

In this chapter, we have presented correction terms for the classical trapezoid rule, Simpson's $\frac{1}{3}$ rule, and the most common Newton-Cotes integration formulas. These correction terms have

$n = 2^i$	2^4	2^5	2^6	2^7	2^8	2^9	2^{10}	2^{11}	2^{12}	2^{13}
Error T.R. (E_i^∞)	3.32470e-03	8.68748e-04	6.75714e-05	3.27956e-04	1.48027e-04	5.34071e-05	6.25827e-06	1.73014e-05	1.21226e-05	6.24818e-06
O_i	-	1.9362	3.6845	-2.279	1.1476	1.4708	3.0932	-1.4671	0.51319	0.95619
Error C.T.R. (E_i^∞)	4.16334e-17	5.55112e-17	5.55112e-17	5.55112e-17	6.93889e-17	2.08167e-16	2.49800e-16	4.44089e-16	6.52256e-16	1.99840e-15
O_i	-	-	-	-	-	-	-	-	-	-
$n = 2^i + 1$	$2^4 + 1$	$2^5 + 1$	$2^6 + 1$	$2^7 + 1$	$2^8 + 1$	$2^9 + 1$	$2^{10} + 1$	$2^{11} + 1$	$2^{12} + 1$	$2^{13} + 1$
Error S. 1/3 R. (E_i^∞)	2.51799e-03	2.89379e-03	2.24835e-04	2.60974e-04	3.99048e-04	6.95012e-05	1.42677e-05	1.33435e-05	2.70634e-05	6.48331e-06
O_i	-	-0.20069	3.686	-0.21504	-0.61266	2.5215	2.2843	0.096619	-1.0202	2.0615
Error C.S. 1/3 R. (E_i^∞)	2.77556e-17	4.16334e-17	2.77556e-17	4.16334e-17	4.16334e-17	4.16334e-17	4.16334e-17	4.16334e-17	4.16334e-17	4.16334e-17
O_i	-	-	-	-	-	-	-	-	-	-

Table 2.1: Grid refinement analysis in the infinity norm for the integral shown in (2.61) using two composite quadrature rules. The first part of the table shows the trapezoidal rule (T.R.) and the corrected trapezoidal rule (C.T.R.). The bottom part shows the Simpson's 1/3 Rule (S. 1/3 R.) and the corrected Simpson's rule (C.S. 1/3 R.).

an explicit closed formula that allows keeping the global accuracy attained by classical formulas at smooth zones even when the data contains discontinuities in the function or the derivatives. The correction terms can be used for the simple or composite classical integration formulas and it is possible to compute the integral using these formulas and then, as post-processing, add the correction terms to raise the accuracy. Correction terms for any other integration rule can be found following analogous processes to the ones shown in this work. We have also given correction terms for the most widely used Newton-Cotes quadrature formulas and we have proved that the use of these correction terms assures the expected theoretical accuracy. We have shown that the correction terms depend on the jumps of the function that is to be integrated and its derivatives. All the numerical experiments that we have presented, confirm the theoretical results obtained.

$C_{1,1}$	$\frac{(-h+2\alpha)}{2}[f] + \frac{(h\alpha-\alpha^2)}{2}[f']$
$C_{2,1}$	$\left(\alpha - \frac{h}{3}\right)[f] + \frac{\alpha}{6}(3\alpha - 2h)[f'] + \frac{\alpha^2}{6}(\alpha - h)[f'']$
$C_{2,2}$	$-\left(\alpha - \frac{h}{3}\right)[f] + \frac{\alpha}{6}(3\alpha - 2h)[f'] - \frac{\alpha^2}{6}(\alpha - h)[f'']$
$C_{3,1}$	$\left(\alpha - \frac{3}{8}h\right)[f] + \left(\frac{3}{8}h\alpha - \frac{1}{2}\alpha^2\right)[f'] + \left(-\frac{3}{16}h\alpha^2 + \frac{1}{6}\alpha^3\right)[f''] + \left(\frac{1}{16}h\alpha^3 - \frac{1}{24}\alpha^4\right)[f''']$
$C_{3,2}$	$\left(\alpha - \frac{1}{2}h\right)[f] + \left(\frac{1}{2}h\alpha - \frac{1}{2}\alpha^2 - \frac{1}{8}h^2\right)[f'] + \left(-\frac{1}{8}h\alpha^2 - \frac{1}{48}h^3 + \frac{1}{8}h^2\alpha + \frac{1}{6}\alpha^3\right)[f''] + \left(\frac{1}{48}h^3\alpha + \frac{1}{48}h^4 - \frac{1}{24}\alpha^4 - \frac{1}{16}h^2\alpha^2 + \frac{1}{12}h\alpha^3\right)[f''']$
$C_{3,3}$	$\left(-\alpha + \frac{3}{8}h\right)[f] + \left(-\frac{1}{2}\alpha^2 + \frac{3}{8}h\alpha\right)[f'] + \left(-\frac{1}{6}\alpha^3 + \frac{3}{16}h\alpha^2\right)[f''] + \left(-\frac{1}{24}\alpha^4 + \frac{1}{16}h\alpha^3\right)[f''']$
$C_{4,1}$	$\left(-\frac{14}{45}h + \alpha\right)[f] + \left(-\frac{1}{2}\alpha^2 + \frac{14}{45}h\alpha\right)[f'] + \left(\frac{1}{6}\alpha^3 - \frac{7}{45}h\alpha^2\right)[f''] + \left(-\frac{1}{24}\alpha^4 + \frac{7}{135}h\alpha^3\right)[f'''] + \left(\frac{1}{120}\alpha^5 - \frac{7}{540}h\alpha^4\right)[f^{(4)}]$
$C_{4,2}$	$\left(\alpha - \frac{11}{15}h\right)[f] + \left(-\frac{17}{90}h^2 + \frac{11}{15}h\alpha - \frac{1}{2}\alpha^2\right)[f'] + \left(\frac{1}{90}h^3 + \frac{17}{90}h^2\alpha - \frac{11}{30}h\alpha^2 + \frac{1}{6}\alpha^3\right)[f''] + \left(\frac{11}{90}h\alpha^3 - \frac{1}{24}\alpha^4 + \frac{11}{1080}h^4 - \frac{1}{90}h^3\alpha - \frac{17}{180}h^2\alpha^2\right)[f'''] + \left(\frac{17}{540}h^2\alpha^3 + \frac{1}{180}h^3\alpha^2 - \frac{11}{360}h\alpha^4 - \frac{11}{1080}h^4\alpha - \frac{1}{216}h^5 + \frac{1}{120}\alpha^5\right)[f^{(4)}]$
$C_{4,3}$	$\left(-\alpha + \frac{11}{15}h\right)[f] + \left(-\frac{17}{90}h^2 + \frac{11}{15}h\alpha - \frac{1}{2}\alpha^2\right)[f'] + \left(-\frac{1}{6}\alpha^3 + \frac{11}{30}h\alpha^2 - \frac{17}{90}h^2\alpha - \frac{1}{90}h^3\right)[f''] + \left(\frac{11}{90}h\alpha^3 - \frac{1}{24}\alpha^4 + \frac{11}{1080}h^4 - \frac{1}{90}h^3\alpha - \frac{17}{180}h^2\alpha^2\right)[f'''] + \left(-\frac{17}{540}h^2\alpha^3 + \frac{11}{1080}h^4\alpha + \frac{11}{360}h\alpha^4 - \frac{1}{180}h^3\alpha^2 + \frac{1}{216}h^5 - \frac{1}{120}\alpha^5\right)[f^{(4)}]$
$C_{4,4}$	$\left(\frac{14}{45}h - \alpha\right)[f] + \left(-\frac{1}{2}\alpha^2 + \frac{14}{45}h\alpha\right)[f'] + \left(-\frac{1}{6}\alpha^3 + \frac{7}{45}h\alpha^2\right)[f''] + \left(-\frac{1}{24}\alpha^4 + \frac{7}{135}h\alpha^3\right)[f'''] + \left(-\frac{1}{120}\alpha^5 + \frac{7}{540}h\alpha^4\right)[f^{(4)}]$

Table 2.2: Correction terms to be subtracted from the most common integration formulas.

$(c-a)$	$\frac{1}{2}$	$\frac{1}{4}$	$\frac{1}{8}$	$\frac{1}{16}$	$\frac{1}{32}$	$\frac{1}{64}$	$\frac{1}{128}$	$\frac{1}{256}$	$\frac{1}{512}$	$\frac{1}{1024}$
Error T.R. (E_i)	5.55384e-01	2.87374e-01	1.41312e-01	6.97373e-02	3.46224e-02	1.72492e-02	8.60914e-03	4.30072e-03	2.14940e-03	1.07446e-03
O_i	-	0.95056	1.024	1.0189	1.0102	1.0052	1.0026	1.0013	1.0006	1.0003
Error C.T.R. (E_i)	8.73231e-02	8.36720e-03	8.18010e-04	8.67118e-05	9.84247e-06	1.16748e-06	1.41995e-07	1.75028e-08	2.17243e-09	2.70590e-10
O_i	-	3.3835	3.3546	3.2378	3.1391	3.0756	3.0395	3.0202	3.0102	3.0051
Error S. 1/3 R. (E_i)	1.65392e-01	8.75298e-02	4.48262e-02	2.26680e-02	1.13966e-02	5.71378e-03	2.86074e-03	1.43133e-03	7.15906e-04	3.58013e-04
O_i	-	0.91804	0.96543	0.98368	0.99206	0.99608	0.99806	0.99903	0.99952	0.99976
Error C.S. 1/3 R. (E_i)	3.64440e-04	8.31101e-06	1.04180e-06	7.25089e-08	4.61560e-09	2.88760e-10	1.80198e-11	1.12481e-12	7.02849e-14	4.37150e-15
O_i	-	5.4545	2.9959	3.8448	3.9736	3.9986	4.0022	4.0018	4.0003	4.007
Error S. 3/8 R. (E_i)	3.80713e-02	2.11065e-02	1.10144e-02	5.61914e-03	2.83719e-03	1.42546e-03	7.14440e-04	3.57647e-04	1.78930e-04	8.94916e-05
O_i	-	0.85102	0.9383	0.97097	0.98588	0.99304	0.99654	0.99828	0.99914	0.99957
Error C.S. 3/8 R. (E_i)	3.23113e-04	5.67780e-06	9.29742e-08	1.52212e-09	2.56990e-11	4.60409e-13	9.00668e-15	2.02095e-16	5.63785e-18	1.92988e-17
O_i	-	5.8306	5.9324	5.9327	5.8882	5.8026	5.6758	5.4779	5.1637	-1.7753

Table 2.3: Grid refinement analysis for the simple quadrature rules. The first part of the table shows the trapezoidal rule (T.R.) and the corrected trapezoidal rule (C.T.R.). The central part shows the Simpson's 1/3 Rule (S. 1/3 R.) and the corrected Simpson's rule (C.S. 1/3 R.). Finally the bottom part shows the Simpson's 3/8 Rule (S. 3/8 R.) and the corrected Simpson's 3/8 rule (C.S. 3/8 R.). We have used the function in (2.54).

$n = 2^i$	2^4	2^5	2^6	2^7	2^8	2^9	2^{10}	2^{11}	2^{12}	2^{13}
Error T.R. (E_i)	3.14564e-01	3.00647e-02	4.44922e-02	2.21224e-02	1.83580e-02	1.83086e-03	2.74401e-03	1.37153e-03	1.14264e-03	1.14245e-04
O_i	-	3.3872	-0.56548	1.008	0.2691	3.3258	-0.58377	1.0005	0.26341	3.3222
Error C.T.R. (E_i)	2.63164e-03	6.16553e-04	1.49283e-04	3.66601e-05	9.09938e-06	2.26614e-06	5.65427e-07	1.41201e-07	3.52844e-08	8.81900e-09
O_i	-	2.0937	2.0462	2.0258	2.0104	2.0055	2.0028	2.0016	2.0006	2.0003
Error S. 3/8 R. (E_i)	2.33932e-01	7.25343e-03	4.45169e-02	1.28813e-02	1.37617e-02	4.56764e-04	2.74410e-03	7.99969e-04	8.56956e-04	2.85576e-05
O_i	-	5.0113	-2.6176	1.7891	-0.095376	4.9131	-2.5868	1.7783	-0.099277	4.9073
Error C.S. 3/8 R. (E_i)	1.74854e-05	9.70184e-07	5.58112e-08	3.36499e-09	2.07176e-10	1.28564e-11	8.00249e-13	5.06262e-14	1.77636e-15	8.88178e-16
O_i	-	4.1717	4.1196	4.0519	4.0217	4.0103	4.0059	3.9825	4.8329	1
$n = 2^i + 1$	$2^4 + 1$	$2^5 + 1$	$2^6 + 1$	$2^7 + 1$	$2^8 + 1$	$2^9 + 1$	$2^{10} + 1$	$2^{11} + 1$	$2^{12} + 1$	$2^{13} + 1$
Error S. 1/3 R. (E_i)	3.81374e-02	1.36672e-01	9.79905e-03	3.41046e-02	2.43374e-03	8.53020e-03	6.09443e-04	2.13230e-03	1.52298e-04	5.33090e-04
O_i	-	-1.8414	3.8019	-1.7993	3.8087	-1.8094	3.807	-1.8068	3.8074	-1.8075
Error C.S. 1/3 R. (E_i)	4.59121e-06	4.99040e-08	1.72994e-08	2.08413e-10	6.81162e-11	8.00249e-13	2.65565e-13	1.77636e-15	5.32907e-15	7.10543e-15
O_i	-	6.5236	1.5284	6.3751	1.6134	6.4114	1.5914	7.224	-1.585	-0.41504

Table 2.4: Grid refinement analysis for the composite quadrature rules. The first part of the table shows the trapezoidal rule (T.R.) and the corrected trapezoidal rule (C.T.R.). The central part shows the Simpson's 3/8 Rule (S. 3/8 R.) and the corrected Simpson's rule (C.S. 3/8 R.). Finally the bottom part shows the Simpson's 1/3 Rule (S. 1/3 R.) and the corrected Simpson's 1/3 rule (C.S. 1/3 R.). We have used the function in (2.54).

Chapter 3

Adapting cubic Hermite splines to the presence of singularities through correction terms

3.1 Introduction

In this chapter, it is our aim to design a nonlinear cubic Hermite spline interpolation adapted to the presence of singularities and constructed using the point-values discretization, i.e. using the data values $f(x)$ at the positions $x = x_j, j = 0, \ldots, m$. In this case, we try to obtain fully accurate first order derivatives and interpolation even close to the singularities (by full accuracy we mean the highest theoretically possible accuracy that we can obtain through our spline), but trying to preserve the jumps in the function and its derivatives in the reconstruction. The resulting method presents a high order of accuracy in the whole domain and provides piecewise C^2 regularity at both sides of the singularities. In order to reach our objective, we are inspired by the construction of the Immersed Interface Method (IIM) [3, 48, 49], in the sense that we design correction terms that allow us to fulfil our objectives. This method has been mostly used for the solution of elliptic equations with singularities in the context of fluid-structure interaction and it is based on an accurate tracking of the singularities and the modification of the finite difference scheme close to them.

Let us start by describing in brief detail the discretization of data that we shall use. The point-values sampling process used to obtain the pairs of data $(x_j, f(x_j)), j = 0, \ldots, m$, from a function f that may contain jump discontinuities implies the loss of the information regarding the exact position of these jump discontinuities, as it only preserves local information at the positions x_j. Even so, it is possible to detect the interval that contains the discontinuity [50]. The described kind of discretization would only allow for the detection and location of the position of discontinuities in the first order derivative (kinks in the function) [50, 51]. Yet, if we assume that the data come from a discretization through local averages of the function $f(x)$, i.e. the cell-averages setting

[50], then it is indeed possible to locate jump discontinuities in $f(x)$. In this work we use data discretized in the point-values. Further research could cover the results using cell-averages.

Let us continue by describing the classical Hermite interpolation and by exposing some classical results. Classical cubic Hermite interpolation is based on the construction of a cubic polynomial using the values $f_j = f(x_j), f_{j+1} = f(x_{j+1})$ of the function f, and its first order derivatives, $f'_j = f'(x_j)$ at the positions x_j, x_{j+1}. These four pieces of data allow to obtain the four unknowns in a cubic polynomial. Then, continuity conditions on the function and its first and second order derivatives are imposed at the x_j in order to set a system of equations that provides a global solution for the considered interval. That way, piecewise cubic Hermite interpolation is known to be fourth order accurate for smooth functions. Assuming that the data is smooth, if the spline uses approximations of the first order derivatives $\tilde{f}'_j \approx f'_j$, (from now on, if not stated otherwise, we use the tilde˜to represent approximations of different values: the function, the derivatives, the location of the singularity, etc.), then the maximum accuracy of the piecewise cubic Hermite interpolant is known to be $O(h^4)$ if the approximation of the first order derivatives is $O(h^3)$ accurate. If f presents singularities between the nodes (from here on we will use the word *node* as a synonym for the points of union of the different polynomial pieces of the spline), even good approximations of the first order derivatives at the nodes will lead to inaccurate approximations of the function inside the interval that contains the singularity. Discontinuities in the data lead either to classical Hermite splines showing Gibbs oscillations close to discontinuities in the function, or the smearing of singularities if the discontinuity is in the derivatives. This is logical considering that Hermite interpolation can be expressed in terms of the Hermite basis, represented in Figure 3.1, which is composed of polynomials that are smooth, two of them being non-monotone. The smearing of discontinuities in the first order derivative can be clearly explained through the smoothness of the base. The occurrence of oscillations close to jumps in the function will be justified later on, showing that the non-monotone elements of the base are multiplied by non-zero coefficients close to discontinuities.

Thus, our aim is twofold: to design a technique that allows for the obtention of the first order derivatives of the function at the nodes of the spline with full accuracy even close to singularities, and to use the computed first order derivatives to obtain a fully accurate spline. These two objectives will be reached through the computation of correction terms.

3.2 Some preliminaries about classical cubic Hermite splines

In this section we briefly introduce the classical way of constructing the cubic Hermite spline. Then, we introduce some new techniques that allow for the adaption of the classical interpolant to the presence of singularities. The objective is to design a technique that enables the obtention of sharp reconstructions of functions with discontinuities in the function or the derivatives, avoiding the smearing of the singularity or the appearance of Gibbs oscillations.

There is an extensive list of references that treat the field of the construction and the study of the properties of cubic Hermite splines. For example, [52] or [53] contain a in-depth revision of

the classical theoretical results in the field. The idea behind the construction of the spline is to compute a piecewise polynomial function of degree three between the data nodes. The resulting function must be C^2, i.e. the function and the first two derivatives must be continuous. The basis used to construct the polynomial between the nodes varies in the literature. Some authors start from $m+1$ pairs of values $(x_j, y_j), j = 0, \ldots, m$ and write the expression of the polynomial at a particular interval $[x_j, x_{j+1}]$ as

$$g_j(x) = a_j(x - x_j)^3 + b_j(x - x_j)^2 + c_j(x - x_j) + d_j. \tag{3.1}$$

Sometimes it is more convenient to use the alternative expression

$$g_j(x) = a_j(x - x_j)^2(x - x_{j+1}) + b_j(x - x_j)^2 + c_j(x - x_j) + d_j, \tag{3.2}$$

which easily provides a bound for the error of the Hermite interpolation. In any of both cases, regularity conditions must be imposed at the nodes in order to obtain a piecewise defined function that is C^2. Basically, we need to impose the continuity of the function and the two first order derivatives at the nodes. If y_j, y_{j+1} denote the values of the function at the nodes x_j, x_{j+1}, and D_j, D_{j+1} the values of the first order derivatives at the same nodes, imposing the continuity of the function and the first and second order derivatives at the nodes, it is straightforward to obtain the following expression for the coefficients in (3.1) (see for example [36] for a complete deduction of the formulas),

$$\begin{aligned} a_j &= \frac{h_{j+1}D_{j+1} + D_j h_{j+1} + 2y_j - 2y_{j+1}}{h_{j+1}^3}, \\ b_j &= -\frac{h_{j+1}D_{j+1} + 2D_j h_{j+1} + 3y_j - 3y_{j+1}}{h_{j+1}^2}, \\ c_j &= D_j, \\ d_j &= y_j, \end{aligned} \tag{3.3}$$

where $h_{j+1} = x_{j+1} - x_j$.

As mentioned before, the expression of the Hermite spline (3.1) can be expressed in terms of the Hermite basis, represented in Figure 3.1 for cubic splines. By replacing the coefficients of the spline in (3.1) by the values found in (3.3) we obtain,

$$\begin{aligned} g_j(x) = &\frac{h_{j+1}D_{j+1} + D_j h_{j+1} + 2y_j - 2y_{j+1}}{h_{j+1}^3}(x - x_j)^3 \\ &- \frac{h_{j+1}D_{j+1} + 2D_j h_{j+1} + 3y_j - 3y_{j+1}}{h_{j+1}^2}(x - x_j)^2 + D_j(x - x_j) + y_j. \end{aligned} \tag{3.4}$$

Moreover, the change of variables $s = \frac{x - x_j}{h_{j+1}}$ returns the expression of the spline in terms of the

cubic Hermite basis,

$$\begin{aligned} g_j(s) &= (h_{j+1}D_{j+1} + D_j h_{j+1} + 2y_j - 2y_{j+1})\, s^3 - (h_{j+1}D_{j+1} + 2D_j h_{j+1} + 3y_j - 3y_{j+1})\, s^2 + D_j h_{j+1} s + y_j \\ &= \left(1 - s^2(3-2s)\right) y_j + s^2(3-2s) y_{j+1} + \left(s^3 - 2s^2 + s\right) h_{j+1} D_j + \left(s^3 - s^2\right) h_{j+1} D_{j+1} \\ &= b_1(s) y_{j+1} + b_2(s) y_j + b_3(s) h_{j+1} D_j + b_4(s) h_{j+1} D_{j+1}, \end{aligned} \tag{3.5}$$

for $s \in [0, 1]$.

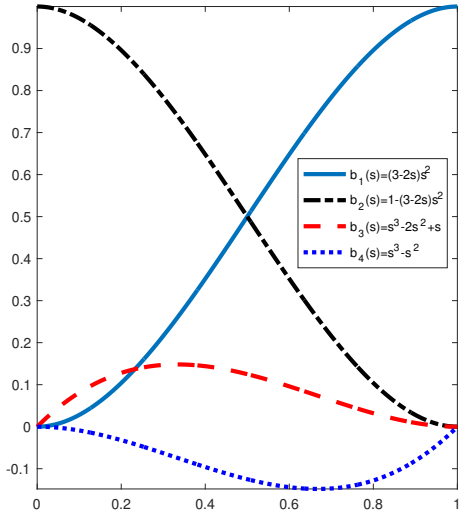

Figure 3.1: Representation of the Hermite basis for $s \in [0, 1]$.

The values of the first order derivatives at the nodes D_j can be known a priori, as with the Hermite interpolation, or they can be obtained by imposing the continuity of the second order derivatives at the nodes, as with the Hermite spline. Thus, the Hermite spline relies on the solution of a linear system of equations for the D_j, which needs two boundary conditions. Common options for the boundary conditions that can be found in the literature are: *natural* boundary conditions, *not-a-knot condition*, *complete cubic spline*, etc. The complete cubic spline consists of imposing slope boundary conditions,

$$g_0'(x_0) = D_0, \quad g_{m-1}'(x_m) = D_m,$$

and we have chosen it for our spline. If the first order derivatives are not available at the boundaries, they can be replaced by $O(h^3)$ approximations.

Imposing the continuity of the second order derivatives of the spline leads to the following equation for each interval between the nodes

$$\frac{D_{j-1}}{h_j} + 2\left(\frac{1}{h_j} + \frac{1}{h_{j+1}}\right) D_j + \frac{D_{j+1}}{h_{j+1}} = 3\left(\frac{y_{j+1} - y_j}{h_{j+1}^2} + \frac{y_j - y_{j-1}}{h_j^2}\right).$$

Thus we easily obtain a linear system for the first order derivatives D_j at the nodes,

$$\begin{bmatrix} 2\left(\frac{1}{h_1}+\frac{1}{h_2}\right) & \frac{1}{h_2} & 0 & \cdots & 0 & 0 \\ \frac{1}{h_2} & 2\left(\frac{1}{h_2}+\frac{1}{h_3}\right) & \frac{1}{h_3} & \cdots & 0 & 0 \\ \cdots & \cdots & \cdots & \cdots & \cdots & \cdots \\ 0 & 0 & 0 & \cdots & \frac{1}{h_{m-1}} & 2\left(\frac{1}{h_{m-1}}+\frac{1}{h_m}\right) \end{bmatrix} \begin{bmatrix} D_1 \\ D_2 \\ \cdots \\ D_{m-1} \end{bmatrix} = 3 \begin{bmatrix} \frac{\delta_2}{h_2}+\frac{\delta_1}{h_1}-\frac{D_0}{3h_1} \\ \frac{\delta_3}{h_3}+\frac{\delta_2}{h_2} \\ \cdots \\ \frac{\delta_m}{h_m}+\frac{\delta_{m-1}}{h_{m-1}}-\frac{D_m}{3h_m} \end{bmatrix}, \tag{3.6}$$

with $\delta_j = \frac{y_j - y_{j-1}}{h_j}$. We will consider a uniform grid spacing, but the results for non-uniform grid spacing can be obtained in an analogous way. With this consideration, the system in (3.6) transforms into

$$\begin{bmatrix} 4 & 1 & 0 & 0 & \cdots & 0 & 0 \\ 1 & 4 & 1 & 0 & \cdots & 0 & 0 \\ \cdots & \cdots & \cdots & \cdots & \cdots & \cdots & \cdots \\ 0 & 0 & 0 & 0 & \cdots & 1 & 4 \end{bmatrix} \begin{bmatrix} D_1 \\ D_2 \\ \cdots \\ D_{m-1} \end{bmatrix} = 6 \begin{bmatrix} \frac{\delta_2+\delta_1}{2}-\frac{D_0}{6} \\ \frac{\delta_3+\delta_2}{2} \\ \cdots \\ \frac{\delta_m+\delta_{m-1}}{2}-\frac{D_m}{6} \end{bmatrix}. \tag{3.7}$$

The existence of a singularity at any place of the domain leads to the computation of inaccurate first order derivatives through the system in (3.7). In case of jump discontinuities in the function, the consequence is the appearance of global Gibbs oscillations in the reconstruction of the spline that will affect the entire domain. A discussion about the size of the oscillations close to the discontinuity can be found in [36]. If a discontinuity is found in the derivatives, the singularity is smeared. In the next sections we will propose correction terms for preserving the accuracy of the spline close to the singularities.

We can also consider now the accuracy of the Hermite interpolation and its second order derivatives. These are classical results that will be used later, and which proofs can be found in pages 58 and 59 of [54].

Theorem 4 *(Error of classical cubic Hermite interpolation)*

Given a sufficiently smooth function f, the error for the cubic Hermite interpolation is given by

$$|f(x) - g_j(x)| \leq \frac{\max|f^{(4)}(\xi)|}{384} h^4, \quad x, \xi \in [x_j, x_{j+1}], \tag{3.8}$$

for all $h > 0$.

Corollary 2 *(Error of the second order derivative of classical cubic Hermite interpolation)*

Given a sufficiently smooth function f, the error for the second order derivative of the cubic Hermite interpolation is given by

$$|f''(x) - g_j''(x)| \leq \frac{\max|f^{(4)}(\xi)|}{2} h^2, \quad x, \xi \in [x_j, x_{j+1}], \tag{3.9}$$

for all $h > 0$.

Remark 2 *If the first order derivatives D_j, D_{j+1} are approximated, an accuracy of $O(h^3)$ is enough to keep the $O(h^4)$ accuracy of the cubic Hermite interpolation at smooth zones. To confirm this observation, instead of considering the canonical base as in (3.1), let us write the Hermite polynomial in the interval $[x_j, x_{j+1}]$ using the expression in (3.2). As we know the values $f(x_j) = y_j, f(x_{j+1}) = y_{j+1}$ and the first order derivatives of the function $f'(x_j) = D_j, f'(x_{j+1}) = D_{j+1}$, we can just set a system of equations to obtain the Hermite polynomial. It takes the following expression:*

$$g_j(x) = \frac{(D_j + D_{j+1})h + 2(y_{j+1} - y_j)}{h^3}(x - x_j)^2(x - x_{j+1}) + \frac{y_{j+1} - y_j - D_j h}{h^2}(x - x_j)^2 + D_j(x - x_j) + y_j. \tag{3.10}$$

It is clear from the expression in (3.10) that $O(h^3)$ is enough in D_j, D_{j+1} to preserve the $O(h^4)$ accuracy of the cubic Hermite interpolation.

3.3 Accurate approximation of first order derivatives using splines and data in the point-values

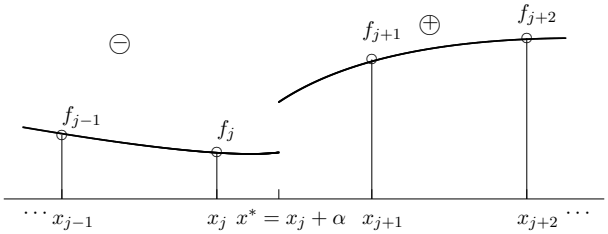

Figure 3.2: In this figure we can see an example of discontinuity in the function and its derivatives placed in the interval $[x_j, x_{j+1}]$ at a position $x^* = x_j + \alpha$.

Let us assume that there is a singularity at $x^* = x_j + \alpha$ in the interval $[x_j, x_{j+1}]$, just as shown in Figure 3.2. For the moment, let us assume that we know the position of the singularity and the jumps in the function and its derivatives. As shown in Figure 3.2, we label all the information about the function to the left of the singularity as $-$. The information to the right is labeled as $+$. Under this configuration, having the values of a sufficiently piecewise smooth function f at the nodes $x_0, x_1 \ldots, x_m$ and the jumps in the function and some of its derivatives at x^*, $[f], [f'], [f''], [f''']$, it is possible to correct the approximations of the first and second order derivatives of the function f computed through the cubic spline (3.4) at the same nodes $x_0, x_1 \ldots, x_m$ to obtain $O(h^3)$ accuracy. Of course, if there is a singularity, the system in (3.7) must be adapted to its presence in order to fulfil the accuracy and regularity requirements. In order to do this, we can modify the right hand side of the system in (3.7). For the general case presented in Figure 3.2, we can adapt the system in (3.7) by modifying the equations corresponding to D_j and D_{j+1}. At smooth zones of the data, it is clear that the system in (3.7) must hold, as the regularity conditions imposed at the nodes

are met. If a singularity is placed in the interval $[x_j, x_{j+1}]$, the system in (3.7) is not valid, as the function cannot be approximated accurately through a polynomial. As each equation of the system in (3.7) is designed to obtain a particular first order derivative D_j at the point x_j, if we encounter a singularity, we can just add a correction term at the right hand side of the system that takes into account the presence of the singularity and that allows for the obtention of the desired accuracy of the first order derivative. Let us summarize all the previous considerations in the following Lemma.

Lemma 5 *If the singularity is placed in the interval $[x_j, x_{j+1}]$, then the local truncation error C_j of the equation for the first order derivatives D_j is equal to*

$$\begin{aligned} C_j =& \left(3\,\frac{[f]}{h} - \frac{1}{24}\,\frac{(-48\,h+72\,\alpha)\,[f']}{h} - \frac{1}{24}\,\frac{\left(-36\,\alpha^2+48\,\alpha\,h-12\,h^2\right)[f'']}{h} \right. \\ & \left. - \frac{1}{24}\,\frac{\left(12\,\alpha^3+12\,h^2\alpha-24\,\alpha^2 h\right)[f''']}{h} \right) - \frac{1}{24}\,\frac{\left(-6\,h^2\alpha^2-3\,\alpha^4+h^4+8\,\alpha^3 h\right)[f^{(4)}]}{h} + O(h^4), \end{aligned} \tag{3.11}$$

and for the first order derivative D_{j+1} it is equal to

$$\begin{aligned} C_{j+1} =& \left(3\,\frac{[f]}{h} + \frac{1}{24}\,\frac{(-72\,\alpha+24\,h)\,[f']}{h} + \frac{1}{24}\,\frac{\left(-24\,\alpha\,h+36\,\alpha^2\right)[f'']}{h} \right. \\ & \left. + \frac{1}{24}\,\frac{\left(12\,\alpha^2 h-12\,\alpha^3\right)[f''']}{h} \right) + \frac{1}{24}\,\frac{\left(3\,\alpha^4-4\,\alpha^3 h\right)[f^{(4)}]}{h} + O(h^4). \end{aligned} \tag{3.12}$$

The equations for the first order derivatives D_j^- and D_{j+1}^+ in (3.7) are

$$\begin{aligned} D_{j-1}^- + 4D_j^- + D_{j+1}^+ &= 6\frac{f_{j+1}^+ - f_{j-1}^-}{2h}, \\ D_j^- + 4D_{j+1}^+ + D_{j+2}^+ &= 6\frac{f_{j+2}^+ - f_j^-}{2h}. \end{aligned} \tag{3.13}$$

Taking into account the presence of the singularity, using Taylor expansions and considering the resulting local truncation error, we can write the expression in (3.13) using quantities only from one side of the discontinuity. Let us denote by C_j^L the correction term for the left hand side of (3.13) and by C_j^R the correction term for the right hand side of (3.13),

$$\begin{aligned} D_{j-1}^- + 4D_j^- + D_{j+1}^+ &= D_{j-1}^- + 4D_j^- + D_{j+1}^- + C_j^L + O(h^4) = \frac{f_{j+1}^+ - f_{j-1}^-}{2h} = \frac{f_{j+1}^- - f_{j-1}^-}{2h} + C_j^R + O(h^4), \\ D_j^- + 4D_{j+1}^+ + D_{j+2}^+ &= D_j^+ + 4D_{j+1}^+ + D_{j+2}^+ + C_{j+1}^L + O(h^4) = \frac{f_{j+2}^+ - f_j^-}{2h} = \frac{f_{j+2}^+ - f_j^+}{2h} + C_{j+1}^R + O(h^4), \end{aligned} \tag{3.14}$$

so we can simply consider that, due to the presence of the singularity,

$$\begin{aligned} D_{j-1}^- + 4D_j^- + D_{j+1}^- &= 6\frac{f_{j+1}^- - f_{j-1}^-}{2h} + C_j + O(h^4), \\ D_j^+ + 4D_{j+1}^+ + D_{j+2}^+ &= 6\frac{f_{j+2}^+ - f_j^+}{2h} + C_{j+1} + O(h^4), \end{aligned} \tag{3.15}$$

where $C_j = C_j^R - C_j^L$ and $C_{j+1} = C_{j+1}^R - C_{j+1}^L$ amount to the local truncation error. These terms will depend on the position of the singularity and the jumps in the function and its derivatives. Thus, we will need the jump relations

$$\begin{aligned} [f] &= f^+(x^*) - f^-(x^*), \\ [f'] &= f_x^+(x^*) - f_x^-(x^*), \\ [f''] &= f_{xx}^+(x^*) - f_{xx}^-(x^*), \\ [f'''] &= f_{xxx}^+(x^*) - f_{xxx}^-(x^*). \end{aligned} \tag{3.16}$$

Looking at Figure 3.2 and (3.13), we can see that, in the equation for D_j^-, f_{j+1}^+ and D_{j+1}^+ belong to the + side of the domain, while D_j^- belongs to the − side. Thus, we can use the Taylor expansions of f_{j+1}^+ and D_{j+1}^+ around x^* and then use the jump relations $[f], [f'], [f''], [f''']$ in (3.16) to express the + values in terms of the − values. Assuming that we know the jump conditions in (3.16), or that we have a good approximation, we are ready to obtain expressions for f_{j+1}^+ in terms of f_{j+1}^- and for f_j^- in terms of f_j^+. Using Taylor expansions, we can write

$$\begin{aligned} f^-(x_j) = f_j^- &= f^-(x^*) - f_x^-(x^*)\alpha + \frac{1}{2}f_{xx}^-(x^*)\alpha^2 - \frac{1}{3!}f_{xxx}^-(x^*)\alpha^3 + O(h^4), \\ f^+(x_j) = f_j^+ &= f^+(x^*) - f_x^+(x^*)\alpha + \frac{1}{2}f_{xx}^+(x^*)\alpha^2 - \frac{1}{3!}f_{xxx}^+(x^*)\alpha^3 + O(h^4), \\ f^-(x_{j+1}) = f_{j+1}^- &= f^-(x^*) + f_x^-(x^*)(h-\alpha) + \frac{1}{2}f_{xx}^-(x^*)(h-\alpha)^2 + \frac{1}{3!}f_{xxx}^-(x^*)(h-\alpha)^3 + O(h^4), \\ f^+(x_{j+1}) = f_{j+1}^+ &= f^+(x^*) + f_x^+(x^*)(h-\alpha) + \frac{1}{2}f_{xx}^+(x^*)(h-\alpha)^2 + \frac{1}{3!}f_{xxx}^+(x^*)(h-\alpha)^3 + O(h^4), \end{aligned} \tag{3.17}$$

and subtracting we obtain

$$\begin{aligned} f_j^+ &= f_j^- + [f] - [f']\alpha + \frac{1}{2}[f'']\alpha^2 - \frac{1}{3!}[f''']\alpha^3 + O(h^4), \\ f_{j+1}^+ &= f_{j+1}^- + [f] + [f'](h-\alpha) + \frac{1}{2}[f''](h-\alpha)^2 + \frac{1}{3!}[f'''](h-\alpha)^3 + O(h^4). \end{aligned} \tag{3.18}$$

By replacing these expressions in the right hand side of (3.13), we obtain the local truncation error

for this part of the equation:

$$\begin{aligned}
\frac{f^+_{j+1}-f^-_{j-1}}{2h} &= \frac{f^-_{j+1}-f^-_{j-1}}{2h}+\frac{1}{2}\frac{[f]}{h}-\frac{1}{2}\frac{(\alpha-h)\,[f']}{h}+\frac{1}{4}\frac{\left(h^2-2\,h\alpha+\alpha^2\right)[f'']}{h}\\
&\quad-\frac{1}{12}\frac{\left(-h^3+3\,h^2\alpha-3\,h\alpha^2+\alpha^3\right)[f''']}{h}\\
&\quad+\frac{1}{48}\frac{\left(h^4-4\,h^3\alpha+6\,h^2\alpha^2-4\,h\alpha^3+\alpha^4\right)[f^{(4)}]}{h}+O(h^4)\\
&= \frac{f^-_{j+1}-f^-_{j-1}}{2h}+C^R_j+O(h^4),\\
\frac{f^+_{j+2}-f^-_{j}}{2h} &= \frac{f^+_{j+2}-f^+_{j}}{2h}+\frac{1}{2}\frac{[f]}{h}-\frac{1}{2}\frac{[f']\,\alpha}{h}+\frac{1}{4}\frac{[f'']\,\alpha^2}{h}-\frac{1}{12}\frac{[f''']\,\alpha^3}{h}\\
&\quad+\frac{1}{48}\frac{[f^{(4)}]\,\alpha^4}{h}+O(h^4)\\
&= \frac{f^+_{j+2}-f^+_{j}}{2h}+C^R_{j+1}+O(h^4).
\end{aligned}\tag{3.19}$$

The same thing can be done for the left hand side of (3.13). We can write that

$$\begin{aligned}
f^-_x(x_j) &= f^-_x(x^*)-f^-_{xx}(x^*)\alpha+\frac{1}{2}f^-_{xxx}(x^*)\alpha^2-\frac{1}{3!}f^-_{xxxx}(x^*)\alpha^3+O(h^4),\\
f^+_x(x_j) &= f^+_x(x^*)-f^+_{xx}(x^*)\alpha+\frac{1}{2}f^+_{xxx}(x^*)\alpha^2-\frac{1}{3!}f^+_{xxxx}(x^*)\alpha^3+O(h^4),\\
f^-_x(x_{j+1}) &= f^-_x(x^*)+f^-_{xx}(x^*)(h-\alpha)+\frac{1}{2}f^-_{xxx}(x^*)(h-\alpha)^2+\frac{1}{3!}f^-_{xxxx}(x^*)(h-\alpha)^3+O(h^4),\\
f^+_x(x_{j+1}) &= f^+_x(x^*)+f^+_{xx}(x^*)(h-\alpha)++\frac{1}{2}f^+_{xxx}(x^*)(h-\alpha)^2+\frac{1}{3!}f^+_{xxxx}(x^*)(h-\alpha)^3+O(h^4).
\end{aligned}\tag{3.20}$$

By subtracting and denoting $D^-_j = f^-_x(x_j), D^+_j = f^+_x(x_j), D^-_{j+1} = f^-_x(x_{j+1})$ and $D^+_{j+1} = f^+_x(x_{j+1})$ we obtain

$$\begin{aligned}
D^+_j &= D^-_j+[f']-[f'']\alpha+\frac{1}{2}[f''']\alpha^2-\frac{1}{3!}[f^{(4)}]\alpha^3+O(h^4),\\
D^+_{j+1} &= D^-_{j+1}+[f']+[f''](h-\alpha)+\frac{1}{2}[f'''](h-\alpha)^2+\frac{1}{3!}[f^{(4)}](h-\alpha)^3+O(h^4).
\end{aligned}\tag{3.21}$$

By replacing now (3.21) in the left hand side of (3.13), we get expressions for C^L_j and C^L_{j+1}:

$$\begin{aligned}
D^-_{j-1}+4D^-_j+D^+_{j+1} &= D^-_{j-1}+4D^-_j+D^-_{j+1}-[f']+[f'']\alpha-\frac{1}{2}[f''']\alpha^2+\frac{1}{3!}[f^{(4)}]\alpha^3+O(h^4)\\
&= D^-_{j-1}+4D^-_j+D^-_{j+1}+C^L_j+O(h^4),\\
D^-_j+4D^+_{j+1}+D^+_{j+2} &= D^+_j+4D^+_{j+1}+D^+_{j+2}+[f']+[f''](h-\alpha)+\frac{1}{2}[f'''](h-\alpha)^2+\frac{1}{3!}[f^{(4)}](h-\alpha)^3+O(h^4)\\
&= D^+_j+4D^+_{j+1}+D^+_{j+2}+C^L_{j+1}+O(h^4).
\end{aligned}\tag{3.22}$$

By replacing the expressions (3.19) in the right hand side of (3.13), and (3.22) in the left hand side, we recover the expression in (3.15):

$$\begin{aligned} D_{j-1}^- + 4D_j^- + D_{j+1}^- &= 6\frac{f_{j+1}^- - f_{j-1}^-}{2h} + C_j + O(h^4), \\ D_j^+ + 4D_{j+1}^+ + D_{j+2}^+ &= 6\frac{f_{j+2}^+ - f_j^+}{2h} + C_{j+1} + O(h^4), \end{aligned} \tag{3.23}$$

with the local truncation errors written as

$$\begin{aligned} C_j = C_j^R - C_j^L &= 3\,\frac{[f]}{h} - \frac{1}{24}\,\frac{(-48\,h + 72\,\alpha)\,[f']}{h} - \frac{1}{24}\,\frac{\left(-36\,\alpha^2 + 48\,\alpha\,h - 12\,h^2\right)[f'']}{h} \\ &\quad - \frac{1}{24}\,\frac{\left(12\,\alpha^3 + 12\,h^2\alpha - 24\,\alpha^2 h\right)[f''']}{h} - \frac{1}{24}\,\frac{\left(-6\,h^2\alpha^2 - 3\,\alpha^4 + h^4 + 8\,\alpha^3 h\right)[f^{(4)}]}{h} \\ &\quad + O(h^4), \\ C_{j+1} = C_{j+1}^R - C_{j+1}^L &= 3\,\frac{[f]}{h} + \frac{1}{24}\,\frac{(-72\,\alpha + 24\,h)\,[f']}{h} + \frac{1}{24}\,\frac{\left(-24\,\alpha\,h + 36\,\alpha^2\right)[f'']}{h} \\ &\quad + \frac{1}{24}\,\frac{\left(12\,\alpha^2 h - 12\,\alpha^3\right)[f''']}{h} + \frac{1}{24}\,\frac{\left(3\,\alpha^4 - 4\,\alpha^3 h\right)[f^{(4)}]}{h} + O(h^4). \end{aligned} \tag{3.24}$$

Note that, if x^* is unknown, we only need to locate the interval that contains the singularity to obtain an accurate computation of the first order derivatives at the nodes through the spline. Then, we can give a rough approximation $\tilde{x}^*$ of x^* inside that interval, and use it to obtain accurate approximations of the jump in the function and its derivatives at the chosen $\tilde{x}^*$ (for example, using one-sided interpolation, as explained in [49]). For the cubic Hermite spline, we need $O(h^4)$ accuracy for $[f]$, $O(h^3)$ accuracy for $[f']$, and so on. This observation is straightforward if we look at the expression of the correction terms in (3.24). Of course, the use of an inaccurate $\tilde{x}^*$ instead of x^* (but still inside the interval that contains the singularity), will produce a large error in the approximation of the function in the interval that contains the singularity (typically an error of order $O(1)$ for jumps in the function and $O(h)$ for jumps in the first order derivative), but not in the approximation of the first order derivatives at the nodes. Moreover, it would also provide a reconstruction of the function without oscillations. Later on (in Remark 5) we will discuss how the approximation of the location of the singularity affects the interpolation of the function through the spline. The location of the interval that contains a jump discontinuity in the function, or the approximated location of a discontinuity in the first order derivative can be done using Harten's ENO-SR (essentially non oscillatory-subcell resolution). A nice discussion about the process, with an improved algorithm for the location, is given in [32].

Let us consider now the Hermite spline in the interval $[a, b]$, constructed using $m + 1$ points belonging to a piecewise continuous function that contains a singularity at $x^* \in [x_j, x_{j+1}]$ and that is at least four times continuously differentiable except at x^*. Let us follow the same notation as before and denote the information to the left of the singularity with the $-$ symbol and to the right

with the + symbol. The system of equations for the first order derivatives at the nodes can be expressed as

$$\begin{bmatrix} 4 & 1 & 0 & \cdots & 0 & 0 & 0 & 0 & \cdots & 0 & 0 \\ 1 & 4 & 1 & \cdots & 0 & 0 & 0 & 0 & \cdots & 0 & 0 \\ \cdots & \cdots & \cdots & \cdots & \cdots & \cdots & \cdots & \cdots & \cdots & \cdots & \cdots \\ 0 & 0 & 0 & \cdots & 1 & 4 & 1 & 0 & \cdots & 0 & 0 \\ 0 & 0 & 0 & \cdots & 0 & 1 & 4 & 1 & \cdots & 0 & 0 \\ \cdots & \cdots & \cdots & \cdots & \cdots & \cdots & \cdots & \cdots & \cdots & \cdots & \cdots \\ 0 & 0 & 0 & \cdots & 0 & 0 & 0 & 0 & \cdots & 1 & 4 \end{bmatrix} \begin{bmatrix} D_1^- \\ D_2^- \\ \cdots \\ D_j^- \\ D_{j+1}^+ \\ \cdots \\ D_{m-1}^+ \end{bmatrix} = 6 \begin{bmatrix} \frac{\delta_1^- + \delta_2^-}{2} - \frac{D_0^-}{6} \\ \frac{\delta_2^- + \delta_3^-}{2} \\ \cdots \\ \frac{f_{j+1}^+ - f_{j-1}^-}{2h} \\ \frac{f_{j+2}^+ - f_j^-}{2h} \\ \cdots \\ \frac{\delta_{m-1}^+ + \delta_m^+}{2} - \frac{D_m^+}{6} \end{bmatrix}. \tag{3.25}$$

Now we can prove the following theorem.

Theorem 5 *(Accuracy of adapted first order derivatives close to singularities)*

Let us consider a piecewise continuous function f that contains a singularity at x^* and that is at least four times continuously differentiable on $R\backslash\{x^*\}$ with uniformly bounded derivatives. The first order derivatives obtained through the non-corrected system of the spline for this function satisfy

$$||f' - D||_{L^\infty} \leq \max\{|C_j|, |C_{j+1}|\}, \tag{3.26}$$

where C_j, C_{j+1} are given in Lemma 5.

The addition of the correction terms $-C_j, -C_{j+1}$ up to $O(h^3)$, i.e. the subtraction of the local truncation errors in (3.24) up to $O(h^3)$, to the right hand side of the equations of the spline for D_j and D_{j+1} in the system (3.25) allows for the computation of first order derivatives that satisfy

$$||f' - D||_{L^\infty} \leq Ch^3 \sup_{c \in R\backslash\{x^*\}} |f^{(4)}(c)| + Kh^3[f^{(4)}], \tag{3.27}$$

for all $h > 0$, with $K, C > 0$ independent of f.

For simplicity we will take a uniform partition of the considered interval. The proof presented in what follows can be extended to a non-uniform partition. Let us represent the system in (3.25) by $AD = d$. Let F and r be the vectors,

$$F = \begin{bmatrix} f'(x_1) \\ f'(x_2) \\ \cdots \\ f'(x_{m-1}) \end{bmatrix}, \quad r = d - AF = A(D - F), \tag{3.28}$$

where $f'(x)$ are the first order derivatives of f at the nodes.

For $i = 1, \ldots, j-1, j+2, \ldots, m-1$ we can use Taylor's expansion to express $y_{i-1} = f(x_{i-1})$ and $y_{i+1} = f(x_{i+1})$ in terms of $f(x_i)$ and the derivatives of f at x_i,

$$r_i = 6\left(\frac{y_{i+1} - y_{i-1}}{2h}\right) - D_{i-1} - 4D_i - D_{i+1}. \tag{3.29}$$

Now we can use Taylor's expansion to express $y_{i-1} = f(x_{i-1})$, $y_{i+1} = f(x_{i+1})$, D_{i-1} and D_{i+1} in terms of $f(x_i)$ and the derivatives of f at x_i,

$$\begin{aligned} r_i &= \frac{3}{h}\Bigg(\left(f(x_i) + hf'(x_i) + \frac{h^2}{2}f''(x_i) + \frac{h^3}{6}f'''(x_i) + \frac{h^4}{24}f^{(4)}(\tau_1) \right) \\ &- \left(f(x_i) - hf'(x_i) + \frac{h^2}{2}f''(x_i) - \frac{h^3}{6}f'''(x_i) + \frac{h^4}{24}f^{(4)}(\tau_2) \right) \Bigg) \\ &- \left(f'(x_i) + hf''(x_i) + \frac{h^2}{2}f'''(x_i) + \frac{h^3}{6}f^{(4)}(\tau_3) \right) - 4f'(x_i) \\ &- \left(f'(x_i) - hf''(x_i) + \frac{h^2}{2}f'''(x_i) - \frac{h^3}{6}f^{(4)}(\tau_4) \right) \\ &= \frac{1}{24}h^3 \left(3f^{(4)}(\tau_1) - 3f^{(4)}(\tau_2) - 4f^{(4)}(\tau_3) + 4f^{(4)}(\tau_4) \right), \end{aligned} \tag{3.30}$$

with $\tau_n \in [x_{i-1}, x_{i+1}], n = 1, \ldots, 4$. Therefore, for $i = 1, \ldots, j-1, j+2, \ldots, m-1$ we obtain

$$|r_i| \leq \frac{7}{12} \sup_{c \in [x_{i-1}, x_{i+1}]} |f^{(4)}(c)| h^3. \tag{3.31}$$

Note that if the boundary conditions D_0^-, D_m^+ are exact, the previous bound holds.

If we assume that the singularity is placed in the interval $[x_j, x_{j+1}]$, just as shown in Figure 3.2, the process to obtain r_j is similar, but we need to follow the same steps taken to obtain the local truncation error in (3.24): use Taylor expansions around x^* to express the values y_{j+1}^+ and $f_x^+(x_{j+1})$ in terms of the $-$ side (or viceversa) using the jump relations as in (3.18) and (3.21). After some basic algebra, we obtain that the r_j that comes from (3.25) satisfies

$$\begin{aligned} r_j &= 6\left(\frac{y_{j+1}^+ - y_{j-1}^-}{2h} \right) - f_x^-(x_{j-1}) - 4f_x^-(x_j) - f_x^+(x_{j+1}) \\ &= 6\left(\frac{y_{j+1}^- - y_{j-1}^-}{2h} \right) + C_j - f_x^-(x_{j-1}) - 4f_x^-(x_j) - f_x^-(x_{j+1}) + O(h^4). \end{aligned}$$

By replicating the process for r_{j+1}, we easily obtain the bound in (3.26), corresponding to the non-corrected spline. Thus, if we subtract to r_j the local truncation error C_j in (3.24) up to $O(h^3)$,

we obtain

$$
\begin{aligned}
r_j - C_j &= 6\left(\frac{y^-_{j+1} - y^-_{j-1}}{2h}\right) - f^-_x(x_{j-1}) - 4f^-_x(x_j) - f^-_x(x_{j+1}) \\
&\quad - \frac{1}{24}\frac{\left(-6\,h^2\alpha^2 - 3\,\alpha^4 + h^4 + 8\,\alpha^3 h\right)[f^{(4)}]}{h} + O(h^4) \\
&= \frac{3}{h}\left(y^-_{j+1} - y^-_{j-1}\right) - f^-_x(x_{j-1}) - 4f^-_x(x_j) - f^-_x(x_{j+1}) \\
&\quad - \frac{1}{24}\frac{\left(-6\,h^2\alpha^2 - 3\,\alpha^4 + h^4 + 8\,\alpha^3 h\right)[f^{(4)}]}{h} + O(h^4) \\
&= \frac{1}{24}h^3\left(3f^{(4)}(\tau_1) - 3f^{(4)}(\tau_2) - 4f^{(4)}(\tau_3) + 4f^{(4)}(\tau_4)\right) \\
&\quad - \frac{1}{24}\frac{\left(-6\,h^2\alpha^2 - 3\,\alpha^4 + h^4 + 8\,\alpha^3 h\right)[f^{(4)}]}{h} + O(h^4),
\end{aligned}
\tag{3.32}
$$

with $\tau_n \in [x_{i-1}, x_{i+1}], n = 1, \ldots, 4$. For the equation of D_{j+1} in (3.25), the result is equivalent. Taking into account the expression of A in (3.25), the norm of its inverse is $||A^{-1}||_{L^\infty} \leq 1$ (see, for example, Theorem 2.1 of [55]), and since $r = A(D - F)$, then $||D - F||_{L^\infty} \leq ||r||_{L^\infty}$. Therefore we obtain the bound in (3.27) by just applying the triangular inequality to the norm of the vector r.

Thus, the subtraction of the local truncation error to the right hand side of the system in (3.25),

$$
\begin{aligned}
&\begin{bmatrix}
4 & 1 & 0 & \cdots & 0 & 0 & 0 & 0 & \cdots & 0 & 0 \\
1 & 4 & 1 & \cdots & 0 & 0 & 0 & 0 & \cdots & 0 & 0 \\
\cdots & \cdots & \cdots & \cdots & \cdots & \cdots & \cdots & \cdots & \cdots & \cdots & \cdots \\
0 & 0 & 0 & \cdots & 1 & 4 & 1 & 0 & \cdots & 0 & 0 \\
0 & 0 & 0 & \cdots & 0 & 1 & 4 & 1 & \cdots & 0 & 0 \\
\cdots & \cdots & \cdots & \cdots & \cdots & \cdots & \cdots & \cdots & \cdots & \cdots & \cdots \\
0 & 0 & 0 & \cdots & 0 & 0 & 0 & 0 & \cdots & 1 & 4
\end{bmatrix}
\begin{bmatrix}
D^-_1 \\ D^-_2 \\ \cdots \\ D^-_j \\ D^+_{j+1} \\ \cdots \\ D^+_{m-1}
\end{bmatrix} \\
&= 6\begin{bmatrix}
\frac{\delta^-_1 + \delta^-_2}{2} - \frac{D^-_0}{6} \\
\frac{\delta^-_2 + \delta^-_3}{2} \\
\cdots \\
\frac{f^+_{j+1} - f^-_{j-1}}{2h} - C_j \\
\frac{f^+_{j+2} - f^-_j}{2h} - C_{j+1} \\
\cdots \\
\frac{\delta^+_{m-1} + \delta^+_m}{2} - \frac{D^+_m}{6}
\end{bmatrix}
= 6\begin{bmatrix}
\frac{\delta^-_1 + \delta^-_2}{2} - \frac{D^-_0}{6} \\
\frac{\delta^-_2 + \delta^-_3}{2} \\
\cdots \\
\frac{f^+_{j+1} - f^-_{j-1}}{2h} \\
\frac{f^+_{j+2} - f^-_j}{2h} \\
\cdots \\
\frac{\delta^+_{m-1} + \delta^+_m}{2} - \frac{D^+_m}{6}
\end{bmatrix}
+ 6\begin{bmatrix}
0 \\ 0 \\ 0 \\ \cdots \\ -C_j \\ -C_{j+1} \\ \cdots \\ 0 \\ 0
\end{bmatrix},
\end{aligned}
\tag{3.33}
$$

allows for the obtention of first order derivatives with the bound for the error given in (3.27).

It is also important to note that, in order to solve the system in (3.33), we need to know its right hand side. The right hand side of the system in (3.33) is composed of finite difference approximations of the first order derivative. Thus, if the positions of the singularities are not known, the processing of these differences can be used to approximate their location. See for example the algorithm described in [50].

Remark 3 *If the data presents more than one singularity, the treatment is exactly the same. If an algorithm for locating the singularity is used, the only requirement is that the singularities are placed far enough from each other, i.e. at such a distance that the location algorithm is capable of distinguishing between two contiguous singularities. In the case of the algorithm presented in [50], singularities must be placed one stencil away from each other (four points for cubic polynomials).*

3.4 Analysis of the absence of the Gibbs phenomenon close to jump discontinuities in the cubic Hermite spline using corrected first order derivatives

In this section we will analyse the absence of the Gibbs phenomenon when using the corrected first order derivatives.

In Theorem 5 we have proved that the accuracy attained in the first order derivatives computed using the corrected system (3.33) is $O(h^3)$ in the infinity norm. With this result, it is posible to prove that, using these derivatives, the Hermite spline does not introduce the Gibbs phenomenon close to jump discontinuities.

We should start by introducing the definition of the Gibbs phenomenon given by D. Gottlieb and C.-W. Shu in [24].

Definition 1 *The Gibbs phenomenon*

Given a punctually discontinuous function f and its sampling, defined by $f(x_i) = f(ih)$, the Gibbs phenomenon deals with the convergence of the function g based on $f(x_i)$ towards f when h goes to zero. It can be characterized by two features ([24]):

1. *Away from the discontinuity, the convergence is rather slow and for any point x*

$$|f(x) - g(x)| = O(h).$$

2. *There is an overshoot, close to the discontinuity, that does not diminish with the reduction of h. Thus,*

$$\max|f(x) - g(x)| \text{ does not tend to zero with } h.$$

With the results about the accuracy of the first order derivatives obtained in Theorem 5 and the previous definition of the Gibbs phenomenon, we can state the following theorem.

Theorem 6 *Absence of the Gibbs phenomenon*

The Hermite spline obtained using the adapted first order derivatives computed through (3.33) does not introduce Gibbs oscillations close to jump discontinuities in the function.

We can analyse two cases. The first one is when the considered interval does not contain a singularity. In this case, Theorem 5 assures $O(h^3)$ accuracy for the first order derivatives. And, as

mentioned in Remark 2, this is enough for the Hermite spline to attain $O(h^4)$ accuracy at smooth zones, so no Gibbs oscillations are possible.

The second case is when the considered interval contains a jump discontinuity in the function. Let us assume that the singularity is in the interval $[x_j, x_{j+1}]$. In (3.27), Theorem 5 assures that the first order derivatives attained through the corrected system in (3.33) also have $O(h^3)$ order of accuracy. Thus, it can be considered that the vector of first order derivatives D that results from solving (3.33) will be

$$||D||_{L^\infty} = O(1). \tag{3.34}$$

Now, considering (3.3) we can write

$$\begin{aligned} a_j &= \frac{hD_{j+1} + D_j h + 2y_j - 2y_{j+1}}{h^3} = \frac{O(h) + O(h) + 2y_j - 2y_{j+1}}{h^3}, \\ b_j &= -\frac{hD_{j+1} + 2D_j h + 3y_j - 3y_{j+1}}{h^2} = -\frac{O(h) + 2O(h) + 3y_j - 3y_{j+1}}{h^2}, \\ c_j &= D_j = O(1), \\ d_j &= y_j. \end{aligned} \tag{3.35}$$

If we consider that there is a jump discontinuity in the interval $[x_j, x_{j+1}]$, then $y_{j+1} - y_j = O(1)$ and

$$\begin{aligned} d_j &= y_j, \\ c_j &= D_j = O(1), \\ b_j &= -\frac{hD_{j+1} + 2D_j h + 3y_j - 3y_{j+1}}{h^2} = -\frac{O(h) + 2O(h) - 3O(1)}{h^2} = \frac{O(1)}{h^2} = O\left(\frac{1}{h^2}\right), \\ a_j &= \frac{hD_{j+1} + D_j h + 2y_j - 2y_{j+1}}{h^3} = \frac{O(h) + O(h) - 2O(1)}{h^3} = \frac{O(1)}{h^3} = O\left(\frac{1}{h^3}\right). \end{aligned} \tag{3.36}$$

And if $x \in [x_j, x_{j+1}]$, the equation of the spline (3.1) transforms into

$$\begin{aligned} g_j(x) &= a_j(x - x_j)^3 + b_j(x - x_j)^2 + c_j(x - x_j) + d_j = O\left(\frac{1}{h^3}\right) O\left(h^3\right) \\ &+ O\left(\frac{1}{h^2}\right) O\left(h^2\right) + O\left(h\right) + y_j = y_j + O(1). \end{aligned} \tag{3.37}$$

This means that the error attained by the Hermite spline with $O(h^3)$ accurate first order derivatives provides $O(h^4)$ accuracy when interpolating the data, except at the interval that contains the discontinuity, where the approximation is $O(1)$ accurate.

Now we only need to check that the approximation provided by the spline is in the interval $[y_j, y_{j+1}]$ when h goes to zero. In order to verify this assumption, we can write the equation of the

spline in (3.1) as

$$\begin{aligned} g_j(x) &= a_j(x-x_j)^3 + b_j(x-x_j)^2 + c_j(x-x_j) + d_j \\ &= \frac{hD_{j+1} + D_j h + 2y_j - 2y_{j+1}}{h^3}(x-x_j)^3 - \frac{hD_{j+1} + 2D_j h + 3y_j - 3y_{j+1}}{h^2}(x-x_j)^2 \\ &+ D_j(x-x_j) + y_j. \end{aligned} \tag{3.38}$$

Introducing the change of variables $s = \frac{x-x_j}{h}$, we get

$$\begin{aligned} g_j(x) &= (hD_{j+1} + D_j h + 2y_j - 2y_{j+1})\, s^3 - (hD_{j+1} + 2D_j h + 3y_j - 3y_{j+1})\, s^2 + D_j h s + y_j, \\ &= \left(1 - s^2(3-2s)\right) y_j + s^2(3-2s) y_{j+1} + \left(s^3 - 2s^2 + s\right) hD_j + \left(s^3 - s^2\right) hD_{j+1} \\ &= b_1(s) y_{j+1} + b_2(s) y_j + b_3(s) hD_j + b_4(s) hD_{j+1}, \end{aligned} \tag{3.39}$$

for $s \in [0,1]$. The expression can also be reformulated as follows:

$$g_j(x) = y_j + \left(s^2(3-2s)\right)(y_{j+1} - y_j) + \left(s^3 - 2s^2 + s\right) hD_j + \left(s^3 - s^2\right) hD_{j+1}, \tag{3.40}$$

where the first two terms of (3.40) are just a dilation and a translation of the Hermite base function $b_1(s) = s^2(3-2s)$. This function presents a minimum at $s = 0$ and a maximum at $s = 1$, so no Gibbs oscillations can be introduced by this element of the Hermite base, as can be seen in Figure 3.1. In this Figure it can be observed that the base functions $b_3(s)$ and $b_4(s)$ oscillate. Thus, Gibbs oscillations can appear if these bases appear multiplied by large coefficients. As we have already mentioned, in (3.40) D_j and D_{j+1} are $O(1)$. With these considerations in mind, it is not difficult to conclude that the last two terms in (3.40) go to zero when $h \to 0$. So no Gibbs oscillation is possible.

It should be noted that an analogous analysis can be done for the classical spline. In this case, the vector of first order derivatives D that results from solving (3.33) without the correction terms will be

$$||D||_{L^\infty} = O\left(\frac{1}{h}\right), \tag{3.41}$$

due to the bound in (3.26) and the expressions for C_j, C_{j+1} given in Lemma 5. Following exactly the same arguments as before and rewriting the expressions from (3.35) to (3.40) taking into account (3.41) in the process, we can easily conclude that the classical spline introduces the Gibbs phenomenon close to jump discontinuities in the function.

3.5 Full accuracy of the adapted Hermite interpolation

Once the first order derivatives have been calculated with $O(h^3)$ accuracy, if we use them directly in the expression in (3.4) without any other enhancement, the interpolation will lose its accuracy at the interval $[x_j, x_{j+1}]$ that contains the singularity, as it has been analysed in Theorem 6. This is logical, as the interpolation in the interval $[x_j, x_{j+1}]$ can be seen as a particularization of a linear combination of the polynomials of the Hermite basis, which are continuous. This situation can be solved by defining a piecewise continuous Hermite polynomial at the interval $[x_j, x_{j+1}]$.

Remark 4 *The exact location of jump discontinuities and the definition of the function at x^* is lost during the point-values discretization. Thus, to obtain a reconstruction at x^*, not only the location of the discontinuity must be provided, but also which of the two definitions corresponds to this point. If the discontinuities are in the derivatives, this problem does not arise, as the function is continuous.*

Let us consider the following lemma.

Lemma 6 *Let us assume that the first order derivatives of the function at the nodes have been obtained with $O(h^3)$ accuracy. Let us assume that the data presents a singularity at x^* with $x_j \leq x^* \leq x_{j+1}$ and, without loss of generality, that we know that $f(x^*)$ belongs to the $-$ side of the function. Then, the local truncation error of the non-corrected spline in the interval $[x_j, x^*]$ is*

$$\begin{aligned} C^-(x) = & \left(3\,\frac{(x-x_j)^2}{h^2} - 2\,\frac{(x-x_j)^3}{h^3} \right)[f] \\ & + \left(-\frac{(-2\,h+3\,\alpha)\,(x-x_j)^2}{h^2} + \frac{(-h+2\,\alpha)\,(x-x_j)^3}{h^3} \right)[f'] \\ & + \left(\frac{\Big(-(h-\alpha)^2 + h\,(h-\alpha)\Big)\,(x-x_j)^3}{h^3} - \frac{\Big(-\frac{3}{2}\,(h-\alpha)^2 + h\,(h-\alpha)\Big)\,(x-x_j)^2}{h^2} \right)[f''] \\ & + \left(\frac{\Big(\frac{1}{2}\,h\,(h-\alpha)^2 - \frac{1}{3}\,(h-\alpha)^3\Big)\,(x-x_j)^3}{h^3} - \frac{\Big(\frac{1}{2}\,h\,(h-\alpha)^2 - \frac{1}{2}\,(h-\alpha)^3\Big)\,(x-x_j)^2}{h^2} \right)[f'''] + O(h^4). \end{aligned} \tag{3.42}$$

In the interval $(x^*, x_{j+1}]$ the local truncation error is

$$C^+(x) = C^-(x) - \left([f] + (x-x^*)[f'] + \frac{1}{2}(x-x^*)^2[f''] + \frac{1}{3!}(x-x^*)^3[f'''] \right) + O(h^4). \tag{3.43}$$

As mentioned in the lemma, we have two possible cases:

- The first one is when the interpolation is being obtained at a position $x_j \leq x \leq x^*$. In this case, the first order derivative D^+_{j+1} and the data point y^+_{j+1} belong to the $+$ side of the singularity while the interpolation point x is at the $-$ side. We can use the same technique applied before to obtain the correction terms for the first order derivatives in order to assure the accuracy of the interpolation. Let us consider again Figure 3.2. In the interval $[x_j, x_{j+1}]$, the Hermite interpolation in (3.4) will have the following expression:

$$\begin{aligned} g_j(x) = & \frac{hD^+_{j+1} + D^-_j h + 2y^-_j - 2y^+_{j+1}}{h^3}(x-x_j)^3 \\ & - \frac{hD^+_{j+1} + 2D^-_j h + 3y^-_j - 3y^+_{j+1}}{h^2}(x-x_j)^2 + D^-_j(x-x_j) + y^-_j. \end{aligned} \tag{3.44}$$

Now we can use (3.18) and (3.21) to obtain an expression of the corrected spline in the interval $[x_j, x^*]$:

$$
\begin{aligned}
g_j(x) = & \frac{hD_{j+1}^- + D_j^- h + 2y_j^- - 2y_{j+1}^-}{h^3}(x-x_j)^3 \\
& - \frac{hD_{j+1}^- + 2D_j^- h + 3y_j^- - 3y_{j+1}^-}{h^2}(x-x_j)^2 + D_j^-(x-x_j) + y_j^- \\
& + \left(3\,\frac{(x-x_j)^2}{h^2} - 2\,\frac{(x-x_j)^3}{h^3}\right)[f] \\
& + \left(-\frac{(-2\,h+3\,\alpha)\,(x-x_j)^2}{h^2} + \frac{(-h+2\,\alpha)\,(x-x_j)^3}{h^3}\right)[f'] \\
& + \left(\frac{\left(-(h-\alpha)^2 + h\,(h-\alpha)\right)(x-x_j)^3}{h^3} - \frac{\left(-\frac{3}{2}\,(h-\alpha)^2 + h\,(h-\alpha)\right)(x-x_j)^2}{h^2}\right)[f''] \\
& + \left(\frac{\left(\frac{1}{2}\,h\,(h-\alpha)^2 - \frac{1}{3}\,(h-\alpha)^3\right)(x-x_j)^3}{h^3} - \frac{\left(\frac{1}{2}\,h\,(h-\alpha)^2 - \frac{1}{2}\,(h-\alpha)^3\right)(x-x_j)^2}{h^2}\right)[f'''] \\
& + O(h^4) \\
& = g_j^-(x) + C^-(x) + O(h^4).
\end{aligned}
\tag{3.45}
$$

In fact, the $O(h^4)$ term in the previous expression can be written as

$$
T_4^-(x) = \left(\frac{\left(\frac{1}{6}\,h\,(h-\alpha)^3 - \frac{1}{12}\,(h-\alpha)^4\right)(x-xj)^3}{h^3} - \frac{\left(\frac{1}{6}\,h\,(h-\alpha)^3 - \frac{1}{8}\,(h-\alpha)^4\right)(x-xj)^2}{h^2}\right)[f^{(4)}] + \cdots
\tag{3.46}
$$

- The second one is when the interpolation is being obtained at a position $x^* < x \leq x_{j+1}$. In this case, the first order derivative D_j^- and the data y_j^- belong to the $-$ side of the singularity

while the interpolation point x is at the + side. Proceeding as before, we have

$$
\begin{aligned}
g_j(x) = & \frac{hD_{j+1}^+ + D_j^+ h + 2y_j^+ - 2y_{j+1}^+}{h^3}(x-x_j)^3 \\
& - \frac{hD_{j+1}^+ + 2D_j^+ h + 3y_j^+ - 3y_{j+1}^+}{h^2}(x-x_j)^2 + D_j^+(x-x_j) + y_j^+ \\
& + \left(-2\,\frac{(x-x_j)^3}{h^3} - 1 + 3\,\frac{(x-x_j)^2}{h^2}\right)[f] \\
& + \left(\frac{(-h+2\,\alpha)\,(x-x_j)^3}{h^3} - \frac{(-2\,h+3\,\alpha)\,(x-x_j)^2}{h^2} + \alpha - x + x_j\right)[f'] \\
& + \left(\frac{\left(h\alpha-\alpha^2\right)(x-x_j)^3}{h^3} - \frac{\left(2\,h\alpha - \frac{3}{2}\,\alpha^2\right)(x-x_j)^2}{h^2} + \alpha\,(x-x_j) - \frac{1}{2}\,\alpha^2\right)[f''] \\
& + \left(\frac{\left(\frac{1}{3}\,\alpha^3 - \frac{1}{2}\,h\alpha^2\right)(x-x_j)^3}{h^3} + \frac{1}{6}\,\alpha^3 - \frac{1}{2}\,\alpha^2\,(x-x_j) - \frac{\left(\frac{1}{2}\,\alpha^3 - h\alpha^2\right)(x-x_j)^2}{h^2}\right)[f'''] + O(h^4) \\
& = g_j^+(x) + C^+(x) + O(h^4) \\
& = g_j^+(x) + C^-(x) - \left([f] + (x-x^*)[f'] + \frac{1}{2}(x-x^*)^2[f''] + \frac{1}{3!}(x-x^*)^3[f''']\right) + O(h^4).
\end{aligned}
\tag{3.47}
$$

In the previous expression, the $O(h^4)$ term can be written as

$$
T_4^+(x) = \left(\frac{\left(-\frac{1}{12}\,\alpha^4 + \frac{1}{6}\,h\alpha^3\right)(x-xj)^3}{h^3} - \frac{\left(-\frac{1}{8}\,\alpha^4 + \frac{1}{3}\,h\alpha^3\right)(x-xj)^2}{h^2} - \frac{1}{24}\,\alpha^4 + \frac{1}{6}\,\alpha^3\,(x-xj)\right)[f^{(4)}] + \cdots
\tag{3.48}
$$

From (3.47), we can see that we obtain again a relation between the correction terms for the spline similar to that obtained for the data in (3.18),

$$
C^+(x) = C^-(x) - \left([f] + (x-x^*)[f'] + \frac{1}{2}(x-x^*)^2[f''] + \frac{1}{3!}(x-x^*)^3[f''']\right) + O(h^4).
$$

Now we have all the necessary tools to prove the following theorem.

Theorem 7 *(Accuracy of the corrected Hermite interpolation close to singularities)*

Let us consider a piecewise continuous function f that contains a singularity at $x^* \in [x_j, x_{j+1}]$ and that is at least four times continuously differentiable on $R\backslash\{x^*\}$. Let us assume, without loss of generality, that we know that $f(x^*)$ belongs to the $-$ side of the function. Let us also consider that the first order derivatives at the nodes are available with at least $O(h^3)$ accuracy. The approximation obtained through the non-corrected Hermite spline for this function satisfies

$$
|f(x) - g_j(x)| \leq \max\{|C^+(x)|, |C^-(x)|\}, x \in [x_j, x_{j+1}],
\tag{3.49}
$$

where $C^+(x), C^-(x)$ are given in Lemma 6.

The addition of the correction terms $-C^-(x)$ when $x \in [x_j, x^*]$ and $-C^+(x)$ when $x \in (x^*, x_{j+1}]$, i.e. the subtraction of the local truncation error given in Lemma 6 to the approximation obtained by the non-corrected Hermite spline results in the accuracy

$$|f(x) - g_j(x)| \leq \begin{cases} \max\left\{\frac{13}{24}h^4|[f^{(4)}]|, \frac{1}{384}h^4 \sup\limits_{\xi\in[x_j,x^*]}|f^{(4)}(\xi)|\right\}, & x \in [x_j, x^*], \\ \max\left\{\frac{2}{3}h^4|[f^{(4)}]|, \frac{1}{384}h^4 \sup\limits_{\xi\in(x^*,x_{j+1}]}|f^{(4)}(\xi)|\right\}, & x \in (x^*, x_{j+1}], \\ \frac{1}{384}h^4 \sup\limits_{\xi\in[x_j,x_{j+1}]}|f^{(4)}(\xi)|, & \textit{in any other case,} \end{cases} \tag{3.50}$$

for all $h > 0$, independent of f.

For smooth functions, the error has been analysed in Theorem 4 and is given in (3.8).

Now we can consider the case when there is a singularity in the interval $[x_j, x_{j+1}]$. Looking at the results obtained in expressions (3.42) and (3.43) of Lemma 6, we can see the local truncation error obtained when approximating the data using the uncorrected spline. We can just change the sign of the local truncation error, i.e isolate $g_j^-(x)$ or $g_j^+(x)$, to write that

$$g_j^-(x) = g_j(x) - C^-(x) + O(h^4), \quad x_j < x \leq x^*, \tag{3.51}$$

$$g_j^+(x) = g_j(x) - C^+(x) + O(h^4), \quad x^* < x < x_{j+1}, \tag{3.52}$$

and to conclude that the addition of the correction terms $-C^-(x)$ in the interval $[x_j, x^*]$ or $-C^+(x)$ in the interval $(x^*, x_{j+1}]$ allows us to keep the accuracy of the spline close to the singularities. In fact, looking at the $O(h^4)$ terms in the local truncation error, we can see that the term in (3.46) can be roughly bounded by

$$|T_4^-(x)| \leq \frac{13}{24}|[f^{(4)}]|h^4, \tag{3.53}$$

and the one in (3.48) can be bounded in the same way by

$$|T_4^+(x)| \leq \frac{2}{3}|[f^{(4)}]|h^4. \tag{3.54}$$

Remark 5 *Let us assume now that we do not know the exact location of the singularity x^* and we approximate it by $\tilde{x}^*$. For simplicity, we can assume that $\tilde{x}^*$ is located to the right of x^* at a distance β (which is the error of location). Then, using Taylor's expansion on the jump in the function or the derivatives, we get*

$$\begin{aligned} [f(\tilde{x}^*)] &= [f] + \beta[f'] + \frac{\beta^2}{2}[f''] + \cdots, \\ \left[f'(\tilde{x}^*)\right] &= [f'] + \beta[f''] + \frac{\beta^2}{2}[f'''] + \cdots \end{aligned} \tag{3.55}$$

Therefore, from replacing these expressions in the local truncation error in (3.42) or (3.43), we derive that an error in the location of the discontinuity leads to an error of the size of the jump of the function in the interval between $\tilde{x}^*$ and x^*. In the case of jumps in the first order derivative, the problem can be solved computing an accurate enough $\tilde{x}^*$. Thus, in order to keep order of accuracy $O(h^4)$ for the cubic spline, we just need the error of location β to be of order $O(h^4)$. It is noteworthy that if there is a false detection of the singularity at a smooth zone, the jumps should be zero (if known a priori) or close enough to zero (if approximated) [49].

Remark 6 *Although we have introduced the corrected cubic Hermite spline for cases where the location of the singularities and the jump in the function and its derivatives are known, this information can be approximated numerically in certain instances.*

When working with data derived from the discretization of piecewise smooth functions, sometimes it is possible to detect the singularities and compute their location. Some kinds of singularities are jump discontinuities in the function and kinks, meaning jumps in the function or the first order derivative respectively. The location of these singularities can be found depending on the discretization of the data used. Kinks can be located using the point-value discretization, i.e. a sampling of the function. There is no way of locating the position of jump discontinuities using this kind of discretization: the exact position is lost during the discretization process. For data discretized using point-values, the location of kinks can be obtained, for example, using the classical approach proposed by Harten for his ENO subcell resolution (ENO-SR) algorithm [51, 50]. In [50], the authors introduce the ENO-SR algorithm and propose its implementation for the point-values discretization of the data.

Once the location of the singularity has been approximated, it is also possible to approximate the jump in the function and its derivatives using one-sided interpolation. See for example [49] for a detailed explanation about this point.

We will verify the previous assertions in the Numerical experiments section.

Corollary 3 *(Error of the second order derivative of the corrected cubic Hermite interpolation)*

Under the assumptions of Theorem (7), the error for the second order derivative of the corrected cubic Hermite interpolation in the interval that contains the singularity is given by

$$|f''(x) - g_j''(x)| \leq \begin{cases} \max\left\{\frac{1}{3}h^2|[f^{(4)}]|, \frac{1}{2}h^2 \sup\limits_{\xi\in[x_j,x^*]}|f^{(4)}(\xi)|\right\}, & x \in [x_j, x^*], \\ \max\left\{\frac{5}{12}h^2|[f^{(4)}]|, \frac{1}{2}h^2 \sup\limits_{\xi\in(x^*,x_{j+1}]}|f^{(4)}(\xi)|\right\}, & x \in (x^*, x_{j+1}], \\ \frac{1}{2}h^2 \sup\limits_{\xi\in[x_j,x_{j+1}]}|f^{(4)}(\xi)|, & \textit{in any other case,} \end{cases} \tag{3.56}$$

for all $h > 0$, independent of f.

If we differentiate the error terms in (3.46) and (3.48) of Lemma (6), it is not difficult to arrive to the expression for the error of the second order derivative of the corrected spline in the intervals

$[x_j, x^*)$ or $(x^*, x_{j+1}]$:

$$\begin{aligned}(T_4^-(x))'' &= \left(-\frac{(\alpha-h)^3(-3\alpha-h+6\alpha h^2(x-x_j)+6h^3(x-x_j))}{12h^2}\right)[f^{(4)}]+\cdots,\\ (T_4^+(x))'' &= \left(\frac{3\alpha^4(h-2(x-xj))-4h\alpha^3(2h-3(x-x_j))}{12h^3}\right)[f^{(4)}]+\cdots\end{aligned} \tag{3.57}$$

Taking into account these results and Corollary 2, we finish the proof:

$$|f''(x)-g_j''(x)| \leq \begin{cases} \max\left\{\frac{1}{3}h^2|[f^{(4)}]|, \frac{1}{2}h^2 \sup\limits_{\xi\in[x_j,x^*]}|f^{(4)}(\xi)|\right\}, & x\in[x_j,x^*],\\ \max\left\{\frac{5}{12}h^2|[f^{(4)}]|, \frac{1}{2}h^2 \sup\limits_{\xi\in(x^*,x_{j+1}]}|f^{(4)}(\xi)|\right\}, & x\in(x^*,x_{j+1}],\\ \frac{1}{2}h^2 \sup\limits_{\xi\in[x_j,x_{j+1}]}|f^{(4)}(\xi)|, & \text{in any other case,}\end{cases} \tag{3.58}$$

Corollary 4 *(Smoothness of the classical Hermite spline with corrected first order derivatives)*
The correction proposed in Theorem 7 leads to a piecewise C^2 spline that preserves the singularity of the function at x^*. Consequently, the use of the adapted first order derivatives obtained in Section 3.3 without the correction proposed in Theorem 7 produces a jump in the second order derivative of the resultant spline $[S''(x)] = S''(x^+) - S''(x^-)$, at x_j and x_{j+1} if the singularity is placed in the interval $[x_j, x_{j+1}]$. This jump is equal to

$$[S''(x_j)] = \frac{6}{h^2}[f] + \frac{(-6\alpha+4h)}{h^2}[f'] + \frac{(3\alpha^2+4\alpha h)}{h^2}[f''] + \frac{(-\alpha^3+2\alpha^2 h)}{h^2}[f'''], \tag{3.59}$$

$$[S''(x_{j+1})] = -\frac{6}{h^2}[f] + \frac{(6\alpha-2h)}{h^2}[f'] + \frac{(-3\alpha^2+10\alpha h)}{h^2}[f''] + \frac{(\alpha^3-\alpha^2 h)}{h^2}[f''']. \tag{3.60}$$

Thus, in this case, the resultant spline is C^1. More specifically, it is C^2 except at x_j and x_{j+1}, if $[x_j, x_{j+1}]$ is the interval that contains the singularity.

Let us consider that we apply the correction terms proposed in Theorem 7. In this case, the modification of the right hand side of the system in (3.33) does not affect the regularity conditions imposed at all the nodes except at x_j and x_{j+1}. This is very easy to verify by computing the jumps $[S''(x_i)]$ and $[S'(x_i)]$ for $x_i, i = 1, \ldots, j-1, j+2, \ldots m-1$, using the expression of the spline in (3.4), and confirming that these jumps are zero. Thus, we only have to consider the jump in the first and second order derivatives at these points. By differentiating once or twice the expression in (3.4) for the spline at x_j^- and the expression in (3.51) for the spline at x_j^+, we obtain $[S'(x_j)] = S'(x_j^+) - S'(x_j^-) = 0$ and $[S''(x_j)] = S''(x_j^+) - S''(x_j^-) = 0$. In the same way,

differentiating once or twice (3.4) for the spline at x_{j+1}^+ and (3.52) for the spline at x_{j+1}^- we obtain $[S''(x_{j+1})] = S''(x_{j+1}^+) - S''(x_{j+1}^-) = 0$ and $[S'(x_{j+1})] = S'(x_{j+1}^+) - S'(x_{j+1}^-) = 0$. This means that the addition of the correction terms shown in Theorem 7 assures piecewise C^2 regularity of the spline everywhere except at the singularity placed at x^*.

By repeating the same calculations but eliminating the correction term $C^-(x)$ in (3.51) or $C^+(x)$ in (3.52) we obtain that the jumps in the first order derivative are still zero at x_j and x_{j+1}, and we obtain the jumps in the second order derivative shown in (3.59) and (3.60) respectively.

The conclusions reached in Corollary 4 will be verified in the Numerical experiments section (Subsection 3.7.3).

3.6 The adaption as a post-processing procedure

In this section we will analyse the possibility of correcting the spline as a post-processing. We have two possibilities: the first one is when we want to obtain a smooth function in the interval that contains the singularity; the second one is when we want to obtain a piecewise continuous function in that interval. In the first case we only have to incorporate the correction of the first order derivatives exposed in Section 3.3. In the second case we need to include also the correction shown in Section 3.5. Let us start by the first case.

3.6.1 The cubic Hermite spline with corrected first order derivatives as a post-processing procedure

Looking at the right hand side of the system in (3.33), we can see that the correction of the first order derivatives of the spline can be done as a post-processing, just adding to the solution of the uncorrected spline the solution of the system considering only as right hand side the sparse vector that contains the correction terms. It is clear that the system can be expressed as

$$A\bar{D} = d + C, \tag{3.61}$$

and it is clear that the term that will add the desired accuracy to the vector is the solution of the system

$$A\tilde{D} = C. \tag{3.62}$$

The solution $\tilde{D}$ of this system will be a vector which, added to the vector of first order derivatives obtained from the classical system of the spline

$$AD = d, \tag{3.63}$$

will provide $O(h^3)$ accuracy for the first order derivatives even close to the singularities. Looking at the expression of the spline in (3.38), if we express each particular first order derivative resulting from (3.61)

$$\bar{D} = D + \tilde{D},$$

then the adapted spline can be expressed as

$$\bar{g}_i(x) = \left(\frac{hD_{i+1} + D_i h + 2y_i - 2y_{i+1}}{h^3}(x - x_i)^3 - \frac{hD_{i+1} + 2D_i h + 3y_i - 3y_{i+1}}{h^2}(x - x_i)^2 \right.$$
$$\left. + D_i(x - x_i) + y_i \right) + \frac{h\tilde{D}_{i+1} + \tilde{D}_i h}{h^3}(x - x_i)^3 - \frac{h\tilde{D}_{i+1} + 2\tilde{D}_i h}{h^2}(x - x_i)^2 + \tilde{D}_i(x - x_i) = g_i(x) + \tilde{g}_i(x). \tag{3.64}$$

The term $\tilde{g}_i(x)$ can be interpreted as a spline where the function values are zero and the first order derivatives are different from zero. It can be added as a post-processing of the classical Hermite spline in order to attain $O(h^3)$ order of accuracy for the first order derivatives at the nodes.

In [52] p. 22, the authors provide a very efficient algorithm for solving tridiagonal systems with dominant main diagonal, like the ones in (3.25) and (3.33). If we have the equations

$$\begin{aligned} b_1 x_1 + c_1 x_2 &= d_1, \\ a_2 x_1 + b_2 x_2 + c_2 x_3 &= d_2, \\ &\cdots \\ a_{m-1} x_{m-2} + b_{m-1} x_{m-1} + c_{m-1} x_m &= d_{m-1}, \\ a_m x_{m-1} + b_m x_m &= d_m, \end{aligned} \tag{3.65}$$

then we can compute for $j = 1, 2, \ldots, m$,

$$\begin{aligned} p_j &= a_j q_{j-1} + b_j, \quad (q_0 = 0), \\ q_j &= -c_j / p_j, \\ u_j &= (d_j - a_j u_{j-1})/p_j, \quad (u_0 = 0). \end{aligned}$$

The successive elimination of $x_1, x_2, \ldots, x_{m-1}$ from the second, third, $\ldots, m$th equations yields the equivalent system of equations

$$\begin{aligned} x_j &= q_j x_{j+1} + u_j, \quad (j = 1, \ldots, m-1), \\ x_m &= u_m, \end{aligned}$$

where $x_m, x_{m-1}, \ldots, x_1$ are evaluated successively. We note that the quantities p_j and q_j depend on the mesh but not on the ordinates at the mesh nodes (that only appear in the d_j in (3.65)). Thus, the correction can be calculated very efficiently once the p_j's and q_j's of the classical spline have been computed, as we are only changing the right hand side of the system of equations of the classical spline, i.e. the d_j's.

3.6.2 The fully accurate cubic Hermite spline as a post-processing procedure

The fully accurate spline presents differences with the one presented in the previous subsection only at the interval $[x_j, x_{j+1}]$ that contains the singularity. Thus, it is possible to express the

corrected spline with corrected first order derivatives inside that interval $g_j(x)$ as

$$g_j^-(x) = g_j(x) + \tilde{g}_j(x) - C^-(x) + O(h^4), \quad x_j < x < x^*, \tag{3.66}$$

$$g_j^+(x) = g_j(x) + \tilde{g}_j(x) - C^+(x) + O(h^4), \quad x^* < x < x_{j+1}. \tag{3.67}$$

3.7 Numerical experiments

In this section we analyse the accuracy obtained when computing the corrected first order derivatives proposed in Section 3.3 and in the interpolation obtained through the corrected Hermite spline described in Section 3.5. We will compare the results of the corrected Hermite spline with those obtained by the classical non-corrected spline.

3.7.1 Accuracy analysis of the interpolation, first and second order derivatives obtained through the classical and corrected splines

Let us try to analyse the accuracy of the interpolation, first and second order derivatives attained by the corrected and non-corrected spline. We will consider that we start from discretized data that comes from the sampling of a function. The location of the discontinuity will be considered known in the case of jump discontinuities in the function. When the jumps are in the first order derivative, we will obtain approximations of its location using the algorithm in [50].

In order to check the accuracy of the spline between the nodes or the first and second order derivatives at the nodes, we can perform a grid refinement analysis. For the approximation of the derivatives, we can just obtain analytically the corresponding derivative of the function and compare it with the approximation of the derivative obtained through the spline for each step of the refinement analysis. The process for this grid refinement analysis will be the following:

1. Sample the function at a high resolution with the mesh size h_0 and keep this data to check the error.

2. Subsample the high resolution data using a mesh size h_1 to obtain the nodes of the spline.

3. Obtain the analytical first and second order derivatives of the function at the nodes obtained in the previous step.

4. Compute the spline with the low resolution nodes.

5. Compute the errors for the first order derivative at the low resolution nodes and for the function and the second order derivative at the high resolution data.

6. Reduce the mesh size for the high resolution data and between nodes so that $h_0 = \frac{h_0}{2}, h_1 = \frac{h_1}{2}$ and go back to step 1.

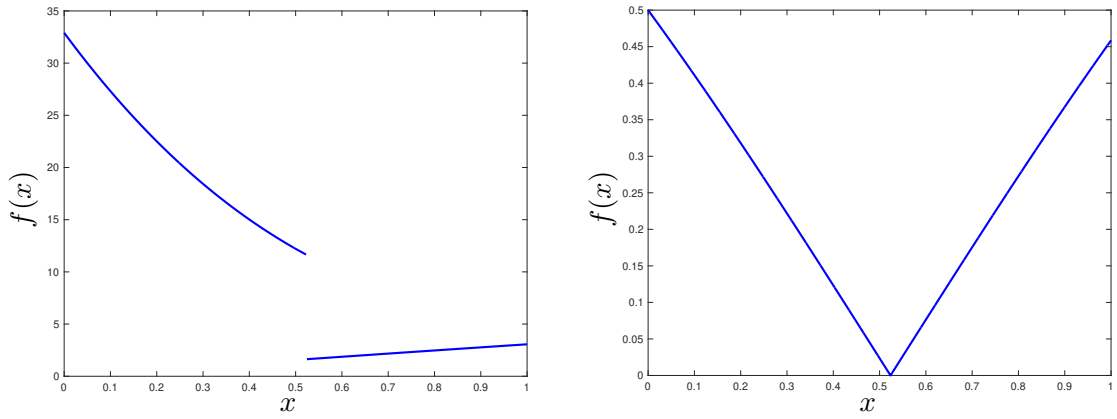

Figure 3.3: Functions in (3.68) and (3.69) used in the numerical experiments.

Once we have the errors for the data, the first, and the second order derivative for all the refinement steps, we can just apply the classical formula for approximating the numerical accuracy,

$$O^l = log_2\left(\frac{E^l}{E^{l+1}}\right),$$

using the infinity norm $E^l = ||f^l - \tilde{f}^l||_{L^\infty}$, where we have denoted the grid refinement step with the super index l.

Experiment 1: a function with a jump discontinuity

For this first experiment we have chosen the function in (3.68), which corresponds to a function with jumps in the function and the first four derivatives:

$$f(x) = \begin{cases} (x-\frac{\pi}{6})(x-\frac{\pi}{6}-3)^3 + 8\sin\left(\frac{\pi x}{8}\right) + 10, & \text{if } 0 \leq x < \frac{\pi}{6}, \\ 8\sin\left(\frac{\pi x}{8}\right), & \text{if } \frac{\pi}{6} \leq x \leq 1. \end{cases} \tag{3.68}$$

In this case, we assume that we know the location of the discontinuity, but we approximate the jumps in the function and the derivatives using one-sided interpolation [49].

In this experiment we have set the relation between the high resolution data and the nodes to $\frac{h_1}{h_0} = 32$, which means that we take one point of every 32 points of the high resolution data to obtain the low resolution data, i.e. the nodes of the spline. Thus, the low resolution nodes have been sampled with $m = 2^l$ nodes and the high resolution data with $32m$ points. The results are shown in Table 3.1 for the interpolation of the spline at the high resolution data obtained from the low resolution data, in Table 3.2 for the first order derivative at the nodes and in Table 3.3 for the second order derivative at the high resolution data points. We can see that the accuracy obtained

by the corrected spline between the nodes tends to $O(h^4)$ when h goes to zero and to $O(1)$ for the classical spline. The accuracy of the first order derivative at the nodes tends to $O(h^3)$ for the corrected spline and to $O(1/h)$ for the classical one. The accuracy of the second order derivative at the high resolution data tends to $O(h^2)$ for the corrected spline and to $O(1/h^2)$ for the classical one. These results have been also presented in Figure 3.4, in a semilogarithmic scale in order to show the numerical decreasing of the error and to compare it with the theoretical one, which has been represented with dashed blue lines. In the plot to the left of this figure we can see the errors obtained by the classical spline (stars in red) and by the corrected spline (stars in blue) at the high resolution nodes. The slope of the dashed lines represents the decreasing of the error of the classical spline with order of accuracy $O(1)$ and with $O(h^4)$ for the corrected spline. At the center we present the errors in the first order derivatives at the low resolution nodes (resulting from the solution of the system of equations of the spline) for each spline with the same markers. The slope of the dashed lines represent again the decreasing of the error for the classical spline with $O\left(\frac{1}{h}\right)$ accuracy and with $O(h^3)$ for the corrected spline. The plot to the right shows the errors obtained in the second order derivative at the high resolution nodes. In this case, the slope of the dashed lines represents the decreasing of the error for the classical spline with $O\left(\frac{1}{h^2}\right)$ accuracy and with $O(h^2)$ for the corrected spline. In Subsection 3.7.2 we show that the loss of accuracy of the classical approach is due, among other things, to Gibbs-like oscillations close to the discontinuity.

$m = 2^l$	2^4	2^5	2^6	2^7	2^8	2^9	2^{10}
Error adapted spline (E^l)	5.54491e-05	1.19648e-05	3.51535e-07	3.59957e-09	2.24858e-10	1.40403e-11	8.81073e-13
Order ($ln(E^l/E^{l+1})$)	-	2.21237	5.08898	6.60970	4.00073	4.00137	3.99417
Error classical spline (E^l)	6.71264	7.41233	5.07078	9.78913	9.79239	9.31633	8.77116
Order ($ln(E^l/E^{l+1})$)	-	-0.14305	0.54772	-0.94897	-0.00048	0.07190	0.08700

Table 3.1: Grid refinement analysis for the accuracy of the corrected and classical splines using the infinity norm at the high resolution nodes. The original data has been sampled from the function in (3.68). The low resolution nodes have been sampled with $m = 2^l$ nodes and the high resolution data with $32m$ points.

$m = 2^l$	2^4	2^5	2^6	2^7	2^8	2^9	2^{10}
Error 1^{st} order derivative corr. spline (E^l)	1.47381e-03	1.83664e-04	2.29231e-05	2.86321e-06	3.57760e-07	4.47014e-08	5.59032e-09
Order ($ln(E^l/E^{l+1})$)	-	3.00440	3.00220	3.00110	3.00057	3.00060	2.99932
Error 1^{st} order derivative class. spline (E^l)	1.03645e+02	2.11761e+02	4.10360e+02	8.07729e+02	1.61958e+03	3.24326e+03	6.49063e+03
Order ($ln(E^l/E^{l+1})$)	-	-1.03078	-0.95445	-0.97698	-1.00367	-1.00183	-1.00091

Table 3.2: Grid refinement analysis for the accuracy of the first order derivative at the low resolution nodes of the corrected and classical splines using the infinity norm. The original data has been sampled from the function in (3.68). The low resolution nodes have been sampled with $m = 2^l$ nodes and the high resolution data with $32m$ points.

$m = 2^l$	2^4	2^5	2^6	2^7	2^8	2^9	2^{10}
Error 2^{nd} order derivative corr. spline (E^l)	1.26490e-01	4.28426e-02	1.73353e-02	4.33295e-03	1.07375e-03	2.63758e-04	6.30744e-05
Order ($ln(E^l/E^{l+1})$)	-	1.56191	1.30533	2.00029	2.01270	2.02537	2.06409
Error 2^{nd} order derivative class. spline (E^l)	5.45724e+03	2.22944e+04	9.00877e+04	3.54527e+05	1.40653e+06	5.60307e+06	2.23662e+07
Order ($ln(E^l/E^{l+1})$)	-	-2.03044	-2.01465	-1.97649	-1.98818	-1.99407	-1.99703

Table 3.3: Grid refinement analysis for the accuracy of the second order derivatives at the high resolution nodes of the corrected and classical splines using the infinity norm. The original data has been sampled from the function in (3.68). The low resolution nodes have been sampled with $m = 2^l$ nodes and the high resolution data with $32m$ points.

Experiment 2: a function with a discontinuity in the derivatives

For the second experiment we have chosen the function in (3.69)

$$f(x) = \left|\sin\left(x - \frac{\pi}{6}\right)\right|, \quad 0 \leq x < 1, \tag{3.69}$$

which corresponds to a function with jumps in the odd derivatives. In this case, we approximate the location of the singularity with $O(h^4)$ accuracy using the algorithm in [50], and we also approximate the jumps in the function (which in this case is zero) and the derivatives [49]. Following the same setting as in the previous experiment, the results are shown in Table 3.4 for the interpolation of the spline, in Table 3.5 for the first order derivatives at the nodes and in Table 3.6 for the second order derivative of the spline at the high resolution data points. It can be observed that with the corrected spline we are capable of obtaining high resolution approximations of the function, the first and the second order derivatives, while with the classical spline the approximations are affected by the presence of the singularity. These results have been presented in Figure 3.5, where the slope of the dashed blue lines represent again the theoretical decreasing of the error for each case. In this figure we represent the results of the grid refinement analysis for the accuracy of the corrected and classical splines and their first and second order derivatives using the infinity norm shown in Tables 3.4, 3.5 and 3.6.

$m = 2^l$	2^4	2^5	2^6	2^7	2^8	2^9	2^{10}
Error adapted spline (E^l)	6.59827e-07	2.78771e-08	1.15987e-09	7.37090e-11	4.64462e-12	2.91434e-13	1.83187e-14
Order ($ln(E^l/E^{l+1})$)	-	4.56494	4.58705	3.97597	3.98821	3.99432	3.99178
Error classical spline (E^l)	1.86023e-02	7.32441e-03	5.24429e-03	1.32151e-03	6.43286e-04	3.04237e-04	1.40813e-04
Order ($ln(E^l/E^{l+1})$)	-	1.34469	0.48196	1.98856	1.03865	1.08026	1.11141

Table 3.4: Grid refinement analysis for the accuracy of the corrected and classical splines using the infinity norm at the high resolution nodes. The original data has been sampled from the function in (3.69). The low resolution nodes have been sampled with $m = 2^l$ nodes and the high resolution data with $32m$ points.

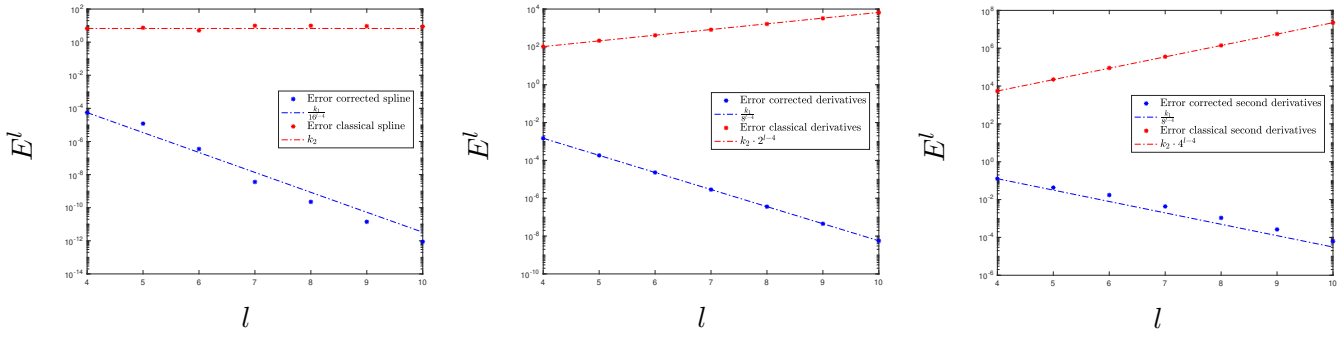

Figure 3.4: In this figure we represent the results of the grid refinement analysis for the accuracy of the corrected and classical splines and their first and second order derivatives using the infinity norm shown in Tables 3.1, 3.2 and 3.3. The original data has been sampled from the function in (3.68). In the first row we show the error E^l for the corrected and classical spline, in the second one we show the error for the first order derivative, and finally, the error for the second order derivative. The x axis represents de resolution level l: the increase of l implies the reduction of the grid-spacing of the low resolution data. Thus, the slope of the dashed lines represents the accuracy of each method.

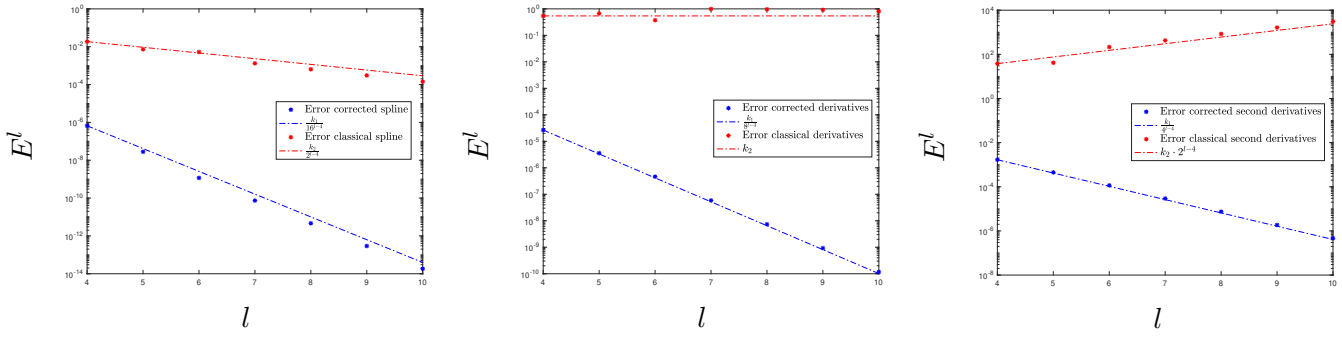

Figure 3.5: In this figure we represent the results of the grid refinement analysis for the accuracy of the corrected and classical splines and their first and second order derivatives using the infinity norm shown in Tables 3.4, 3.5 and 3.6. The original data has been sampled from the function in (3.69). As in Figure 3.4, in the first row we show the error E^l for the corrected and classical spline, in the second one we show the error for the first order derivative, and finally, the error for the second order derivative. The x axis represents de resolution level l: the increase of l implies the reduction of the grid-spacing of the low resolution data. Thus, the slope of the dashed lines represents the accuracy of each method.

$m = 2^l$	2^4	2^5	2^6	2^7	2^8	2^9	2^{10}
Error 1^{st} order derivative corr. spline (E^l)	2.66070e-05	3.57412e-06	4.61924e-07	5.86765e-08	7.39272e-09	9.27689e-10	1.16387e-10
Order ($ln(E^l/E^{l+1})$)	-	2.89614	2.95186	2.97680	2.98861	2.99439	2.99471
Error 1^{st} order derivative class. spline (E^l)	5.42186e-01	6.68854e-01	3.73696e-01	9.94572e-01	9.68398e-01	9.16048e-01	8.11350e-01
Order ($ln(E^l/E^{l+1})$)	-	-0.30290	0.83983	-1.41221	0.03848	0.08018	0.17510

Table 3.5: Grid refinement analysis for the accuracy of the first order derivative at the nodes of the corrected and classical splines using the infinity norm. The original data has been sampled from the function in (3.69). The low resolution nodes have been sampled with $m = 2^l$ nodes and the high resolution data with $32m$ points.

$m = 2^l$	2^4	2^5	2^6	2^7	2^8	2^9	2^{10}
Error 2^{nd} order derivative corr. spline (E^l)	1.67571e-03	4.48916e-04	1.15908e-04	2.94324e-05	7.41473e-06	1.86069e-06	4.66252e-07
Order ($ln(E^l/E^{l+1})$)	-	1.90025	1.95346	1.97751	1.98894	1.99455	1.99666
Error 2^{nd} order derivative class. spline (E^l)	3.78943e+01	4.14111e+01	2.14565e+02	4.26291e+02	8.41072e+02	1.63595e+03	3.08695e+03
Order ($ln(E^l/E^{l+1})$)	-	-0.12804	-2.37332	-0.99043	-0.98039	-0.95982	-0.91606

Table 3.6: Grid refinement analysis for the accuracy of the second order derivatives at the high resolution nodes of the corrected and classical splines using the infinity norm. The original data has been sampled from the function in (3.69). The low resolution nodes have been sampled with $m = 2^l$ nodes and the high resolution data with $32m$ points.

3.7.2 Elimination of the Gibbs phenomenon using adapted first order derivatives

In this section we will analyse the behaviour of the corrected spline, the classical spline with corrected first order derivatives and the classical spline close to discontinuities. In order to do so, we will use the function in (3.68), which presents a jump discontinuity. As in Subsection 3.7.1, we assume that we know the location of the discontinuity for this function, but we approximate the jumps in the function and the derivatives using one-sided interpolation [49]. The results of the experiments are shown in Figure (3.6). In the first row, we present the approximation (red circles) of the function in (3.68) sampled with a high resolution of 256 points (blue crosses) and then subsampled to obtain 16 points (solid black circles) in order to obtain the low resolution data. We can see that the classical spline (first row, plot to the left) shows Gibbs oscillations close to the discontinuity. If we correct the first order derivatives of the spline and we do not use any correction for the spline itself (first row, central plot), we obtain an approximation that is free of oscillations close to the discontinuity, but that presents diffusion in the interval that contains the discontinuity. If we use the corrected first order derivatives and we also correct the approximation of the spline close to the discontinuity (first row, plot to the right), we can obtain a piecewise continuous function without oscillations close to the discontinuity. The second row of Figure 3.6 shows the error obtained in the computation of the first order derivatives at the low resolution nodes for each spline: to the left we show the result of the classical spline and at the center and to the right, the error for corrected first order derivatives (which are the same both for the classical

spline with corrected first order derivatives and for the corrected spline). The third row shows the error at the high resolution nodes attained by each of the splines in the same order. From these plots we can see that the use of corrected first order derivatives leads to the elimination of the Gibbs oscillations close to the discontinuities. If we also correct the interpolation of the spline, it is possible to obtain a piecewise continuous function with high accuracy even close to the discontinuities.

3.7.3 Regularity

In this subsection we will analyse the behaviour of the first and second order derivatives between the nodes for the classical spline, the classical spline with corrected first order derivatives and the corrected spline with corrected first order derivatives. As before, for the function in (3.68), we assume that we know the location of the discontinuity, and, for the function in (3.69), we approximate the location of the singularity with $O(h^4)$ [50]. In both cases we approximate the jumps in the function and the derivatives using one-sided interpolation [49]. Figures 3.7 and 3.8 show the results obtained for the functions in (3.68) and (3.69) respectively. In both figures, the approximation of the first order derivative of the functions is shown in the first column, and the approximation for the second order derivatives is shown in the second column. Functions in (3.68) and (3.69) are sampled with 16 points to obtain the low resolution data. Then, each polynomial piece of the spline is differentiated once or twice to obtain the results shown in Figures 3.7 and 3.8. We have represented some points of the first or the second order derivative of the function with blue dots. The stars represent a sampling of the first or the second order derivatives of each one of the polynomial pieces of the spline $g(x)$. Each polynomial piece is represented with a different colour. Our objective is just to compare qualitatively the first and second order derivatives of the functions, and the approximations obtained through each spline. In each of the two figures, the first row presents the result for the classical spline, and the second row shows the result for the classical spline with corrected first order derivatives. Finally, the third row shows the results for the corrected spline with corrected first order derivatives. It is clear that the classical spline introduces oscillations in the first and the second order derivatives close to the singularities, but maintains the C^2 regularity in the whole domain. The results also show that the modification of the right hand side of the system of equations of the spline in (3.33) eliminates the oscillations in the function outside the interval that contains the singularity, but leads to the loss of the regularity in the second order derivative if the spline is not corrected, as discussed in Corollary 4. Only the corrected spline with corrected first order derivatives, discussed in Section 3.5, allows for the elimination of the oscillations and keeps the correct piecewise regularity of the function from which the data has been obtained.

3.8 Conclusions

In this chapter we have presented a new technique that allows for the correction of the first order derivatives and the approximation obtained through cubic Hermite splines close to singularities.

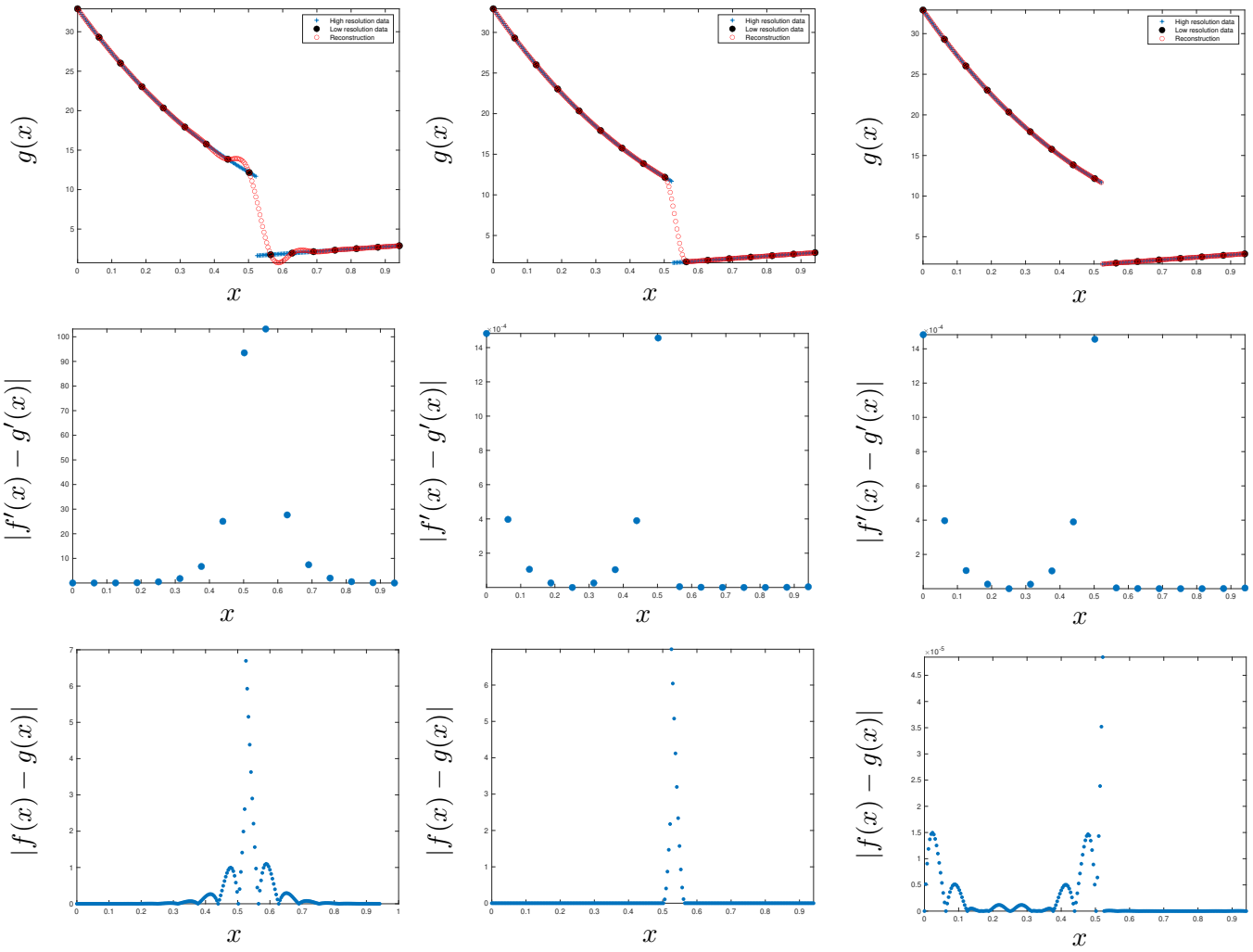

Figure 3.6: In the first row, we present the reconstruction or approximation $g(x)$ of the function in (3.68) with red circles. Initially we sample the function at a high resolution of 256 points and we represent it with blue crosses. Then we subsample the data to obtain a low resolution version of 16 points, and we represent it with solid black circles. The second and third row are dedicated to present the error in the first and second order derivatives, respectively. The first column presents the results of the classical cubic Hermite spline, the second one presents those obtained by the classical cubic Hermite spline with corrected first order derivatives. Finally, the third one presents the results attained by the corrected cubic Hermite spline with corrected first order derivatives.

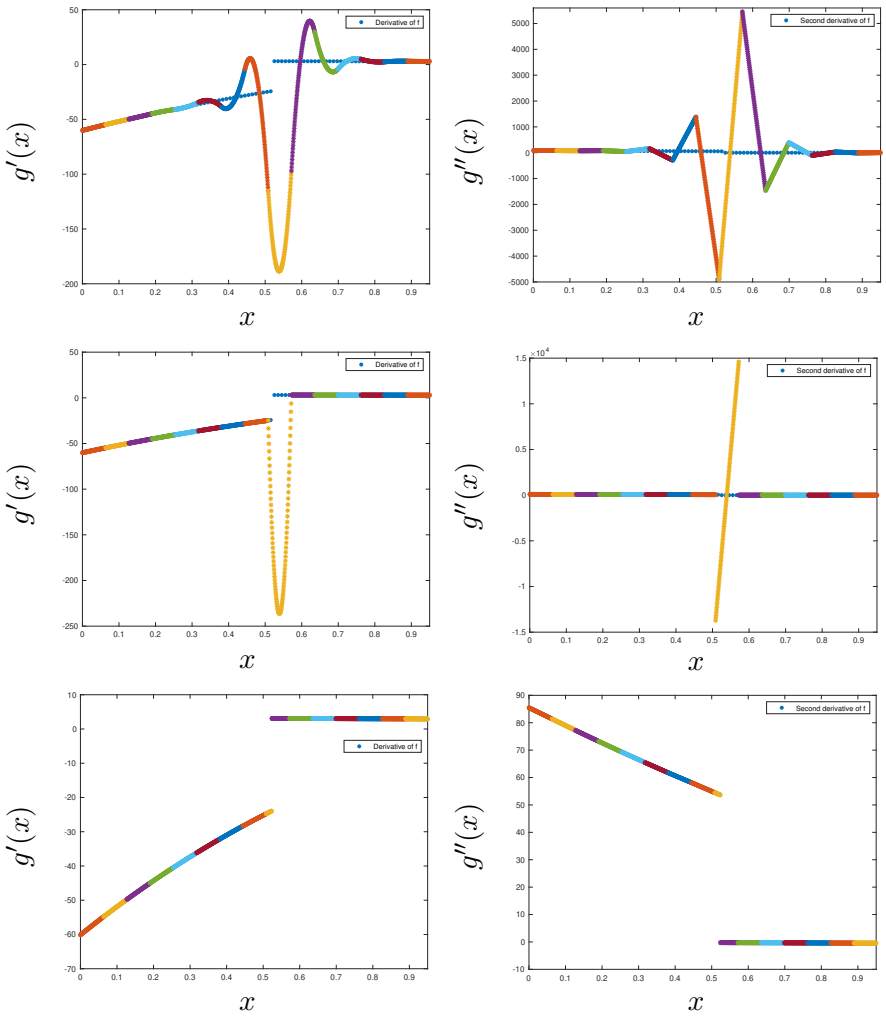

Figure 3.7: Approximation of the first order derivative (first column), and second order derivative (second column) of the function in (3.68) sampled with 16 points to obtain the low resolution data. The blue dots represent the first or the second order derivative of the function. The coloured stars represent the first or the second order derivatives of the polynomial pieces of the spline $g(x)$. Each colour of the stars represents a different polynomial piece of the spline. The first row presents the result for the classical spline. The second row shows the result for the classical spline with corrected first order derivatives. The third row shows the results for the corrected spline with corrected first order derivatives.

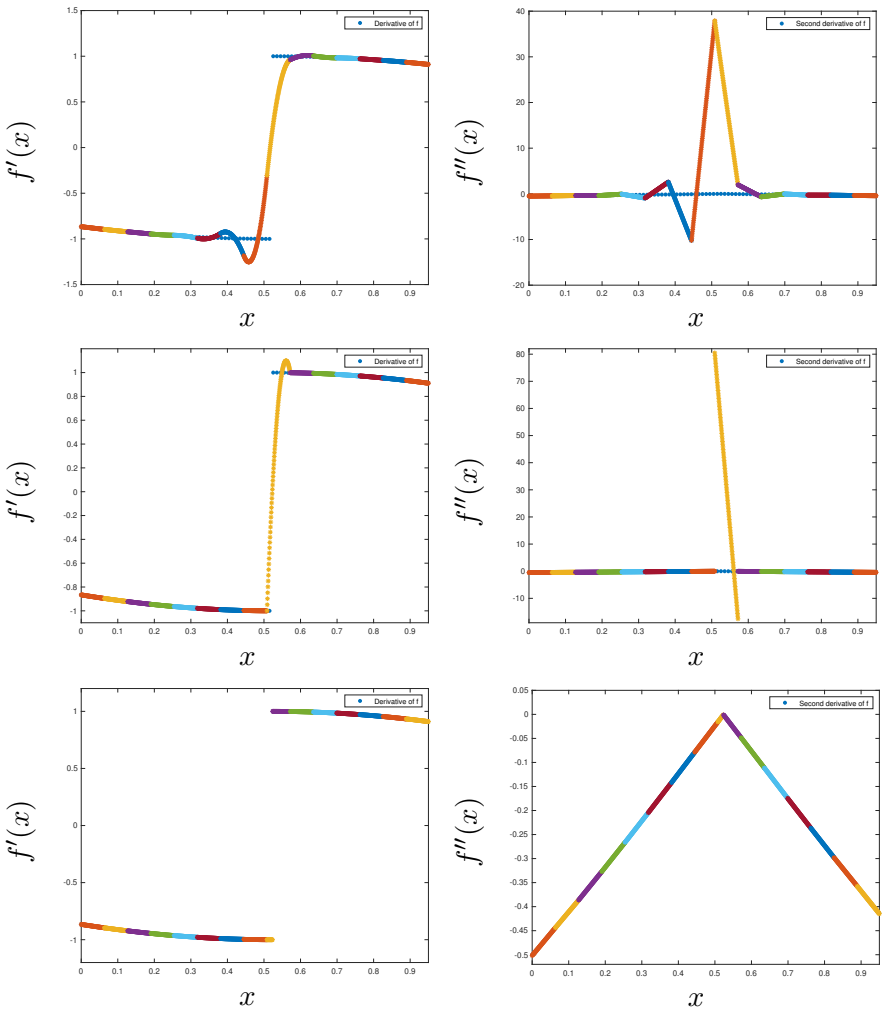

Figure 3.8: Approximation of the first order derivative (first column) and second order derivative (second column) of the function in (3.69) sampled with 16 points to obtain the low resolution data. The blue dots represent the first or the second order derivative of the function. The coloured stars represent the first or the second order derivatives of the polynomial pieces of the spline $g(x)$. Each colour of the stars represents a different polynomial piece of the spline. The first row presents the result for the classical spline. The second row shows the result for the classical spline with corrected first order derivatives. The third row shows the results for the corrected spline with corrected first order derivatives.

The technique consists in taking into account the effect introduced by the singularity by adding correction terms, in order to assure a high order of accuracy close to the singularities. The correction can be included in the right hand side of the system of the spline, allowing for its application as a post-processing. It has been shown theoretically that the correction of the first order derivatives eliminates the Gibbs phenomenon introduced by the classical spline close to jump discontinuities. Through the correction introduced in the system of equations of the spline, we obtain accurate first order derivatives even close to the singularities. Thus we have also discussed the theoretical accuracy in the infinity norm obtained through the correction of the first order derivatives. Even so, diffusion is always present in the interval that contains a jump discontinuity if we only correct the first order derivatives of the spline. If the correction is also introduced in the equation of the spline (3.1) in the interval that contains the singularity, it is possible to approximate accurately piecewise continuous functions. Proofs for the accuracy attained through the corrected spline in the infinity norm have been provided. The new technique requires the knowledge of the location of the singularities and the jumps in the function and its derivatives at the singularities, or high order of accuracy approximations. We have also discussed the order of accuracy needed in the approximated location of the singularity to keep the order of the spline. The numerical experiments confirm the theoretical results obtained.

Chapter 4

Image super resolution

It is important to mention here that the super resolution topic was the starting point of this thesis. Then, we continued with the other two paths of research presented in the previous chapters, which successfully led us to obtain enough results for the conclusion of this work. In this part of the thesis, we briefly expose the line of research that we followed at that stage.

4.1 Introduction

Super resolution, within the context of Harten's multiresolution algorithms, is a powerful technique for enhancing the quality and detail of images or data. Operating within Harten's framework, super resolution aims to improve the resolution of data by incorporating information from various scales in the multiresolution process. This is achieved through data-dependent reconstruction operators, enabling the generation of more precise and detailed representations of the data, especially in areas with abrupt changes or singularities. The adaptability of Harten's multiresolution approach allows for the design of super resolution methods to specific problems or dataset requirements, making them particularly effective enhancing data quality in applications such as image processing or signal processing. We will center our attention in the super resolution of images using a specific prediction operator. We will start by introducing the Harten's framework for multiresolution and then explain how we have used it to try to create a super resolution algorithm based on this framework.

In recent years, the research carried out in signal processing, and more particularly, in problems of compression, denoising, pattern recognition and others, has made this field one of the most studied in the area of Applied Mathematics. A common problem in approximation theory is the reconstruction of a function from a set of discrete data that give information about the function itself. This information is usually given as point values or cell averages of the function over a finite set of points or cells, respectively. The function is then approximated by an interpolant, that is, by another function whose point values or cell averages coincide with those of the original function. This interpolant can be constructed using linear interpolation or even more sophisticated

procedures that take into account the presence of discontinuity points in the data. In the first case, the accuracy of the approximation near a singularity is limited and depends on the regularity of the data, so that if we construct the interpolating polynomial based on a set of points (stencil) crossing the singularity, we will obtain a poor approximation. The second approach aims to solve or at least reduce these problems.

In the past years, several attempts to improve the properties of linear subdivision schemes have given rise to nonlinear subdivision schemes, which study the behavior of functions close to discontinuities. These schemes are data-dependent, so it is necessary to study their stability, which may be affected by perturbations that are present in the data. For nonlinear subdivision schemes, few general convergence or stability results are available, see for example [56, 57, 58, 59, 60, 61]. Starting with a discrete set of data, subdivision schemes generate new data by following a set of well-established rules, and thus, obtaining another new set of data denser than the previous one. This process can be repeated several times in order to refine the original data sequence. Some examples of subdivision schemes are the family of schemes based on Lagrange interpolation, the family of spline subdivision schemes related to spline spaces, the Chaikin algorithm, which is another example of a spline subdivision scheme converging to C^2 functions, the ENO interpolation [62, 63, 64, 65, 66, 67, 68, 57, 69, 70], improved by the WENO (weighted ENO) interpolations [70, 71, 72, 73, 74, 75, 76, 77, 78, 79, 80, 81, 82, 83, 84, 85, 86, 87, 88, 89, 90, 91], as well as the PPH interpolation [56]. Some of these algorithms could be adapted to construct super resolution algorithms.

In the construction of subdivision schemes, the application of the rules which allow us to create, from an initial fixed set of points, another denser set, also allows us to carry out several zoom stages, and thus successive enlargements of the image. The subdivision schemes can be interpreted from the prediction operator that appears in Harten's multiresolution. Harten's multiresolution [92] is a very efficient tool for image processing. The goal of multiresolution is to obtain a multi-scale rearrangement of the information contained in a discrete data set. To perform the transformation between the different levels of multiresolution, we use the decimation and prediction operators. The prediction operator is the one we use to zoom, since it increases the resolution of the initial data set. The prediction and decimation operators are closely related to the reconstruction and discretisation operators, which connect the different discrete levels of resolution to a suitable functional space, which depends on the applications. The feature that makes Harten's multiresolution more attractive than other techniques is the fact that it easily allows the introduction of non-linearity in the schemes.

In what follows, we introduce Harten's framework for multiresolution and then we explain very briefly how to use it to construct a super resolution algorithm.

4.2 Harten's framework for multiresolution

Digital image processing can benefit from multiresolution representations of data. The cell-average setting is a common framework for these applications. To adapt well to singularities, nonlinear

methods are desirable. Therefore, one has to ensure the stability of these representations. A discussion about Harten's multiresolution can be found in [92, 93, 94].

Given a data vector f^L where L represents a resolution level, a multiresolution representation of f^L is any sequence of the type $\{f^0, d^1, \ldots, d^L\}$ where f^k is an approximation of f^L at resolution level $k < L$, and d^{k+1} represents the details required to obtain f^{k+1} from f^k. This representation is then processed and modified to produce a new multi-scale representation $\{\hat{f}^0, \hat{d}^1, \hat{d}^2, \ldots, \hat{d}^L\}$ that is close to the original one, i.e. such that (in some norm)

$$||\hat{f}^0 - f^0|| \leq \epsilon_0 \qquad ||\hat{d}^k - d^k|| \leq \epsilon_k \quad 1 \leq k \leq L,$$

where the user specifies the truncation parameters $\epsilon_0, \epsilon_1, \ldots, \epsilon_L$ according to some criteria. The simplest data compression procedure is to set to zero all the scale coefficients that are below a given tolerance. We define

$$\hat{d}^k = \mathbf{tr}(d^k; \epsilon_k) = \begin{cases} 0 & |d^k| \leq \epsilon_k, \\ d^k & \text{otherwise.} \end{cases} \tag{4.1}$$

We call this operation truncation. This type of data compression mainly reduces the *dimensionality* of the data, eliminating part of the information contained in the original data. Another strategy, which reduces the digital representation of the data, is *quantization*, which can be modelled by

$$\hat{d}^k = \mathbf{qu}(d^k; \epsilon_k) = 2\epsilon_k \cdot \text{ round } \left[\frac{d^k}{2\epsilon_k}\right]. \tag{4.2}$$

Here round $[\cdot]$ means the integer obtained by rounding. Note that if $|d^k| < \epsilon_k$ then $\mathbf{qu}(\mathrm{d}^k; \epsilon_k) = 0$ and that the following expression holds for both cases

$$|d^k - \hat{d}^k| \leq \epsilon_k.$$

When we decode the processed representation, we get a discrete set $\hat{f}^L$ that is supposed to be *close* to the original discrete set f^L. For this to happen, some kind of stability is necessary, i.e. we have to demand that

$$||\hat{f}^L - f^L|| \leq \sigma(\epsilon_0, \epsilon_1, \ldots, \epsilon_L),$$

where $\sigma(\cdot, \ldots, \cdot)$ has the following property

$$\lim_{\epsilon_l \to 0,\ 0 \leq l \leq L} \sigma(\epsilon_0, \epsilon_1, \ldots, \epsilon_L) = 0.$$

Wavelet decompositions serve as fundamental tools commonly employed in image analysis and compression. While these decompositions are known for their stability, it's important to note that the underlying theory is built upon their linearity. Nevertheless, the effectiveness of wavelet decompositions in image compression is frequently constrained by the existence of discontinuities or edges. On one hand, the detail coefficients d^k that hold numerical significance are primarily

associated with wavelet supports that intersect these discontinuities. On the other hand, in order to capture only a small number of significant coefficients in the smoother parts of the signal, it requires the use of highly oscillating wavelets, which inherently have larger supports. Consequently, this results in a greater number of significant coefficients associated with discontinuities. Harten's framework for multiresolution offers a well-suited environment for crafting discrete multiresolution representations, as discussed in [92, 95], and [96]. In this framework, discrete resolution levels are connected through inter-resolution operators known as decimation (transitioning from fine resolution k to coarser resolution $k-1$) and prediction (transitioning from coarser to finer resolutions). These inter-scale operators have a direct correlation with the discretization and reconstruction processes. These processes bridge the continuous level, where a function denoted as f (and related to the discrete data) lives, to each discrete level, where f^k is placed. Both decimation and prediction operators act within linear vector spaces represented as V^k, each of which signifies different resolution levels. Notably, as k increases, the resolution becomes finer:

$$\mathbf{D}_k^{k-1} : V^k \to V^{k-1} \tag{4.3}$$

$$\mathbf{P}_{k-1}^{k} : V^{k-1} \to V^{k} \tag{4.4}$$

They must meet two algebraic prerequisites:

1. $\mathbf{D}_k^{k-1}$ must be a linear operator.
2. $\mathbf{D}_k^{k-1}\mathbf{P}_{k-1}^{k} = I_{V^{k-1}}$ (consistency), where $I_{V^{k-1}}$ is the identity operator at the lower-resolution level. This condition simply means that if we decimate the data obtained through the prediction operator, we must obtain the original data from which we started.

One of the most significant strengths of Harten's framework lies in its adaptability. The role played by the reconstruction operator enables the implementation of adaptive techniques specifically created for handling singularities. In most cases, these techniques involve the use of data-dependent reconstruction operators, resulting in non-linear prediction methods and consequently leading to non-linear multiresolution decompositions (as discussed in [95] and [96]).

A significant advance towards non-linear adaptation near singularities has been made possible by the Essentially Non Oscillatory (ENO) reconstruction methods, which have been detailed in [95] and [92]. When considering image examples, such as those in [67, 97], and [98], it becomes evident that non-linear processing allows for a more finely-tuned treatment of edges. Specifically, this approach ensures that edges do not yield as many prominent detail coefficients as is typical in standard wavelet transforms.

4.3 The Cell-average Multiresolution Setting

A discussion about this kind of discretization can be found in [92, 99]. We consider a set of nested grids in $[0, 1]$:

$$X^k = \{x_j^k\}_{j=0}^{J_k}, \quad x_j^k = jh_k, \quad h_k = 2^{-k}/J_0, \quad J_k = 2^k J_0,$$

where J_0 is a fixed integer. We employ the discretization process defined as:

$$\mathcal{D}_k : L^1[0,1] \to V^k, \qquad f_j^k = (\mathcal{D}_k f)_j = \frac{1}{h_k}\int_{x_{j-1}^k}^{x_j^k} f(x)dx, \quad 1 \le j \le J_k, \tag{4.5}$$

where $L^1[0,1]$ represents the space of functions in $[0,1]$ with finite integrals, and V^k is the space of sequences with J_k elements. Using the additivity of the integral, we obtain the decimation steps:

$$f_j^{k-1} = (\mathbf{D}_k^{k-1} f^k)_j = \frac{1}{h_{k-1}}\int_{x_{j-1}^{k-1}}^{x_j^{k-1}} f(x)dx = \frac{1}{2h_k}\int_{x_{2j-2}^k}^{x_{2j}^k} f(x)dx = \frac{1}{2}(f_{2j-1}^k + f_{2j}^k).$$

The consistency requirement for $\mathbf{P}_{k-1}^k$ can be expressed as:

$$f_j^{k-1} = (\mathbf{D}_k^{k-1}\mathbf{P}_{k-1}^k f^{k-1})_j = \frac{1}{2}((\mathbf{P}_{k-1}^k f^{k-1})_{2j-1} + (\mathbf{P}_{k-1}^k f^{k-1})_{2j}).$$

Thus, if $f^{k-1} = \mathbf{D}_k^{k-1} f^k$, then the prediction errors can be obtained from the last two equations and satisfy:

$$d_{2j-1}^k = f_{2j-1}^k - (\mathbf{P}_{k-1}^k f^{k-1})_{2j-1} = (\mathbf{P}_{k-1}^k f^{k-1})_{2j} - f_{2j}^k = -d_{2j}^k.$$

This indicates that the prediction error contains some redundancy.

Now, if we only consider the prediction errors at, for example, the odd points of the grid X^k, we achieve a one-to-one mapping:

$$f_j^{k-1} = \frac{f_{2j}^k + f_{2j-1}^k}{2}, d_j^k = f_{2j-1}^k - (P_{k-1}^k f^{k-1})_{2j-1},$$

$$f_{2j-1}^k = (P_{k-1}^k f^{k-1})_{2j-1} + d_j^k, f_{2j}^k = 2f_j^{k-1} - f_{2j-1}^k. \tag{4.6}$$

We can proceed to consider the primitive function and follow the same procedure as before: We consider the sequence $\{F_j^k\}$ on the k-grid defined by

$$F_j^k = h_k \sum_{i=1}^{j} f_i^k = \int_0^{x_j^k} f(x)dx = F(x_j^k) \quad \Rightarrow \quad f_j^k = \frac{F_j^k - F_{j-1}^k}{h_k}, \tag{4.7}$$

where the function $F(x)$ is a primitive of $f(x)$ and the sequence $\{F_j^k\}$ is a discretization by point-values of $F(x)$ on the grid X^k (a sampling of $F(x)$ on that grid).

Let $\mathcal{I}_{k-1}(x; F^{k-1})$ be a reconstruction of F

$$\mathcal{I}_{k-1}(x_j^{k-1}; F^{k-1}) = F_j^{k-1}.$$

Hence, we can obtain an approximation, $\tilde{f}_j^k$, of f_j^k:

$$\tilde{f}_j^k = (\mathcal{I}_{k-1}(x_j^k, F^{k-1}) - \mathcal{I}_{k-1}(x_{j-1}^k, F^{k-1}))/h_k. \tag{4.8}$$

The prediction error follows the expression

$$0 = \frac{\varepsilon_{2j-1}^k + \varepsilon_{2j}^k}{2},$$

therefore, we can define the details as

$$d_j^k = \varepsilon_{2j-1}^k, \quad 1 \le j \le J_{k-1},$$

then, we have all the information we need because

$$\begin{aligned} \varepsilon_{2j-1}^k &= d_j^k, \qquad 1 \le j \le J_{k-1}, \\ \varepsilon_{2j}^k &= -d_j^k, \quad 1 \le j \le J_{k-1}. \end{aligned}$$

Now, knowing that P_{k-1}^k is the prediction operator, we get

$$f_{2j-1}^k = (P_{k-1}^k f^{k-1})_{2j-1} + d_j^{k-1}. \tag{4.9}$$

A nonlinear multiresolution results from a nonlinear interpolation. To get an adapted nonlinear multiresolution in the cell-average framework we can apply nonlinear schemes to the primitive function. In the linear case we get back biorthogonal wavelet algorithms [100].

We will generally consider the family of prediction operators defined by

$$(P_{k-1}^k f^{k-1})_{2j-1} = f_j^{k-1} + F(\delta f_j^{k-1}, \delta f_{j+1}^{k-1}), \tag{4.10}$$

where δ is a linear operator but F can be nonlinear.

The cell-average framework has L^1 as the natural functional space, which makes this setting more appropriate for image processing applications than the point-values framework, where the functional space is the continuous functions. We will use this framework to build our super resolution algorithm. In the following section, we explain the relation between multiresolution and subdivision schemes.

4.4 Relationship between multiresolution schemes and subdivision schemes (zoom)

If in these multiresolution algorithms, we focus only on the signal decoding stage or ascending through the multiresolution pyramid, what we have is a subdivision scheme. Therefore, a subdivision scheme S is defined through the prediction operator P_{k-1}^k that is used. In this case, for a discrete sequence, it is defined as:

$$f^k = Sf^{k-1} = P_{k-1}^k f^{k-1}.$$

In the case of interpolation, where the discretization is given by values of a function on a grid, the subdivision scheme takes the form:

$$f^k = Sf^k \begin{cases} f^k_{2j} = (Sf^{k-1})_{2j} = f^{k-1}_j & 1 \leq j \leq J_{k-1}, \\ f^k_{2j-1} = (Sf^{k-1})_{2j-1} = I_{k-1}(x^k_{2j-1}; f^{k-1}) & 0 \leq j \leq J_{k-1}. \end{cases} \tag{4.11}$$

In this case, the fact that reconstructions are equivalent to interpolations simplifies their design significantly, especially when we consider that the most common interpolations are of polynomial kind.

4.5 Towards a super resolution algorithm

Firstly, it is necessary to mention that in order to apply a super resolution algorithm, two or more images are needed at a resolution lower than the one we want to reconstruct [101]. In addition, these images must be the result of a registration in which the pixel spacing between the two images must be less than 1 pixel [101]. In our case, we will obtain these low-resolution images from a high-resolution image.

To do this, we will choose the pixels located at positions $(2n+1, 2n+1)$ for the first image and the pixels located at positions $(2n, 2n)$ for the second image. Figure 4.1 shows an example for a high-resolution image of 8×8 pixels. Once we have two or more low-resolution images, it is necessary to know the pixel spacing existing between the mentioned low-resolution images and the high-resolution image. In our case, we assume that two pixels located in the same position in the low-resolution images are spaced 0.5 pixels in diagonal direction. To perform the super resolution process it is necessary to obtain the multiresolution pyramid of both images, and then to interpolate the values of the coefficients and the details of the matrix. For the interpolation, we used tensor product and some linear and non linear algorithms, like the Lagrange interpolation, the PPH scheme or the ENO method in the point values and the cell averages.

The results obtained were not completely satisfactory, so we gave preference to the other lines of research that we have presented in previous chapters. This line of research remains opened as possible future work.

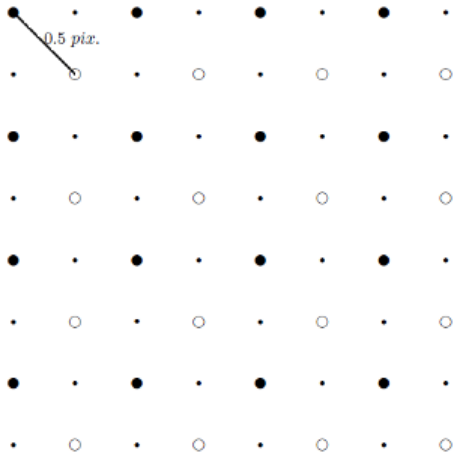

Figure 4.1: High resolution mesh where two low resolution images have been placed (represented by large black dot and large white dot) separated by 0.5 pixels in diagonal direction. The points where we do not have information from the two low-resolution images are represented by a small black dot.

Chapter 5

Conclusions and future works

5.1 Conclusions

In this thesis we have designed and analyzed some numerical methods that try to handle with the presence of discontinuities in the data. As mentioned in the introduction, we have fundamentally explored two approaches: classical approximations plus correction terms and multiresolution algorithms. Our research has lead us to propose three nonlinear algorithms that we have included in the previous chapters of this document. More especifically:

- In Chapter 2 we have introduced correction terms for classical numerical integration methods such as the trapezoid rule, Simpson's $\frac{1}{3}$ rule, and various Newton-Cotes formulas. These correction terms are given through explicit closed formulas, ensuring the preservation of global accuracy when the data is smooth, but also when the underlying data contains discontinuities in either the function or its derivatives. Notably, these correction terms can be added to both simple and composite rules of classical integration formulas, offering the possibility of using the new technique as a post-processing to enhance accuracy. It is possible to extend the results obtained in our study to other integration rules following a similar process. Furthermore, we have provided correction terms for other Newton-Cotes quadrature formulas, assuring that their application guarantees the expected theoretical accuracy. We have found that the correction terms presented depend on the jumps in the function to be integrated and its derivatives. The empirical validation through numerical experiments has corroborated the theoretical findings.

- In Chapter 3 we introduced a novel technique for correcting the first-order derivatives and approximations obtained using cubic Hermite splines near singularities. This method is based on the use of correction terms to take into account the influence of singularities in the approximation, ensuring a high level of accuracy in their vicinity. These corrections can be included into the spline's system of equations, making it suitable for post-processing applications. The theoretical analysis demonstrates that correcting the first-order derivatives

effectively eliminates the Gibbs phenomenon typically associated with classical splines near jump discontinuities. By introducing corrections directly into the spline equation within the singularity's interval, accurate first-order derivatives can be achieved even close to the singularities. The Chapter also explores the theoretical accuracy in the infinity norm resulting from the correction of the first-order derivatives. However, it's important to note that some diffusion is still present in intervals containing jump discontinuities if only the first-order derivatives are corrected. When corrections are applied to the spline equation within the discontinuity interval, the technique becomes capable of accurately approximating piecewise continuous functions. Implementing this new technique imposes the knowledge of the singularity locations, along with information regarding the jumps in the function and its derivatives at those singularities. The accuracy of the corrected spline in the infinity norm is supported by theoretical proofs. The article also addresses the required order of accuracy for approximating singularity locations while maintaining the spline's order. Numerical experiments validate the theoretical findings presented in this chapter.

- Chapter 4 focuses on the creation of nonlinear algorithms for super resolution using multiresolution, with a particular emphasis on the use of Harten's framework. In the context of Harten's multiresolution algorithms, super resolution is a possible application for improving the quality and detail of images or data. Usually, these algorithms are designed to achieve higher data resolution by incorporating information from various scales during the multiresolution process, aided by data-dependent reconstruction operators. This adaptability allows the customization of super resolution methods to specific problem or dataset needs, particularly beneficial for applications like image or signal processing. The chapter introduces Harten's multiresolution and explains how we started this thesis trying to develop a super resolution algorithm within this framework.

5.2 Future lines of research

The findings presented in this thesis leave some open paths for future research in the context of numerical methods and approximation techniques. One possible direction is the extension of the correction techniques introduced here to a broader spectrum of numerical methods. For instance, it is challenging to design correction terms for alternative approximation techniques, including other kinds of splines, subdivision schemes, or entirely different techniques such as methods to approximate the solution of ordinary differential equations (ODEs). The exploration of these possible paths can lead to some extensions of the methods proposed here and to more analysis, that we might continue in the future. Another possible direction for future research lies in the further exploration and advancement of super resolution techniques within the context explained in Chapter 4. The potential for enhancing the quality and detail of images or data using Harten's multiresolution framework is still something that can be explored. Using non linear algorithms to process the multiresolution pyramid, there are possibilities of finding paths of research that allow to refine and expand these methods, optimizing their performance and adaptability.

References

[1] S. Amat, Z. Li, J. Ruiz-Álvarez, C. Solano, J. C. Trillo, Numerical integration rules with improved accuracy close to discontinuities, Mathematics and Computers in Simulation, 210, 593-614, (2023), https://doi.org/10.1016/j.matcom.2023.03.032.

[2] S. Amat, Z. Li, J. Ruiz-Álvarez, C. Solano, J. C. Trillo, Adapting Cubic Hermite Splines to the Presence of Singularities Through Correction Terms. Journal of Scientific Computing, 95, 84 (2023), https://doi.org/10.1007/s10915-023-02191-9.

[3] R. J. LeVeque, Z. Li, The immersed interface method for elliptic equations with discontinuous coefficients and singular sources, SIAM J. Numer. Anal. 31 (4) (1994) 1019–1044.

[4] J. T. Beale, M.-C. Lai, A method for computing nearly singular integrals, SIAM Journal on Numerical Analysis, 38 (6) (2001) 1902–1925.

[5] G. Monegato, L. Scuderi, Numerical integration of functions with boundary singularities, Journal of Computational and Applied Mathematics 112 (1) (1999) 201–214.

[6] E. De Doncker, R. Piessens, Algorithm 32 – automatic computation of integrals with singular integrand, over a finite or an infinite range, Computing 17 (1976) 265–279.

[7] P. J. Davis, P. Rabinowitz, Ignoring the singularity in approximate integration, Journal of the Society for Industrial and Applied Mathematics Series B Numerical Analysis 2 (3) (1965) 367–383.

[8] B. Grier, E. Alyanak, M. White, J. Camberos, R. Figliola, Numerical integration techniques for discontinuous manufactured solutions, J. Comput. Phys. 278 (2014) 193–203.

[9] A. Tornberg, Multi-dimensional quadrature of singular and discontinuous functions, BIT Numer. Math. 42 (2002) 644–669.

[10] W. Boehm, Multivariate spline methods in CAGD, Comput. Aided Des. 18 (2) (1986) 102–104.

[11] J. A. Cottrell, T. J. R. Hughes, Y. Bazilevs, Isogeometric Analysis: Toward Integration of CAD and FEA, Vol. 27, John Wiley and Sons, Ltd., Chichester, 2009.

[12] G. J. Hettinga, J. Kosinka, A multisided C^2 B-spline patch over extraordinary vertices in quadrilateral meshes, Comput. Aided Des. 127 (2020) 102855.

[13] M. Sarfraz, A rational spline with tension: some CAGD perspectives, in: Proceedings. 1998 IEEE Conference on Information Visualization. An International Conference on Computer Visualization and Graphics, 1998, pp. 178–183.

[14] M. L. de Silanes, M. Parra, M. Pasadas, J. Torrens, Spline approximation of discontinuous multivariate functions from scattered data, J. Comput. Appl. Math. 131 (1–2) (2001) 281 – 298.

[15] M. Bloor, M. Wilson, Representing PDE surfaces in terms of B-splines, Comput. Aided Des. 22 (6) (1990) 324–331.

[16] A. Kouibia, M. Pasadas, M. Rodríguez, Construction of ODE curves, Numer. Algorithms 34 (2003) 367–377.

[17] M. Pasadas, M. L. Rodríguez, Multivariate approximation by PDE splines, J. Comput. Appl. Math. 218 (2) (2008) 556–567.

[18] B. Forster, Splines and Multiresolution Analysis, Springer New York, New York, NY, 2015, pp. 1675–1716.

[19] T. M. Lehmann, C. Gonner, K. Spitzer, Addendum: B-spline interpolation in medical image processing, IEEE Trans. Med. Imag. 20 (7) (2001) 660–665.

[20] M. Unser, Splines: a perfect fit for signal and image processing, IEEE Signal Process. Mag. 16 (6) (1999) 22–38.

[21] Z. Zhang, C. F. Martin, Convergence and Gibbs' phenomenon in cubic spline interpolation of discontinuous functions, J. Comput. Appl. Math. 87 (2) (1997) 359 – 371.

[22] F. Richards, A Gibbs phenomenon for spline functions, J. Approx. Theory. 66 (3) (1991) 334 – 351.

[23] E. Hewitt, R. E. Hewitt, The Gibbs-Wilbraham phenomenon: An episode in Fourier analysis, Arch. Hist. Exact. Sci. 21 (1979) 129–160.

[24] D. Gottlieb, C.-W. Shu, On the Gibbs phenomenon and its resolution, SIAM Rev. 39 (4) (1997) 644–668.

[25] J.-H. Jung, B. D. Shizgal, On the numerical convergence with the inverse polynomial reconstruction method for the resolution of the Gibbs phenomenon, J. Comput. Phys. 224 (2) (2007) 477–488.

[26] S. D. Marchi, Mapped polynomials and discontinuous kernels for Runge and Gibbs phenomena, to appear in SEMA SIMAI Springer Series.

[27] D. Gottlieb, C.-W. Shu, A general theory for the resolution of the gibbs phenomenon, Tricomi's Ideas and Contemporary Applied Mathematics, Accademia Nazionale Dei Lincy, ATTI Dei Convegni Lincey 147 (1998) 39–48.

[28] D. Gottlieb, C.-W. Shu, A. Solomonoff, H. Vandeven, On the gibbs phenomenon i: recovering exponential accuracy from the fourier partial sum of a nonperiodic analytic function, J. Comput. Appl. Math. 43 (1992) 81–92.

[29] D. Gottlieb, C.-W. Shu, On the gibbs phenomenon iii: recovering exponential accuracy in a sub-interval from the spectral sum of piecewise analytic function, SIAM J. Numer. Anal. 33 (1996) 280–290.

[30] D. Gottlieb, C.-W. Shu, On the gibbs phenomenon iv: recovering exponential accuracy in a subinterval from a gegenbauer partial sum of a piecewise analytic function, Math. Comput. 64 (1995) 1081–1095.

[31] D. Gottlieb, C.-W. Shu, On the gibbs phenomenon v: recovering exponential accuracy from collocation point values of a piecewise analytic function, Numer. Math. 71 (1995) 511–526.

[32] S. Gottlieb, J.-H. Jung, S. Kim, A review of david gottlieb's work on the resolution of the gibbs phenomenon, Commun. Comput. Phys. 9 (3) (2011) 497–519.

[33] B. D. Shizgal, J.-H. Jung, Towards the resolution of the gibbs phenomena, J. Comput. Appl. Math. 161 (1) (2003) 41–65.

[34] K. S. Eckhoff, Accurate reconstructions of functions of finite regularity from truncated fourier series expansions, Math. Comp. 64 (1995) 671–690.

[35] K. S. Eckhoff, On a high order numerical method for functions with singularities, Math. Comp. 67 (1998) 1063–1087.

[36] S. Amat, J. Ruiz-Álvarez, C.-W. Shu, J. C. Trillo, On a class of splines free of Gibbs phenomenon, ESAIM: Mathematical Modelling and Numerical Analysis. 55 (2021) S29–S64.

[37] S. Amat, D. Levin, J. Ruiz-Álvarez, J. C. Trillo, D. F. Yañez, A class of C^2 quasi-interpolating splines free of Gibbs phenomenon, to appear in Num. Algoritms.

[38] K. E. Atkinson, An introduction to numerical analysis, 2nd edn., John Wiley and Sons, 1989.

[39] E. Isaacson, H. Keller, Analysis of numerical methods, Wiley, New York, 1966.

[40] Z. Li, On convergence of the immersed boundary method for elliptic interface problems, Math. Comput. 84 (293) (2015) 1169–1188.

[41] F. Tong, W. Wang, X. Feng, J. Zhao, Z. Li, How to obtain an accurate gradient for interface problems?, Journal of Computational Physics 405 (2020) 109070.

[42] J. T. Beale, A. T. Layton, On the accuracy of finite difference methods for elliptic problems with interfaces, Commun. Appl. Math. Comput. Sci. 1 (2006) 91–119.

[43] K. Gürlebeck, A. Hommel, On finite difference potentials and their applications in a discrete function theory, Mathematical Methods in the Applied Sciences 25 (16-18) (2002) 1563–1576.

[44] W. Hackbusch, Elliptic Differential Equations: Theory and Numerical Treatment, Vol. 18 of Springer Series in Computational Mathematics, Springer-Verlag, Berlin, 1992.

[45] G. F. Lawler, Intersections of Random Walks, Probability and its Applications, Birkhäuser Boston Inc., Boston, MA, 1991.

[46] Y. Mori, Convergence proof of the velocity field for a Stokes flow immersed boundary method, Communications on Pure and Applied Mathematics 61 (9) (2008) 1213–1263.

[47] V. Thomée, Discrete interior Schauder estimates for elliptic difference operators, SIAM Journal on Numerical Analysis 5 (3) (1968) 626–645.

[48] Z. Li, K. Ito, The Immersed Interface Method: Numerical Solutions of PDEs Involving Interfaces and Irregular Domains (Frontiers in Applied Mathematics), Society for Industrial and Applied Mathematics (SIAM), Philadelphia, PA, USA, 2006.

[49] S. Amat, Z. Li, J. Ruiz, On a new algorithm for function approximation with full accuracy in the presence of discontinuities based on the immersed interface method, J. Sci. Comput. 75 (3) (2018) 1500–1534.

[50] F. Aràndiga, A. Cohen, R. Donat, N. Dyn, Interpolation and approximation of piecewise smooth functions, SIAM J. Numer. Anal. 43 (1) (2005) 41–57.

[51] A. Harten, ENO schemes with subcell resolution, J. Comput. Phys. 83 (1) (1989) 148 – 184.

[52] J. Ahlberg, E. Nilson, J. Walsh, The theory of splines and their applications, Vol. 38 of Mathematics in Science and Engineering, Elsevier, 1967.

[53] C. de Boor, A Practical Guide to Splines, Vol. 27, Springer-Verlag New York, 1980.

[54] J. Stoer, R. Bulirsch, Introduction to numerical analysis. Third edition, Texts in applied mathematics, Springer, 2002.

[55] Z. Zhang, C. F. Martin, Convergence and Gibbs' phenomenon in cubic spline interpolation of discontinuous functions, J. Comput. Appl. Math. 87 (2) (1997) 359 – 371.

[56] Amat S. and Liandrat J., (2005). On the stability of the PPH nonlinear multiresolution, *Appl. Comp. Harm. Anal.*, **18**(2), 198-206.

[57] A. Cohen, N. Dyn, B. Matei, Quasi linear subdivision schemes with applications to ENO interpolation, Appl. Comput. Harmon. Anal. 15 (2003) 89 – 116.

[58] Daubechies I., Runborg O. and Sweldens W., (2004). Normal multiresolution approximation of curves, *Const. Approx.*, **20** 3, 399–463.

[59] Donoho D., Yu T.P.-Y, (2000). Nonlinear pyramid transforms based on median interpolation. *SIAM J. Math. Anal.*, **31**(5), 1030-1061.

[60] Floater M. S. and Michelli C.A., (1998). Nonlinear stationary subdivision, *Approximation theory: in memory of A.K. Varna, edt: Govil N.K, Mohapatra N., Nashed Z., Sharma A., Szabados J.*, 209-224.

[61] Oswald P., (2004). Smoothness of Nonlinear Median-Interpolation Subdivision, *Adv. Comput. Math.*, **20**(4), 401-423.

[62] A. Harten, S. Osher, Uniformly high-order accurate nonoscillatory schemes. I, SIAM J. Numer. Anal. 24 (2) (1987) 279 – 309.

[63] A. Harten, B. Engquist, S. Osher, S. R. Chakravarthy, Uniformly high order accurate essentially non-oscillatory schemes, III, J. Comput. Phys. 71 (2) (1987) 231 – 303.

[64] C.-W. Shu, S. Osher, Efficient implementation of essentially non-oscillatory shock-capturing schemes, J. Comput. Phys. 77 (2) (1988) 439 – 471.

[65] C.-W. Shu, S. Osher, Efficient implementation of essentially non-oscillatory shock-capturing schemes II, J. Comput. Phys. 83 (1) (1989) 32 – 78.

[66] F. Arandiga, A. Cohen, R. Donat, N. Dyn, B. Matei, Approximation of piecewise smooth functions and images by edge-adapted (ENO-EA) nonlinear multiresolution techniques, Appl. Comput. Harmon. Anal. 24 (2) (2008) 225 – 250, Special Issue on Mathematical Imaging – Part II.

[67] S. Amat, F. Aràndiga, A. Cohen, R. Donat, G. Garcia, M. von Oehsen, Data compression with ENO schemes: A case study, Appl. Comput. Harmon. Anal. 11 (2) (2001) 273 – 288.

[68] S. Serna, A. Marquina, Power ENO methods: a fifth-order accurate weighted power ENO method, J. Comput. Phys. 194 (2) (2004) 632 – 658.

[69] S. Amat, S. Busquier, J. C. Trillo, On multiresolution schemes using a stencil selection procedure: applications to ENO schemes, Numer. Algorithms 44 (1) (2007) 45 – 68.

[70] C.-W. Shu, High Order ENO and WENO Schemes for Computational Fluid Dynamics, Springer, Berlin, Heidelberg, 1999, pp. 439 – 582.

[71] F. Aràndiga, A. Baeza, A. M. Belda, P. Mulet, Analysis of WENO schemes for full and global accuracy, SIAM J. Numer. Anal. 49 (2) (2011) 893–915.

[72] F. Aràndiga, A. Belda, P. Mulet, Point-value WENO multiresolution applications to stable image compression, J. Sci. Comput. 43 (2) (2010) 158–182.

[73] A. K. Henrick, T. D. Aslam, J. M. Powers, Mapped weighted essentially non-oscillatory schemes: Achieving optimal order near critical points, J. Comput. Phys. 207 (2) (2005) 542 – 567.

[74] M. Castro, B. Costa, W. S. Don, High order weighted essentially non-oscillatory WENO-Z schemes for hyperbolic conservation laws, J. Comput. Phys. 230 (5) (2011) 1766 – 1792.

[75] S. Rathan, G. N. Raju, A modified fifth-order WENO scheme for hyperbolic conservation laws, Comput. Math. Appl. 75 (5) (2018) 1531 – 1549.

[76] C. Huang, L. L. Chen, A simple smoothness indicator for the WENO scheme with adaptive order, J. Comput. Phys. 352 (2018) 498 – 515.

[77] J. Zhu, J. Qiu, A new type of modified WENO schemes for solving hyperbolic conservation laws, SIAM J. Sci. Comput. 39 (3) (2017) A1089 – A1113.

[78] B. S. van Lith, J. H. ten Thije Boonkkamp, W. L. IJzerman, Embedded WENO: A design strategy to improve existing WENO schemes, J. Comput. Phys. 330 (2017) 529 – 549.

[79] Y.-T. Zhang, C.-W. Shu, Chapter 5 - ENO and WENO schemes, in: R. Abgrall, C.-W. Shu (Eds.), Handbook of Numerical Methods for Hyperbolic Problems. Basic and Fundamental Issues, Vol. 17 of Handbook of Numerical Analysis, Elsevier, 2016, pp. xxi – xxiii.

[80] D. Sun, F. Qu, C. Yan, An efficient adaptive high-order scheme based on the WENO process, Comput. Fluids 140 (2016) 81 – 96.

[81] J. Zhu, J. Qiu, A new fifth order finite difference WENO scheme for solving hyperbolic conservation laws, J. Comput. Phys. 318 (2016) 110 – 121.

[82] X. Zhang, C.-W. Shu, Positivity-preserving high order finite difference WENO schemes for compressible euler equations, J. Comput. Phys. 231 (5) (2012) 2245 – 2258.

[83] G. A. Gerolymos, D. Sénéchal, I. Vallet, Very-high-order WENO schemes, J. Comput. Phys. 228 (23) (2009) 8481 – 8524.

[84] Y. Shen, G. Zha, Improvement of the WENO scheme smoothness estimator, Int. J. Numer. Methods Fluids 64 (6) (2010) 653–675.

[85] Y. Liu, C.-W. Shu, M. Zhang, High order finite difference WENO schemes for nonlinear degenerate parabolic equations, SIAM J. Sci. Comput. 33 (2) (2011) 939–965.

[86] T. Sun, Numerical smoothness and error analysis on WENO for the nonlinear conservation laws, Numer. Methods. Partial Differ. Equ. 29 (6) (2013) 1881–1911.

[87] F. Aràndiga, M. C. Martí, P. Mulet, Weights design for maximal order WENO schemes, J. Sci. Comput. 60 (3) (2014) 641 – 659.

[88] Q. Li, P. Liu, H. Zhang, Piecewise polynomial mapping method and corresponding WENO scheme with improved resolution, Commun. Comput. Phys. 18 (5) (2015) 1417 – 1444.

[89] D. S. Balsara, S. Garain, C.-W. Shu, An efficient class of WENO schemes with adaptive order, J. Comput. Phys. 326 (C) (2016) 780 – 804.

[90] C.-W. Shu, Essentially non-oscillatory and weighted essentially non-oscillatory schemes for hyperbolic conservation laws, Springer, Berlin, Heidelberg, 1998, pp. 325 – 432.

[91] C.-W. Shu, High order weighted essentially nonoscillatory schemes for convection dominated problems, SIAM Review 51 (1) (2009) 82–126.

[92] Aràndiga F. and Donat R., (2000). Nonlinear Multi-scale Decomposition: The Approach of A.Harten, Numerical Algorithms, **23**, pp. 175-216.

[93] Ruiz J. and Trillo J.C. (2018). N-dimensional error control multiresolution algorithms for the cell average discretization. Math. Comput. Simul. 144, C , 153-161.

[94] Amat S. , Liandrat J. , Ruiz J. , Trillo J.C. (2015). On a family of nonlinear cell-average multiresolution schemes for image processing: An experimental study. Math. Comput. Simul. 118, 30-48.

[95] Harten A., (1993). Discrete multiresolution analysis and generalized wavelets, *J. Appl. Numer. Math.*, **12**, 153-192.

[96] Harten A., (1996). Multiresolution representation of data II, *SIAM J. Numer. Anal*, **33**(3), pp. 1205-1256.

[97] Amat S., Busquier S. and Trillo J.C., (2005). Non-linear Harten's Multiresolution on the Quincunx Pyramid , *J. of Comp. and App. Math.*, **189** (1-2), 555-567.

[98] Amat S., Donat R., Liandrat J. and Trillo J.C. (2006), Analysis of a New Nonlinear Subdivision Scheme. Applications in Image Processing., *Foundations of Computational Mathematics*, **6** 2, 193-225.

[99] Amat S., Ruiz J. and Trillo J.C., (2009). Fast multiresolution algorithms and their related variational problems for image denoising. *Journal of Scientific Computing*. Accepted, November 2009. Doi: 10.1007/s10915-009-9336-7.

[100] Cohen A., Daubechies I. and Feauveau J.C., (1992). Biorthogonal bases of compactly supported wavelets, *Comm. in Pure and Appl. Math.*, **45**, 485-560.

[101] Chan, R. H., Chan, T., Shen, L., Shen, Z. (2003). Wavelet algorithms for high-resolution image reconstruction. SIAM Journal on Scientific Computing, 24(4), 1408-1432.